Acoustic Doppler Current Profiler observations during the Coastal Mixing and Optics experiment: R/V Endeavor cruises from 14 August to 1 September 1996 and 25 April to 15 May 1997

Stephen D. Pierce
John A. Barth
P. Michael Kosro

College of Oceanic and Atmospheric Sciences
Oregon State University
Corvallis, Oregon 97331-5503

Data Report 169
Reference 98-2
December 1998

http://diana.oce.orst.edu/cmoweb

We present velocity observations from a shipboard acoustic Doppler current profiler (ADCP) on R/V *Endeavor* during cruises E9608 (14 August to 1 September 1996) and E9704 (25 April to 15 May 1997). The cruises were conducted as part of the Office of Naval Research Coastal Mixing and Optics Accelerated Research Initiative. The objective was to rapidly survey a region in the Middle Atlantic Bight south of Cape Cod, Massachusetts. The ADCP was an RD Instruments hull-mounted 307-kHz unit. Data were collected nearly continuously during both cruises, in a region about 80 km square around 40.5°N, 70.5°W. Vertical bin length was 4 m and the typical depth range in open water was 200 m. To reference the velocities to earth coordinates, we used bottom-tracking supplemented by differential global positioning system (GPS) navigation. A GPS attitude system was also used, in combination with the ship's gyrocompass, to determine heading. This report describes the ADCP processing steps and presents the observed velocities. In addition, we apply an empirical tidal model to estimate and then remove the barotropic tidal currents, and we present the resulting subtidal velocities. An online version of this report is available at *http://diana.oce.orst.edu/cmoweb.*

Table of Contents

Introduction 1

Editing 7

Calibration 12

Navigation 18

Synopsis of uncertainties 18

Determination of subtidal flow 18

Data presentation 27

Acknowledgments 28

References 29

E9608 observed and subtidal velocity vectors at standard depths 31

E9608 subtidal east and north velocity sections 77

E9608 soliton sections 117

E9704 observed and subtidal velocity vectors at standard depths 131

E9704 subtidal east and north velocity sections 167

INTRODUCTION

This report presents observations of velocity from a shipboard acoustic Doppler current profiler (ADCP) on the R/V *Endeavor* during cruises E9608 (14 August to 1 September 1996) and E9704 (25 April to 15 May 1997). The cruises were conducted as part of the Office of Naval Research Coastal Mixing and Optics Accelerated Research Initiative. The objective was to rapidly survey a region in the Middle Atlantic Bight using both ADCP and SeaSoar tows, where a set of moorings and a stationary research vessel were also collecting data (Figure 1). The first cruise was in the summer season, a period of strong stratification of the water column, while the second cruise was in the spring, a period of re-stratification

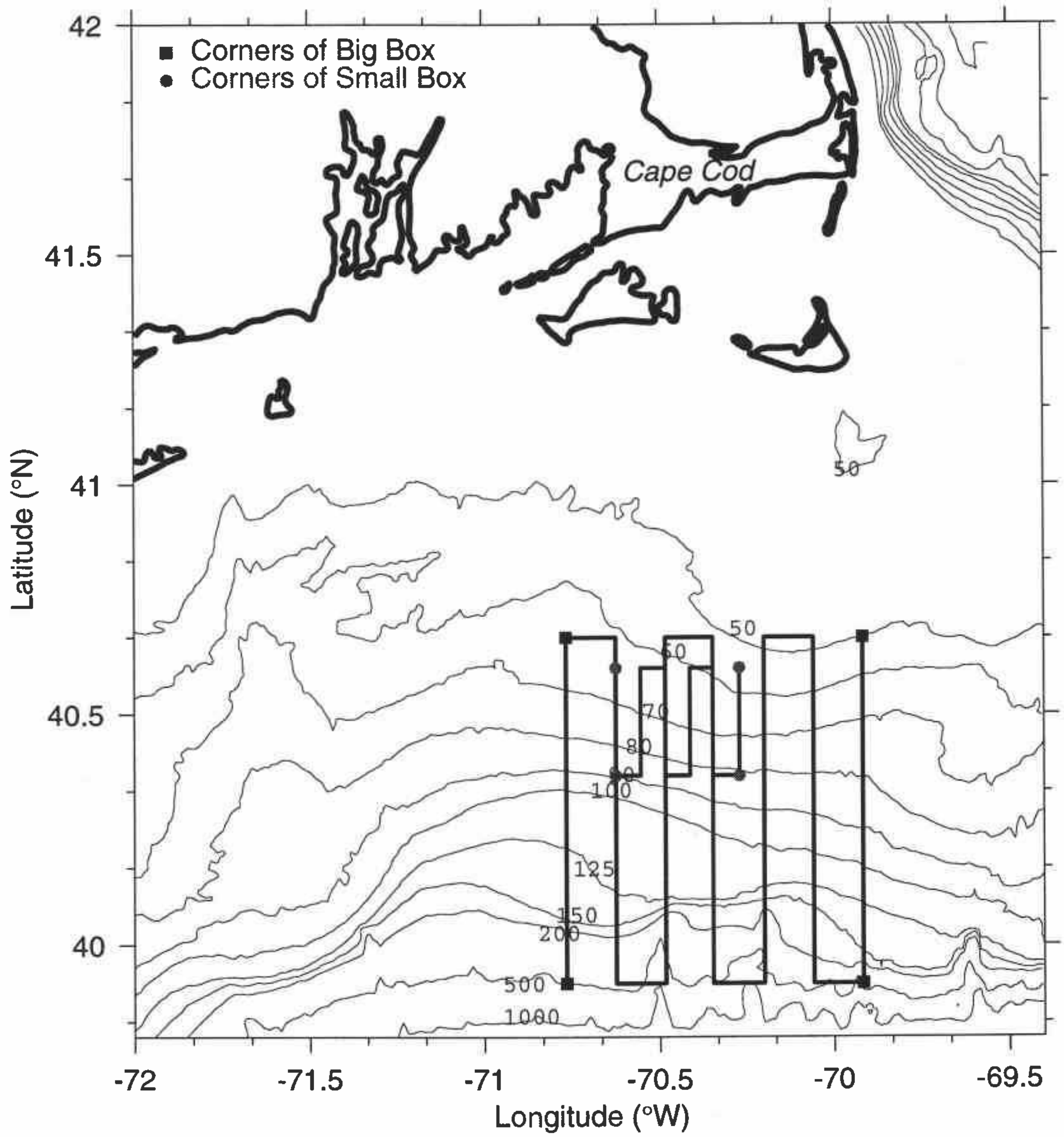

Fig. 1. Map of the study region in the Middle Atlantic Bight. Bottom topography in meters.

Table 1. RDI DAS configuration file.

e9608.cnf

```
AD,SI,HUNDREDTHS     150.00 Sampling interval
AD,NB,WHOLE              75 Number of Depth Bins
AD,BL,WHOLE               2 Bin Length
AD,PL,WHOLE               4 Pulse Length
AD,BK,TENTHS            2.0 Blank Beyond Transmit
AD,PE,WHOLE               1 Pings Per Ensemble
AD,PC,HUNDREDTHS       1.00 Pulse Cycle Time
AD,PG,WHOLE              25 Percent Pings Good Threshold
XX,OD2,WHOLE              5 [SYSTEM DEFAULT, OD2]
XX,TE,HUNDREDTHS       0.00 [SYSTEM DEFAULT, TE]
AD,US,BOOLE             YES  Use Direct Commands on StartUp
DP,TR,BOOLE              NO  Toggle roll compensation
DP,TP,BOOLE              NO  Toggle Pitch compensation
DP,TH,BOOLE             YES  Toggle Heading compensation
DP,VS,BOOLE             YES  Calculate Sound Velocity from TEMP/Salinity
DP,UR,BOOLE             YES  Use Reference Layer
DP,FR,WHOLE               3 First Bin for reference Layer
DP,LR,WHOLE               6 Last Bin for reference Layer
DP,BT,BOOLE             YES  Use Bottom Track     /* for depths < 200 m */
DP,B3,BOOLE             YES  Use 3 Beam Solutions /* for depths > 110 m */
/* [for E9704, no 3 beam solutions are used] */
DP,EV,BOOLE             YES  Use Error Velocity as Percent Good Criterion
DP,ME,TENTHS          100.0 Max. Error Velocity for Valid Data (cm/sec)
DR,RD,BOOLE             YES  Recording on disk
DR,RX,BOOLE             YES  Record N/S (FORE/AFT) Vel.
DR,RY,BOOLE             YES  Record E/W (FORT/STBD) Vel.
DR,RZ,BOOLE             YES  Record vertical vel.
DR,RE,BOOLE             YES  Record error Good
DR,RB,BOOLE             YES  Bytes of user prog. buffer
DR,RP,BOOLE             YES  Record Percent good
DR,RA,BOOLE             YES  Record average AGC/Bin
DR,RN,BOOLE             YES  Record Ancillary data
DR,AP,BOOLE             YES  Auto-ping on start-up
XX,LDR,TRI                3 [SYSTEM DEFAULT, LDR]
XX,RB2,WHOLE            192 [SYSTEM DEFAULT, RB2]
DR,RC,BOOLE              NO  Record CTD data
XX,FB,WHOLE               1 [SYSTEM DEFAULT, FB]
XX,PU,BOOLE              NO  [SYSTEM DEFAULT, PU]
GC,TG,TRI                 1 DISPLAY (NO/GRAPH/TAB)
GC,ZV,WHOLE               1 ZERO VELOCITY REFERENCE (S/B/M/L)
GC,VL,WHOLE             -50 LOWEST VELOCITY ON GRAPH
CG,VH,WHOLE              50 HIGHEST VELOCITY ON GRAPH
GC,DL,WHOLE               0 LOWEST DEPTHS ON GRAPH
GC,DH,WHOLE             500 HIGHEST DEPTHS ON GRAPH
GC,SW,BOOLE             YES  SET DEPTHS WINDOW TO INCLUDE ALL BINS
GC,MP,WHOLE              25 MINIMUM PERCENT GOOD TO PLOT
SG,PNS,BOOLE            YES  PLOT NORTH/SOUTH VEL.
SG,PEW,BOOLE            YES  PLOT EAST/WEST VEL.
SG,PVT,BOOLE            YES  PLOT VERTICAL VEL.
SG,PEV,BOOLE            YES  PLOT ERROR VEL.
SG,PPE,BOOLE            YES  PLOT PERCENT ERROR
SG,PMD,BOOLE             NO  PLOT MAG AND DIR
SG,PSW,BOOLE             NO  PLOT AVERAGE SP. W.
SG,PAV,BOOLE             NO  PLOT AVERAGE AGC.
SG,PPG,BOOLE            YES  PLOT PERCENT GOOD
SG,PD1,BOOLE             NO  PLOT DOPPLER 1
SG,PD2,BOOLE             NO  PLOT DOPPLER 2
SG,PD3,BOOLE             NO  PLOT DOPPLER 3
SG,PD4,BOOLE             NO  PLOT DOPPLER 4
SG,PW1,BOOLE             NO  PLOT SP. W. 1
SG,PW2,BOOLE             NO  PLOT SP. W. 2
SG,PW3,BOOLE             NO  PLOT SP. W. 3
SG,PW4,BOOLE             NO  PLOT SP. W. 4
SG,PA1,BOOLE            YES  PLOT AGC 1
SG,PA2,BOOLE            YES  PLOT AGC 2
SG,PA3,BOOLE            YES  PLOT AGC 3
SG,PA4,BOOLE            YES  PLOT AGC 4
SG,PP3,BOOLE             NO  PLOT 3-BEAM SOLUTION
SS,OD,WHOLE             5.0 OffSet for Depth
SS,OH,TENTHS           45.0 OffSet for Heading
SS,OP,TENTHS            0.0 OffSet for Pitch
SS,ZR,TENTHS            0.0 OffSet for Roll
SS,OT,HUNDREDTHS      45.00 OffSet FOR temp
SS,ST,HUNDREDTHS      50.00 Scale for Temp
SS,SL,HUNDREDTHS      33.50 Salinity (PPT)
SS,UD,BOOLE             YES  Toggle UP/DOWN
SS,CV,BOOLE              NO  Toggle concave/Convex  transducerhead
SS,MA,TENTHS           30.0 Mounting angle for transducers.
SS,SS,HUNDREDTHS    1500.00 Speed of Sound (m/sec)
XX,GP,BOOLE             YES  [SYSTEM DEFAULT, GP]
XX,DD,TENTHS            1.0 [SYSTEM DEFAULT, DD]
XX,PT,BOOLE              NO  [SYSTEM DEFAULT, PT]
XX,TU,TRI                 2 [SYSTEM DEFAULT, TU]
TB,FP,WHOLE               1 FIRST BINS TO PRINT
TB,LP,WHOLE              64 LAST BIN TO PRINT
TB,SK,WHOLE               6 SKIP INTERVAL BETWEEN BINS
TB,DT,BOOLE             YES  DIAGNOSTIC TAB MODE
DU,TD,BOOLE              NO  TOGGLE USE OF DUMMY DATA
XX,PN,WHOLE               0 [SYSTEM DEFAULT, PN]
DR,SD,WHOLE               3 Second recording drive
DR,PD,WHOLE               1 First recording drive (1=A:,2=B: ... )
DP,PX,BOOLE              NO  Profiler does XYZE transform
SS,LC,TENTHS            5.0 Limit of Knots change
SS,NW,TENTHS            0.5 Weight of new knots of value
GC,GM,TRI                 2 GRAPHICS CONTROL 0=LO RES, 1=HI RES, 2=ENHANCED
AD,PS,BOOLE              NO  YES=SERIAL/NO=PARALLEL Profiler Link
XX,LNN,BOOLE            YES  [SYSTEM DEFAULT, LNN]
XX,BM,BOOLE             YES  [SYSTEM DEFAULT, BM]
XX,RSD,BOOLE             NO  RECORD STANDARD DEVIATION OF VELOCITIES PER BIN
XX,DRV,WHOLE              0 [SYSTEM DEFAULT, DRV]
XX,PBD,WHOLE              3 [SYSTEM DEFAULT, PBD]
TB,RS,BOOLE             YES  SHOW RHPT STATISTIC
UX,EE,BOOLE             YES  ENABLE EXIT TO EXTERNAL PROGRAM
SS,VSC,TRI                0 Velocity scale adjustment
AD,DM,BOOLE              NO  USE DMA
TB,SC,BOOLE              NO  SHOW CTD DATA
AD,CW,BOOLE             YES  Collect spectral width
DR,RW,BOOLE             YES  Record average SP.W./Bin
DR,RRD,BOOLE             NO  Record last raw dopplers
DR,RRA,BOOLE            YES  Record last raw AGC
DR,RRW,BOOLE             NO  Record last SP.W.
DR,R3,BOOLE              NO  Record average 3-Beam solutions
DR,RBS,BOOLE            YES  Record beam statistic
XX,STD,BOOLE             NO  [SYSTEM DEFAULT, STD]
LR,HB,HUNDREDTHS       0.00 Heading Bias
SL,1,ARRAY5      0    1    8    NONE  19200  PROFILER
SL,2,ARRAY5      0    1    8    NONE   1200  LORAN RECEIVER
SL,3,ARRAY5      0    1    8    NONE   1200  REMOTE DISPLAY
SL,4,ARRAY5      0    1    8    NONE   1200  ENSEMBLE OUTPUT
SL,5,ARRAY5      0    1    8    NONE   1200  AUX 1
SL,6,ARRAY5      0    1    8    NONE   1200  AUX 2
DU,1,ARRAY6     100.00    100.00    60.00    0.00    0.00 YES D1
DU,2,ARRAY6    -100.00   -100.00    60.00    0.00    0.00 YES D2
DU,3,ARRAY6     200.00    200.00    60.00    0.00    0.00 YES D3
DU,4,ARRAY6    -200.00   -200.00    60.00    0.00    0.00 YES D4
DU,5,ARRAY6     200.00     19.00    60.00    0.00    0.00 YES AGC
DU,6,ARRAY6       0.00      0.00    60.00    0.00    0.00 NO  SP. W.
DU,7,ARRAY6       0.00      0.00    60.00    0.00    0.00 NO  ROLL
DU,8,ARRAY6       0.00      0.00    60.00    0.00    0.00 NO  PITCH
DU,9,ARRAY6       0.00      0.00    60.00    0.00    0.00 NO  HEADING
DU,10,ARRAY6      0.00      0.00    60.00    0.00    0.00 NO  TEMPERATURE
DC,1,SPECIAL  "FH00001" MACRO  1
DC,2,SPECIAL  "E0004020099" MACRO  2   /* E9704 case does not include this */
DC,3,SPECIAL  "B009001" MACRO  3
CI,1,SPECIAL "Coastal Mixing and Optics" CRUISE ID GOES HERE
LR,1,SPECIAL " " LORAN FILE NAME GOES HERE
```

following the winter mixing season.

The cruises were organized around the collection of CTD data from a towed undulating vehicle, the SeaSoar, in two areas: a small box pattern covering about a 25 by 30 km area and a big box pattern covering about 70 by 80 km (Figure 1). Each of these boxes was sampled repeatedly during each cruise. In addition to the CTD, the SeaSoar was equipped with a nine-wavelength light absorption and attenuation meter (WETLABS ac-9) and a new microstructure instrument developed at Oregon State University (MicroSoar). The water column was generally sampled by the SeaSoar from the surface to within 5-7 m of the bottom. Between SeaSoar tows, conventional CTD/rosette casts were also made. ADCP and underway surface temperature, salinity, and meteorological measurements were made continuously (Figure 2).

For a full description of the SeaSoar and conventional CTD data and cruise narratives for the two surveys, see O'Malley *et al.* (1998). For descriptions of the spectral light absorption and attenuation measurements, see Barth and Bogucki (1999) and Barth *et al.* (1999). For descriptions of the microstructure observations, see Erofeev *et al.* (1998). Also, online data reports for all data sets are available at *http://diana.oce.orst.edu/cmoweb.*

The reader unfamiliar with basic ADCP principles and terminology used in this report is referred to the helpful *Practical Primer,* RDI (1989). The ADCP was an RD Instruments hull-mounted narrow-band model, with 4 beams oriented 30° from vertical. To achieve higher vertical resolution, the *Endeavor's* standard 153-kHz transducer was replaced with a 307-kHz model borrowed from Oregon State University (OSU). Spool pieces to adapt the OSU transducer to the *Endeavor's* hull opening were fabricated out of 0.5" steel by Modern Heat Inc., Gloucester, Massachusetts.

The ADCP transducer was at a depth of 5 m. We set up the instrument with a pulse length of 4 m, a bin width of 4 m, a blanking interval of 2 m, and an ensemble averaging time of 2.5 min. Bottom-tracking was turned on (off) automatically when the bottom depth was less than (greater than) 200 m. This was accomplished by a watchdog program running on the data acquisition system (DAS) PC, which toggled the bottom-tracking parameter within the configuration file (Table 1) and restarted data acquisition when the 200 m isobath was crossed (C. Flagg, personal communication). Good quality bottom-tracking was available during 92% of the E9608 cruise and 93% of the E9704 cruise. The average number of pings per ensemble was 116. The error velocity threshold for raw pings during data collection was 1 m/s. No corrections for pitch and roll were made; errors associated with these are likely to be small (Kosro, 1985). Additional configuration details can be found in Table 1, a copy of the file used to configure the DAS.

During E9608, one of the 4 ADCP beams had unusually low backscatter amplitudes (Figure 3). This was probably a problem within the #4 transducer head itself. Between the two cruises, the transducer unit was returned to RD Instruments for testing/repair. The problem did not occur during E9704 (Figure 3). RD Instruments provided no explanation of repairs made. The weak beam during E9608 resulted in slightly reduced depth range, although the problem was to some extent remedied by allowing 3-beam solutions when the bottom depth was greater than 110 m (which occurred about 12% of the time

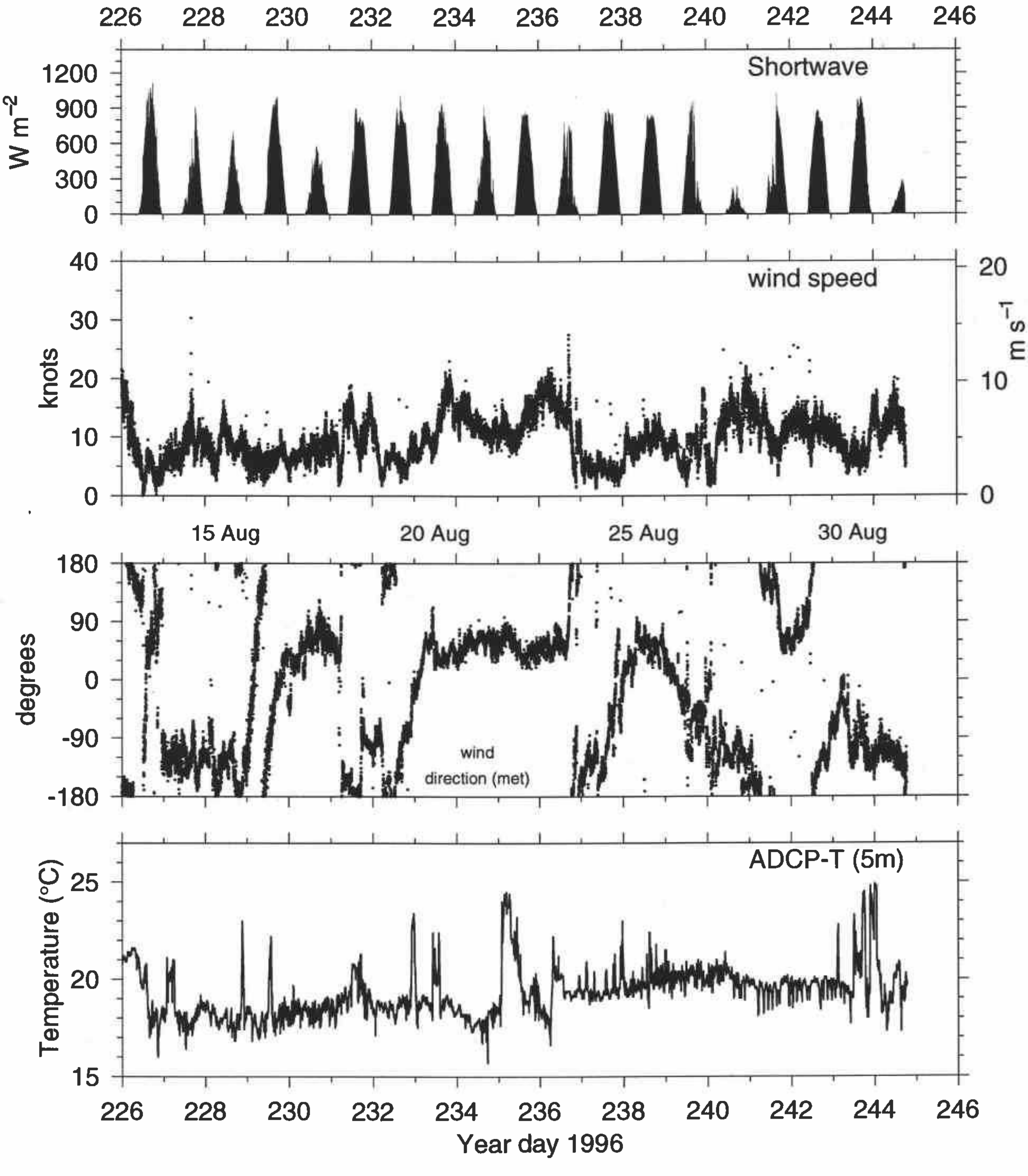

Fig. 2a. Solar radiation, wind speed, wind direction, and 5-m water temperature at the ADCP transducer, during E9608.

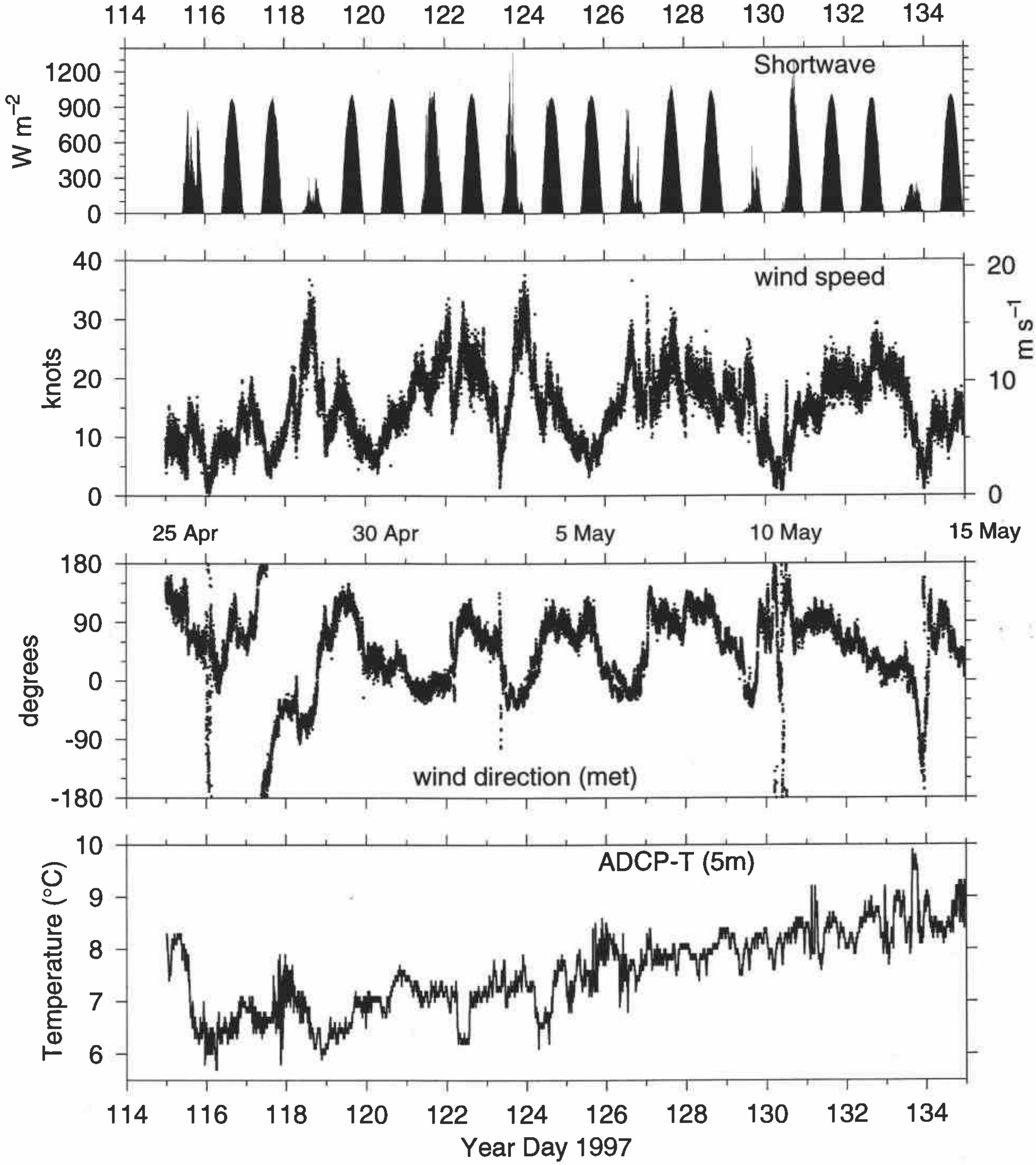

Fig. 2b. Solar radiation, wind speed, wind direction, and 5-m water temperature at the ADCP transducer, during E9704.

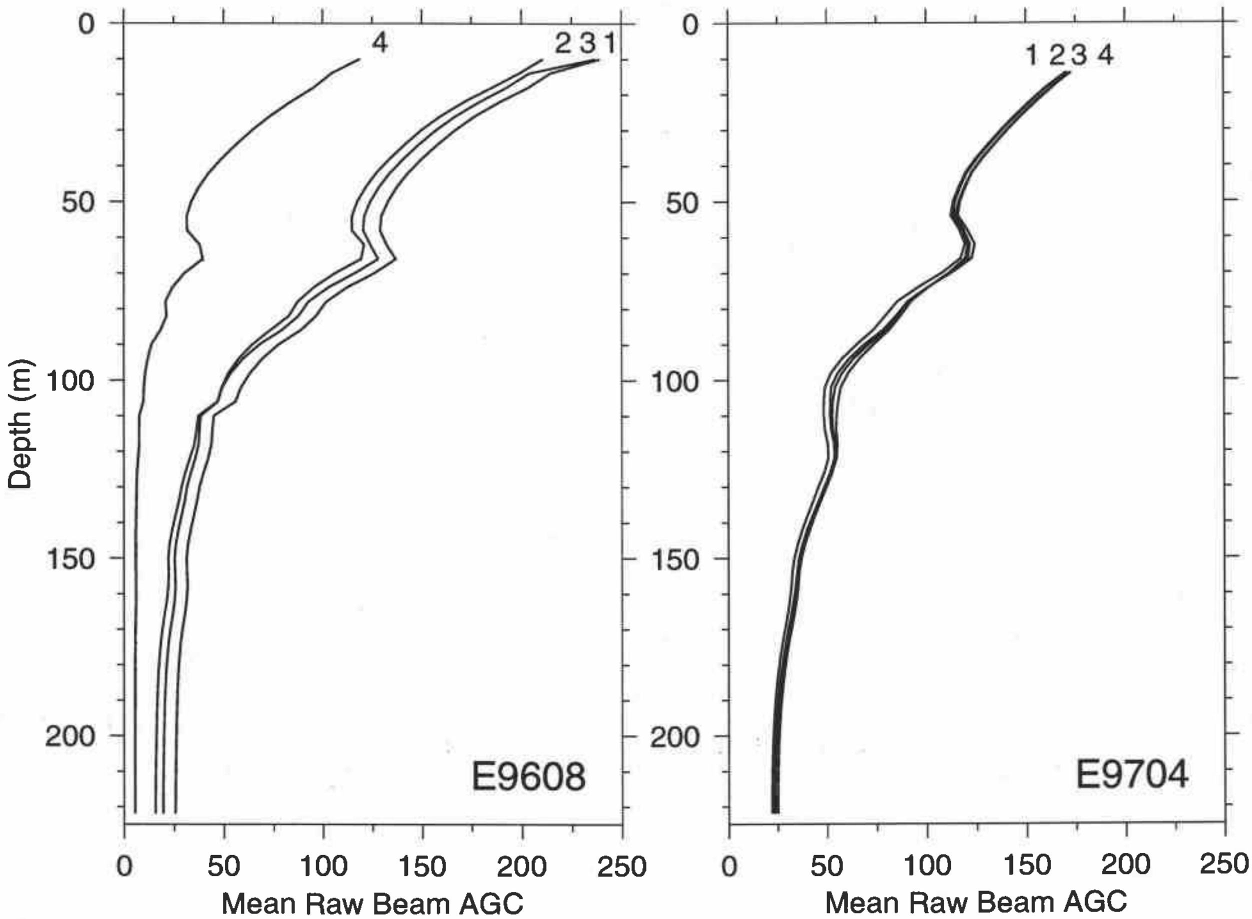

Fig. 3. Mean AGC vs. depth for E9608 (left) and E9704 (right).

during E9608).

During E9608, the shallowest available depth bin was centered at 10 m. During E9704, however, the top two depth bins were judged bad and usually rejected internally by the DAS. The shallowest available depth is thus 18 m. We attempted to remedy this by experimentation with several different ping-to-ping tracking control "E" direct commands, but the changes had no apparent effect.

The ADCP operated continuously except for breakdowns usually caused by DAS-PC "freezes" and planned short interruptions to change system parameters or diskettes. Overall, good data were collected 95% of the time during the E9608 and E9704 cruises. The occasional DAS PC freezes were apparently caused by ship's electrical noise infecting one of the serial communication lines. The source of this noise was investigated but never identified. A hardware watchdog reset program installed on the DAS PC limited these "freeze" gaps to 5 min in most cases. The largest gap was 95 min on year day 234 (Figure 6a), during E9608 Big Box 2 Line C1. This was caused by the failure of a circuit board within the ADCP deck unit. A replacement board was installed and tested successfully. The section was repeated (E9608 Big Box 2 Line C2) in order to obtain a clean section without a gap. The beam-average backscatter amplitude (Figure 4) and percentage-good-pings per ensemble (Figure 5) diagnostics appear reasonable over both cruises. More discussion of these is in the EDITING section below.

The ADCP data were initially processed and displayed in real-time by the RD Instruments program running on the DAS PC. Additional shipboard and shore processing were accomplished using some components of the Common Oceanographic Data Access System (CODAS) software package made available by the University of Hawaii (Firing *et al.*, 1995), running on a Sun Sparc 10. Using the *user exit 4* (*ue4*) program running on the DAS PC, each profile was sent serially to the Sun workstation where a second copy of the raw data was collected by the *monserv* program. Parts of the CODAS software required the Matlab language, and the figures for this report were made using the Gri package (Kelley, 1995).

For position, differential GPS with the U.S. Coast Guard corrective radio broadcasts using a Trimble NavTrac XL receiver were integrated into the ADCP data stream at the end of each 2.5-min ensemble by the *ue4* program. Differential GPS data quality was excellent throughout both cruises. Ship's heading was by a combination of Sperry gyro compass and Trimble TANS vector attitude GPS, which were both recorded at 1 Hz on the Sun workstation. The Trimble TANS vector unit experienced occasional crashes (1-2 a day) which required human intervention and resulted in gaps of about 10 min. The cause of these crashes was unknown. Some software developed at the University of Hawaii to work with Ashtech attitude data (eg. *decash*) was modified and used with the Trimble data. The attitude data were edited and averaged into 2.5 min intervals to match the ADCP ensemble times. More details regarding these steps are discussed below in the CALIBRATION section.

EDITING

As data quality decreases with depth, we must decide on the deepest usable bin for each 2.5 min ensemble. In addition, the data are edited for interference with the sea floor in shallow water and for occasional interference from the CTD hydrographic wire and other objects. To flag and remove suspect data points, several methods were used in combination during post-processing, as recommended by Firing *et al.* (1995) and others:

• The percentage-good-pings per ensemble cutoff was set to 30%; below this point data were not used. The %-good-pings is a record of the proportion of raw pings within the 2.5 min ensemble which are judged good internally by the RDI firmware and subsequently included in the ensemble average.

• The automatic gain control (AGC) gives an indication of the echo return signal strength, scaled such that 1 AGC count corresponds to about a 0.45 dB change in signal power. The AGC decreases with bin depth in general. A small increase with depth may simply indicate the presence of a strong scattering layer due to a large zooplankton population, while a larger increase is probably a reflection off of the sea floor. Individual ensembles were scanned for increases of AGC >30 counts, and the deepest subsequent bin where a local maximum is reached was taken as an indication of sea floor location.

• In the deep water case, where no sea floor echo is detected, the AGC will eventually stop decreasing with depth and become constant. This constant level is the noise floor; the signal of interest is no longer present. We use a noise margin of 10, retaining bins which have AGC greater than 10 above the noise floor.

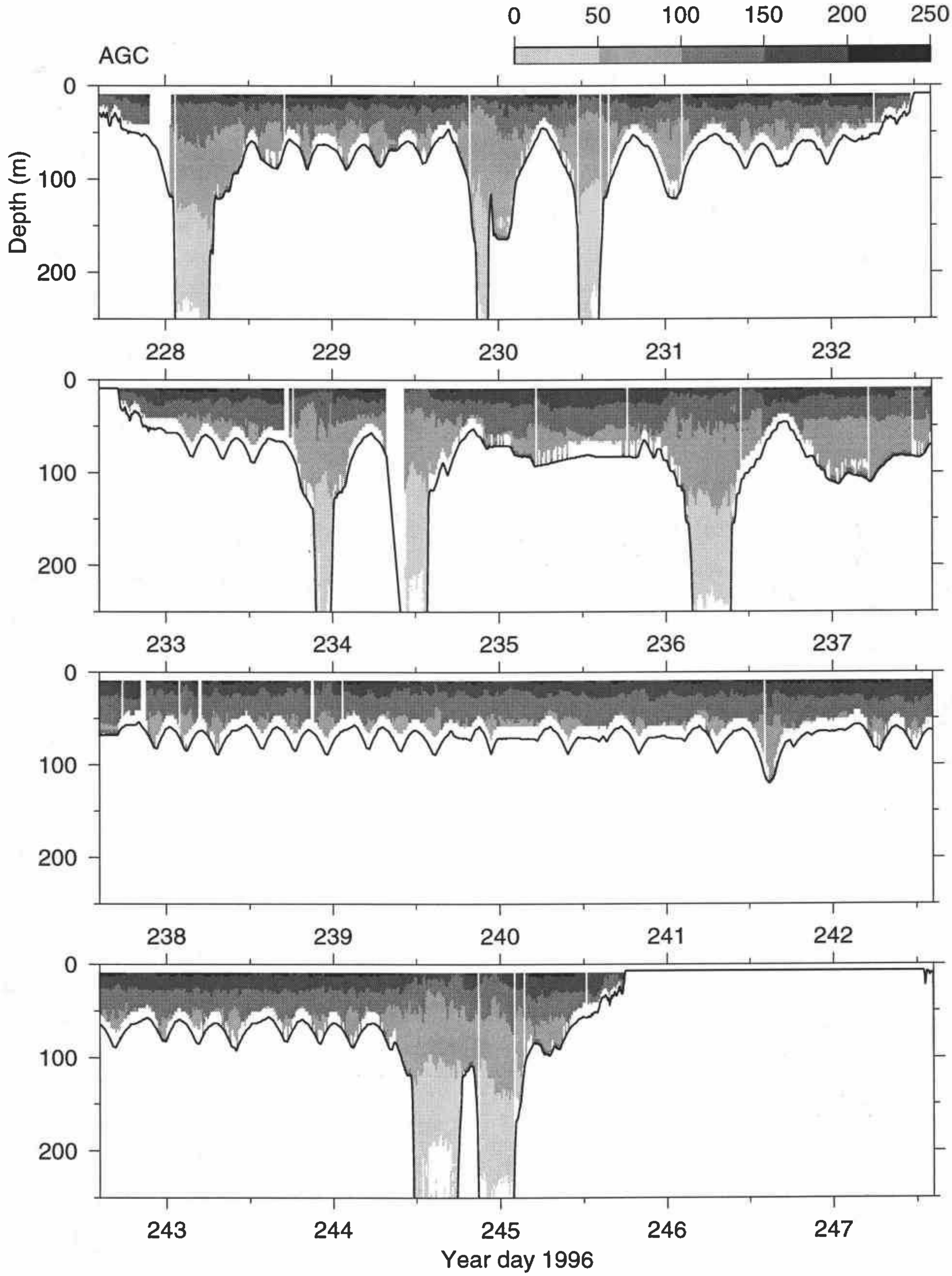

Fig. 4a. Backscatter amplitude (automatic gain control) vs. time and depth, during E9608.

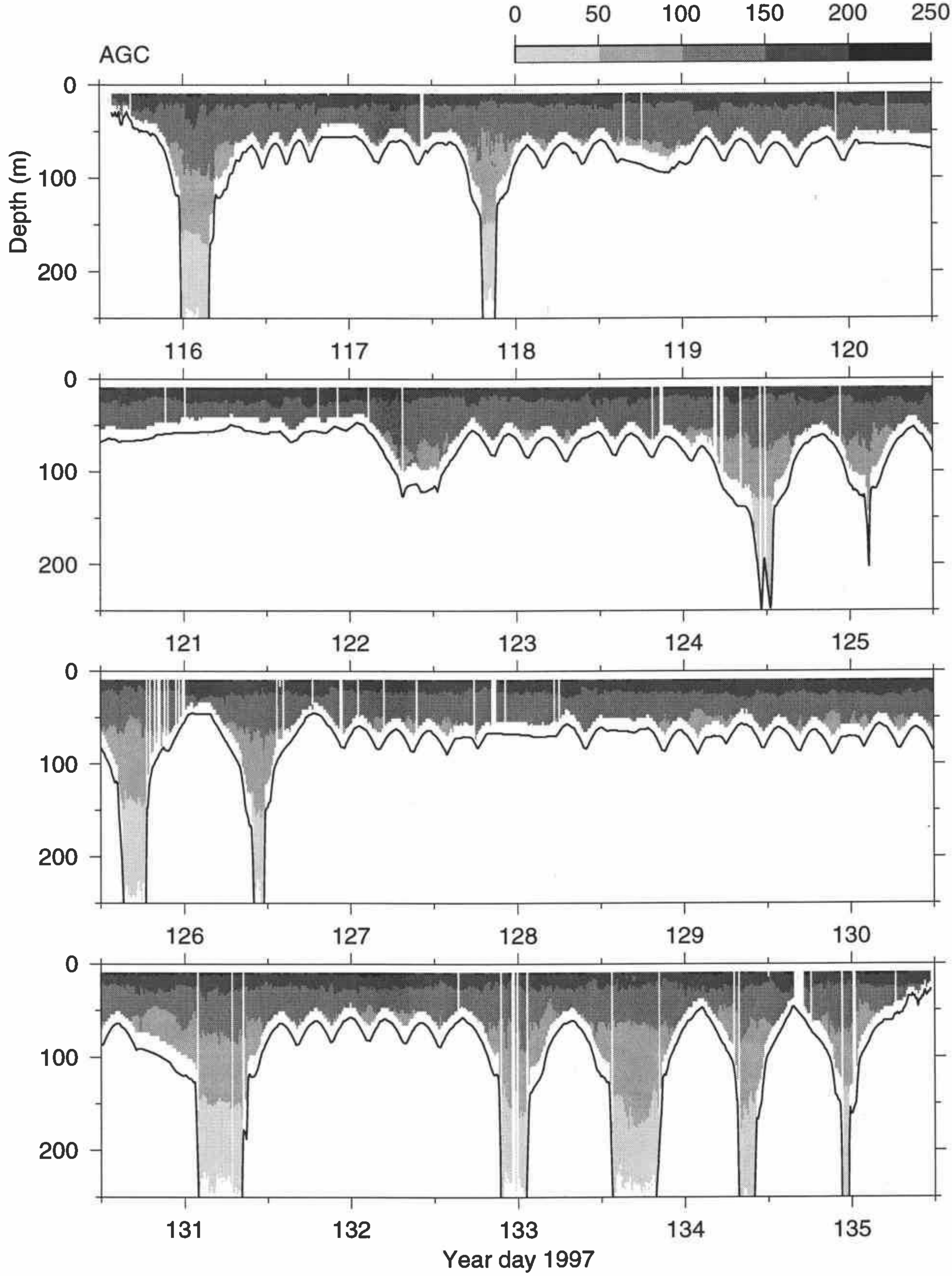

Fig. 4b. Backscatter amplitude (automatic gain control) vs. time and depth, during E9704.

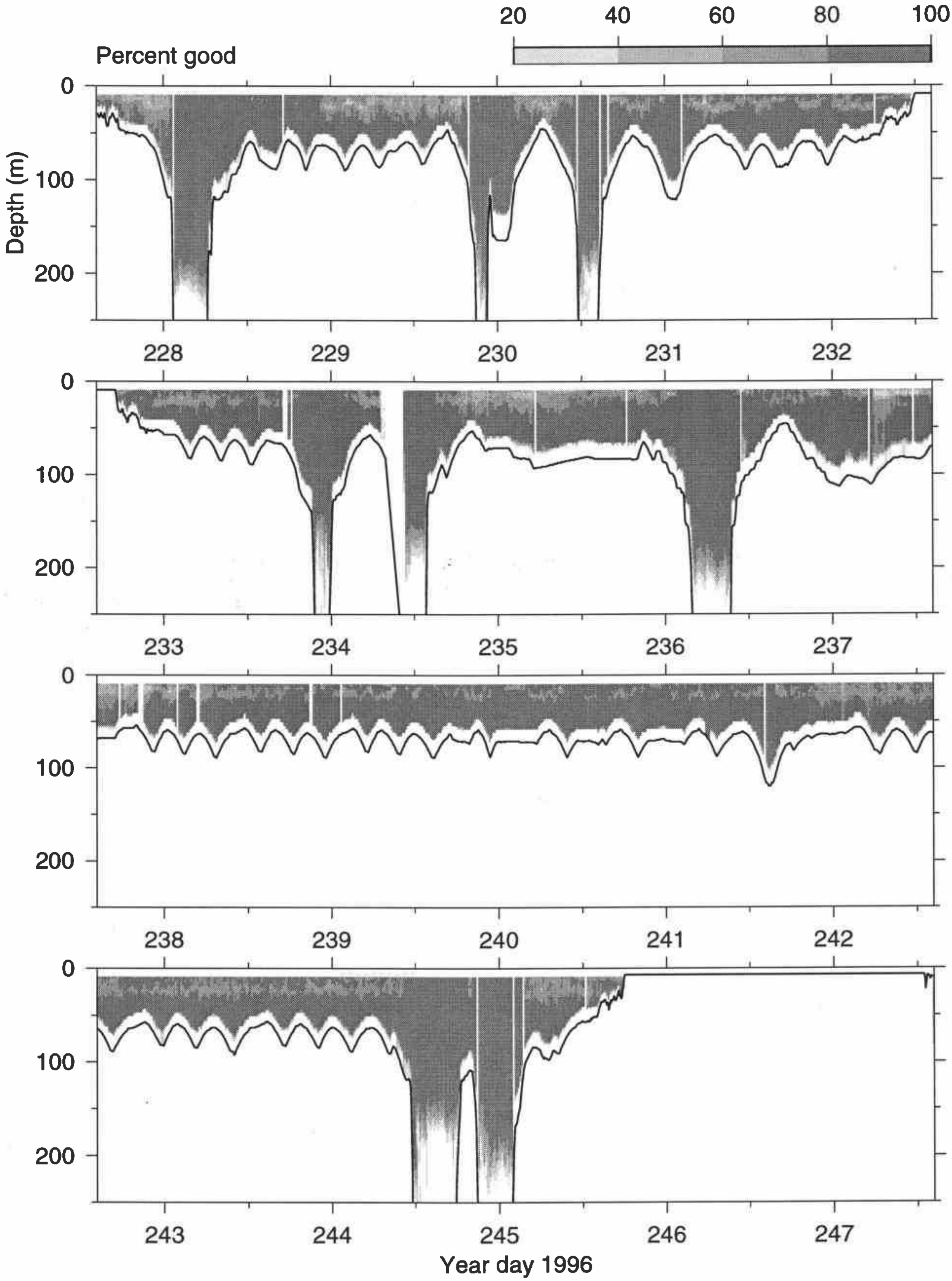

Fig. 5a. Percentage-good-pings vs. time and depth, during E9608.

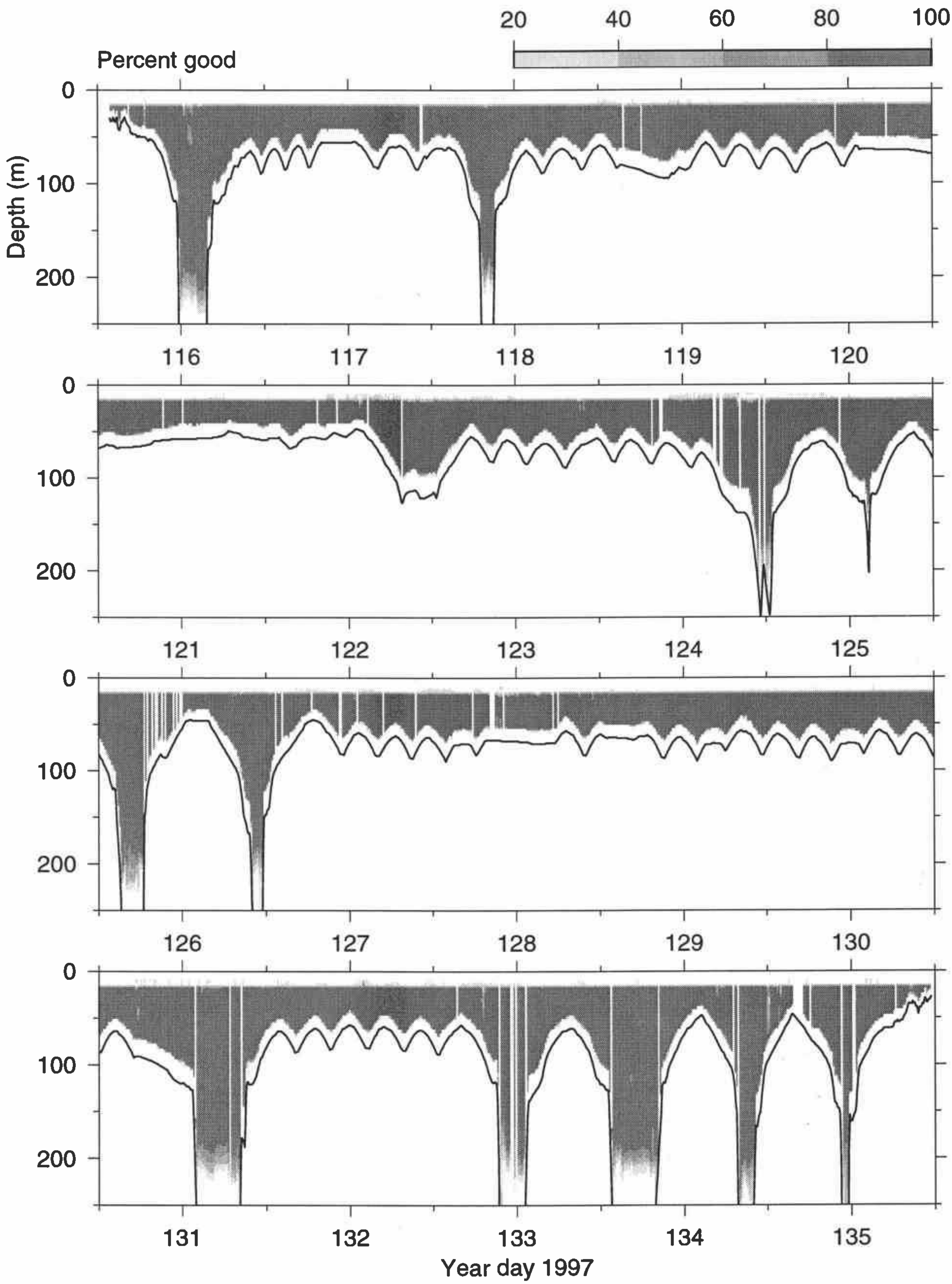

Fig. 5b. Percentage-good-pings vs. time and depth, during E9704.

• Since the ADCP initially measures velocity along the axes of four beams, which are then transformed to the 3-dimensional components u, v, and w, there is redundancy in the scheme. This redundancy is used within the RDI firmware to make two distinct estimates of the vertical velocity w. The difference between these two estimates is called the error velocity and is a useful data quality indicator. A large error velocity indicates an inconsistency among the oceanic velocities sampled by each of the 4 beams. Thus it is another way of detecting interference with one of the beams caused by an object. We reject individual bins which have an error velocity above 10 cm/s, a relatively conservative choice; the results are not very sensitive to the choice.

• The second differences with respect to depth of the horizontal velocities (denoted *d2uv*) and the second differences of the vertical velocities (*d2w*) were calculated for each profile. If *d2uv* or *d2w* exceeded cruise-long 2 standard deviation thresholds, the bin was rejected.

• If the standard deviation of *w* calculated over an entire profile exceeded a cruise-long 3 standard deviation threshold, the profile was rejected.

The result of the editing is shown in Figure 6, where good data points are plotted and missing points appear as white space. Many of the minor blank regions correspond to SeaSoar deployments, recoveries, or CTD stations, where the object in the water interfered briefly with one or more of the four ADCP beams.

CALIBRATION

Sound speed

The system was configured to use sound speed calculated from the ADCP's own thermistor and an assumed constant salinity. The ADCP thermistor (at 5 m depth) was checked against SeaSoar temperatures (from 4.5–5.5 m) when available. This revealed a mean difference of 0.44°C with no apparent trend; the ADCP sound speeds were corrected in post-processing using this constant offset. No correction was applied for salinity, since the largest deviation from the assumed constant salinity and the 4.5–5.5 m SeaSoar salinities was 2.3 psu, corresponding to only a 0.2% change in sound speed. Associated uncertainties in ADCP velocity connected with temperature and salinity are negligible (<1 cm/s) compared to other sources of error.

Attitude GPS

When bottom-tracking is not available, accurate heading information is needed to rotate ADCP velocities from transducer to earth coordinates. The ship's gyro compass usually provides an accurate heading in a long-term sense, but it can experience short-term drifts on the order of 1°. The largest form of error is known as the Schuler oscillation, which tends to be excited by ship accelerations in the north-south sense (Bowditch, 1977).

In recent years, attitude GPS receivers have been developed. These make use of phase differences between a reference antenna and three other antennae to yield a ship's heading, pitch, and roll with potential accuracies of 0.06° (King and Cooper, 1993). Although the attitude GPS receivers are not yet reliable

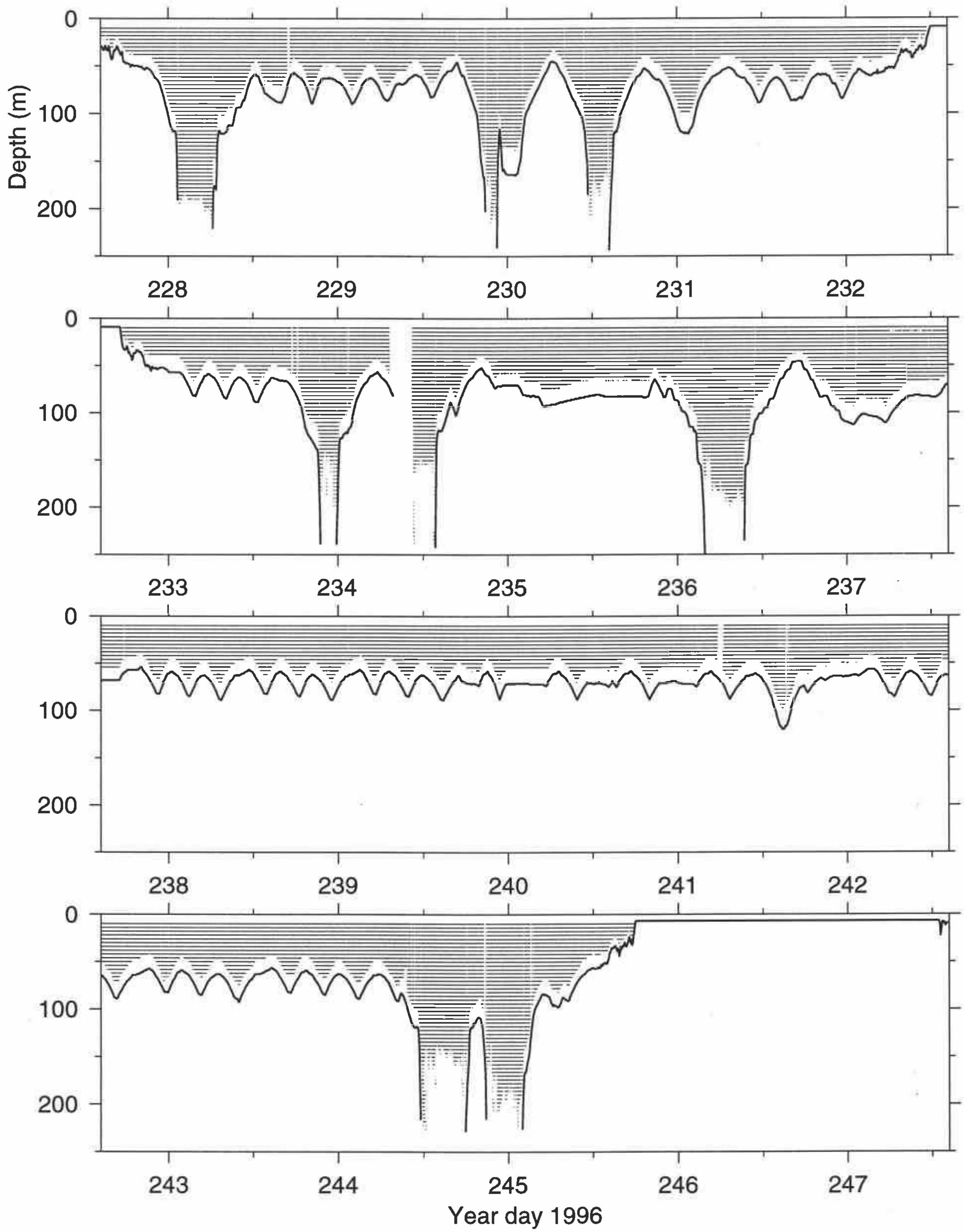

Fig. 6a. ADCP ensembles remaining after editing, for E9608. Bottom depth is also shown.

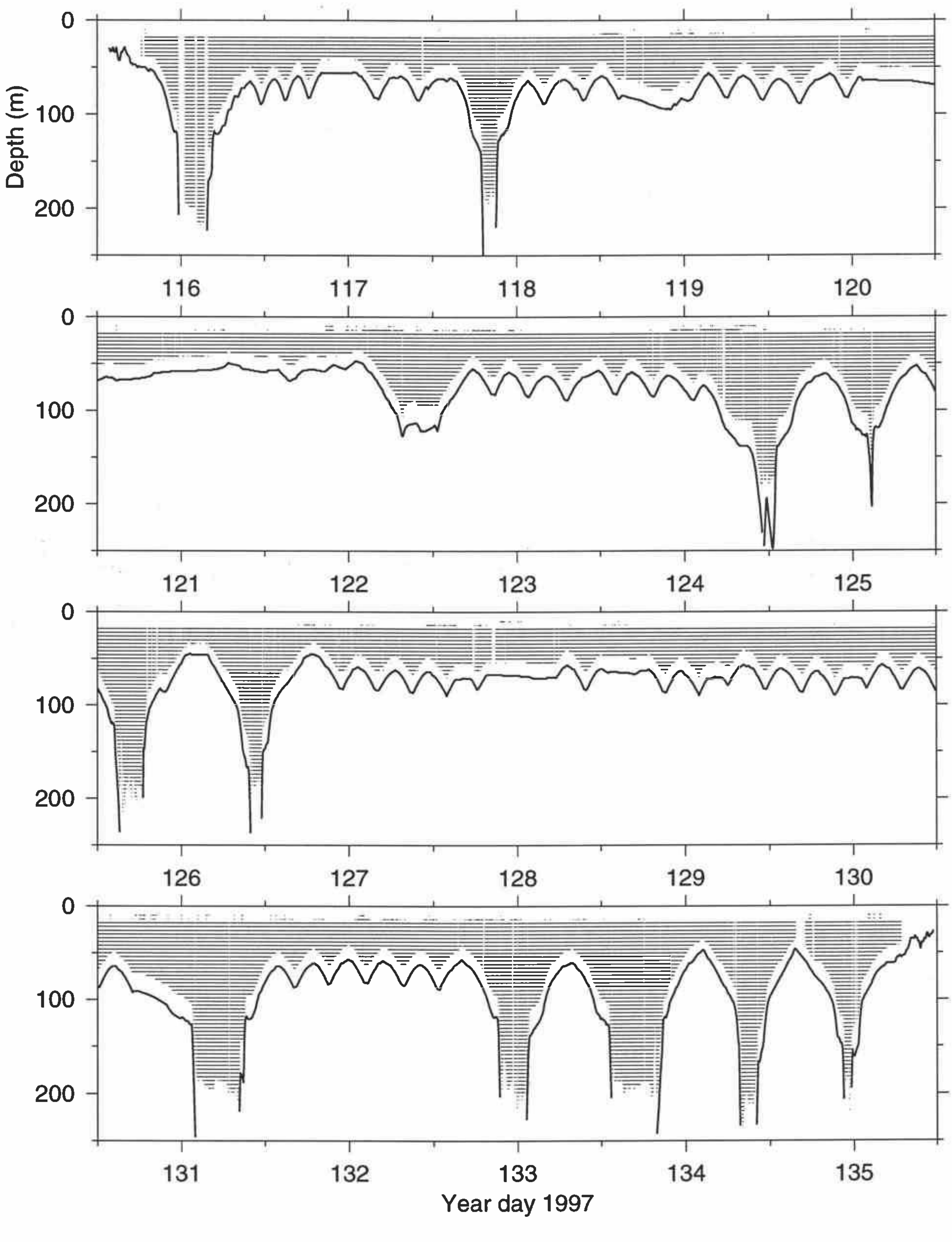

Fig. 6b. ADCP ensembles remaining after editing, for E9704. Bottom depth is also shown.

enough to depend upon completely, in combination with the gyrocompass they are very useful. Initially each ADCP profile uses the gyrocompass heading, as input directly into the DAS PC during data collection. Ultimately, we correct the data set by applying a set of rotation angles, one for each ensemble, based on the difference *dh* between the attitude GPS and gyro headings.

The 1 Hz *dh* (GPS - gyro) data were edited to remove occasional noisy values in the following manner, as suggested by Firing *et al.* (1995): if a *dh* exceeded a running mean of 20 samples by more than 1°, it was rejected. The *dh* as well as the GPS pitch and roll data were then averaged into 2.5 min blocks, to match the ADCP ensemble times. Prior to using these 2.5 min average heading corrections, they were subject to the following additional tests: the *dh* can not exceed 3°, the pitch can not exceed 5°, the roll can not exceed 7°, and each 2.5 min mean must have been formed from at least 10 raw 1 Hz data points. Gaps in the *dh* were filled using linear interpolation. The resulting series of heading corrections for the two cruises are shown in Figures 7a and 7b, with interpolated values plotted as plus symbols. The *dh* swings are probably associated with the numerous north-south ship accelerations experienced during these surveys, but in a complex way. Note that the *dh* corrections only affect the final data set when bottom-tracking is not available. During these cruises, we had good bottom-tracking 92% of the time (indicated by the gray lines of Figure 7).

Sensitivity and Alignment

We use the bottom-track method to determine and correct for the sensitivity error β and the ADCP/gyro misalignment angle α, following Joyce (1989). We assume that the bottom track velocity for each ensemble should be equal and opposite to the ship velocity from navigation. The degree to which this is not true provides values for α and β.

Following some of the recommendations of Trump and Marmorino (1997), for calibration purposes we reject cases where either the ship speed was below 1 m/s or the ship was turning significantly (if the 2.5 min mean ship heading and the momentary heading differed by more than 2°). We also apply a simple median rejection criterion to exclude outliers among the raw α and β estimates. For E9608, we find $\beta = 0.982\pm0.001$ and $\alpha = -1.9\pm0.1°$. For E9704, we find $\beta = 0.985\pm0.001$ and $\alpha = -1.8\pm0.1°$. The actual rotation of the ADCP database velocities is complicated by the heading offset corrections. The CODAS program *rotate* is used to incorporate both the *dh* corrections for each profile and the cruise-long α and β. The α values actually used for the *rotate* runs were -2.2° for E9608 and -2.7° for E9704, since we must correct for both the regular α (ADCP/gyro misalignment) and the cruise-long gyro/GPS misalignments (0.3° and 0.9° for E9608 and E9704 respectively). As a check on the processing steps, the entire calibration procedure was repeated without using the attitude GPS data, and identical results were obtained for the ADCP/gyro calibration parameters.

At worst (at highest ship speed of 5.5 m/s), the β uncertainty implies an unknown bias of 0.5 cm/s in velocity measurement, while the α uncertainty implies an unknown bias of 0.9 cm/s.

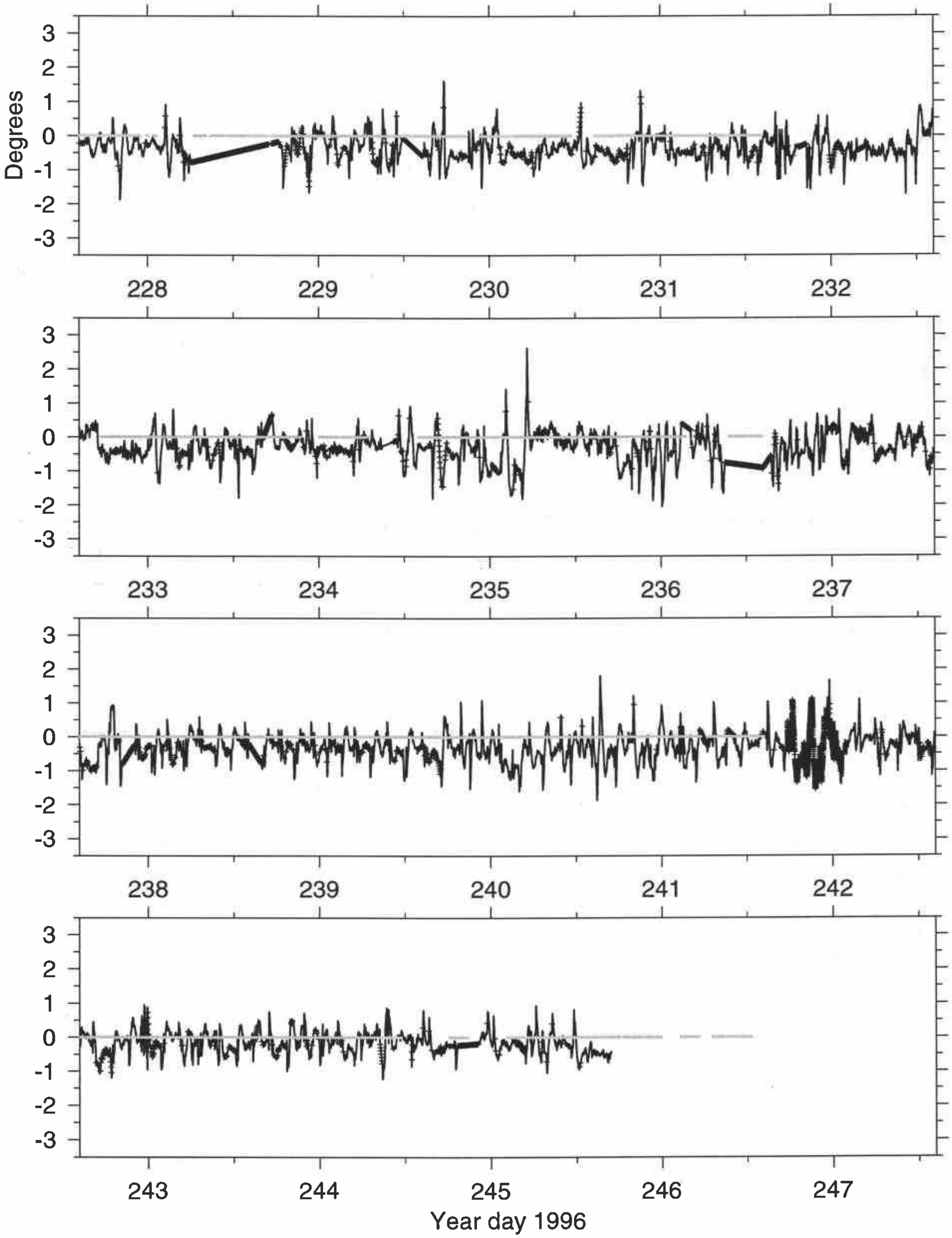

Fig. 7a. Attitude GPS - gyro heading *dh*, for E9608. Interpolated values are plotted as plus symbols (+). Periods of good bottom-tracking are indicated by the gray line.

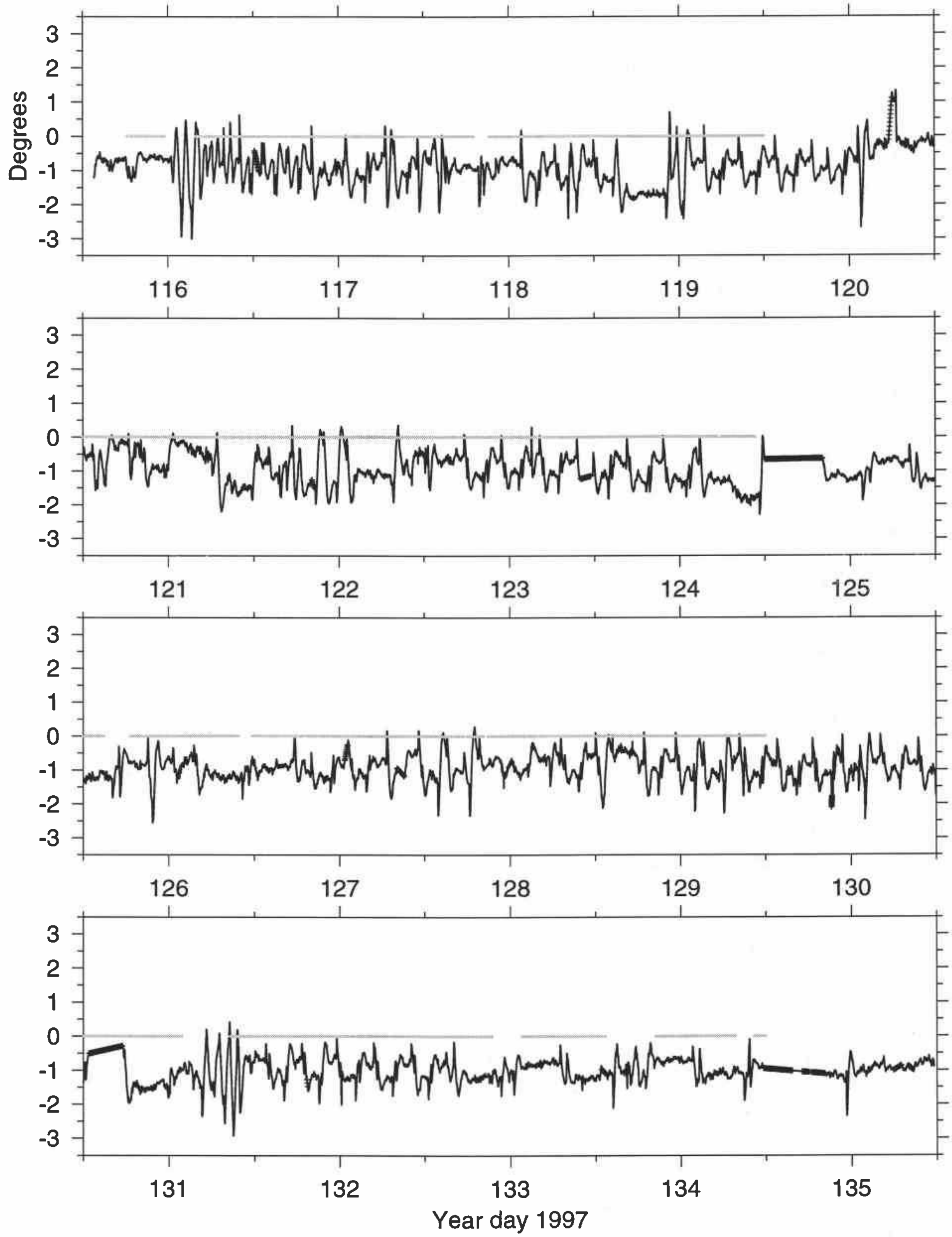

Fig. 7b. Attitude GPS - gyro heading *dh*, for E9704. Interpolated values are plotted as plus symbols (+). Periods of good bottom-tracking are indicated by the gray line.

NAVIGATION

To reference the ADCP velocities to absolute (earth) coordinates, ship velocity is determined by bottom-tracking where possible; elsewhere it must be determined from navigation. In the latter case, the uncertainty in ship velocity is the largest source of ADCP error.

Using a 16–32 m reference layer, we transfer the problem of smoothing ship velocity into the problem of smoothing reference layer velocity. We combine the smoothed ship velocity data and measured ADCP layer velocities relative to the ship to calculate absolute motion of the reference layer (Kosro, 1985; Wilson and Leetmaa, 1988; Firing *et al.*, 1995). The advantage of this step is that our noisy signal is now relatively stationary; conventional linear filtering techniques are now appropriate, and we low-pass filter in a robust manner in the time domain with a Blackman window: $w(t) = 0.42 - 0.5\cos(2\pi t/T) + 0.08\cos(4\pi t/T)$, using a filter width T of 20 min. The resulting smoothed velocities are also integrated back to obtain a new consistent and smooth set of ship positions. This step uses the *smoothr* routine in the CODAS package. After this, the shear profile for each ensemble is added to the reference layer to determine absolute velocities at all depths.

SYNOPSIS OF UNCERTAINTIES

The inherent short-term random uncertainty in an ADCP velocity for a 2.5 min ensemble and 4 m bin is 1.2 cm/s (RDI, 1989) This form of error is reduced with further averaging. For the typical case of 5 min data, the short-term random uncertainty is reduced to 0.9 cm/s.

If bottom-tracking is available, the absolute ADCP velocity may have an unknown bias of 1 cm/s (due to inherent limitations of the bottom-track method, RDI (1989)). If bottom-tracking is not available, the absolute ADCP velocity may have an unknown bias of 1.4 cm/s (combination of sensitivity and alignment errors). In addition, the absolute velocity has a random error due to navigational uncertainty of ±3 cm/s and is low-pass filtered to suppress motions with time scales of less than 20 min (for features present throughout the 16–32 m reference layer).

DETERMINATION OF SUBTIDAL FLOW

Introduction

In this region of the Mid-Atlantic Bight, we expect observed velocities to be significantly affected by tides (Moody *et al.*, 1984). In order to unmask the subtidal flow field, which may be of particular interest, we estimate and then remove barotropic tidal currents from the data sets. We estimate tidal currents in the region using an empirical model fit to both the present ADCP shipboard data sets and a few selected current meter records. A least-squares harmonic method is applied, where the tidal parameters are fit in time and also allowed to vary spatially through polynomial surface trend interpolation. The method is similar to the one applied to a different data set in Chapter 2 of Pierce (1998), and it is a variation on the one introduced by Candela *et al.* (1992).

Data

For the tidal estimation, we use the velocity data sets (depth-averaged):

Name	Type	Location(s)	Time Period	Data source
E9608	Shipboard ADCP	70.03-71.42W, 39.69-41.54N	14-Aug-96 to 1-Sep-96	authors
E9704	Shipboard ADCP	69.90-70.87W, 39.81-40.90N	25-Apr-97 to 15-May-97	authors
OSU Main	Mooring	70.51W, 40.49N	10-Jul-96 to 26-Sep-96	M. Levine/T. Boyd*
Primer	Mooring	70.10W, 40.14N	5-Dec-96 to 15-Feb-97	R. Pickart
Primer	Mooring	71.17W, 40.13N	25-Jul-96 to 4-Aug-96	R. Beardsley

*Boyd *et al.* (1997)

The moored records provide relatively accurate tidal information at three locations (Figure 8). The shipboard ADCP provides less information in a temporal sense, but provides important spatial information to the tidal solution.

Method

A least-squares harmonic method was first used in a tidal estimation problem by Horn (1960), using a room-sized computer. By now such methods applied to stationary current meter data are routine. The method represents the tide in the form:

$$u(t) = u_0 + \sum_{i=1}^{N}[b_i \cos(\omega_i t) + c_i \sin(\omega_i t)] , \tag{1}$$

where ω_i is the frequency of the i_{th} tidal constituent. Observed currents are then regressed onto (1) using least-squares methods to find the coefficients b_i and c_i which minimize the residuals. The other component, $v(t)$, is treated similarly. We use the five primary tidal constituents [$N = 5$ in (1)]: M_2, S_2, K_1, O_1, and N_2. From the Moody *et al.* (1984) analysis of tidal records in the region, these five constituents account for 93% of the total tidal variance.

Candela *et al.* (1992) recognized the inherent flexibility of least-squares methods when they suggested that b_i, c_i in (1) need not be constants. Tidal spatial variability can be modeled by allowing b_i, c_i to be spatially-varying functions, whose unknown coefficients are determined by regression onto the observations, as before. The specific form of the functions might reflect some dynamical knowledge of how the tidal currents vary in space, or they might be sets of arbitrary functions which will hopefully do well at fitting themselves to the spatial structure at hand. Candela *et al.* (1992) successfully use a combination of these two approaches, since they make use of arbitrary polynomials and splines but they also normalize by $1/H$, where $H(x, y)$ is a local bottom depth. This normalization is appropriate in the shallow East China Sea and Amazon Basin (they also estimate the subtidal mean flow, by simultaneous least-squares fitting to spatial functions with no time dependence; we fit only to the tidal flow).

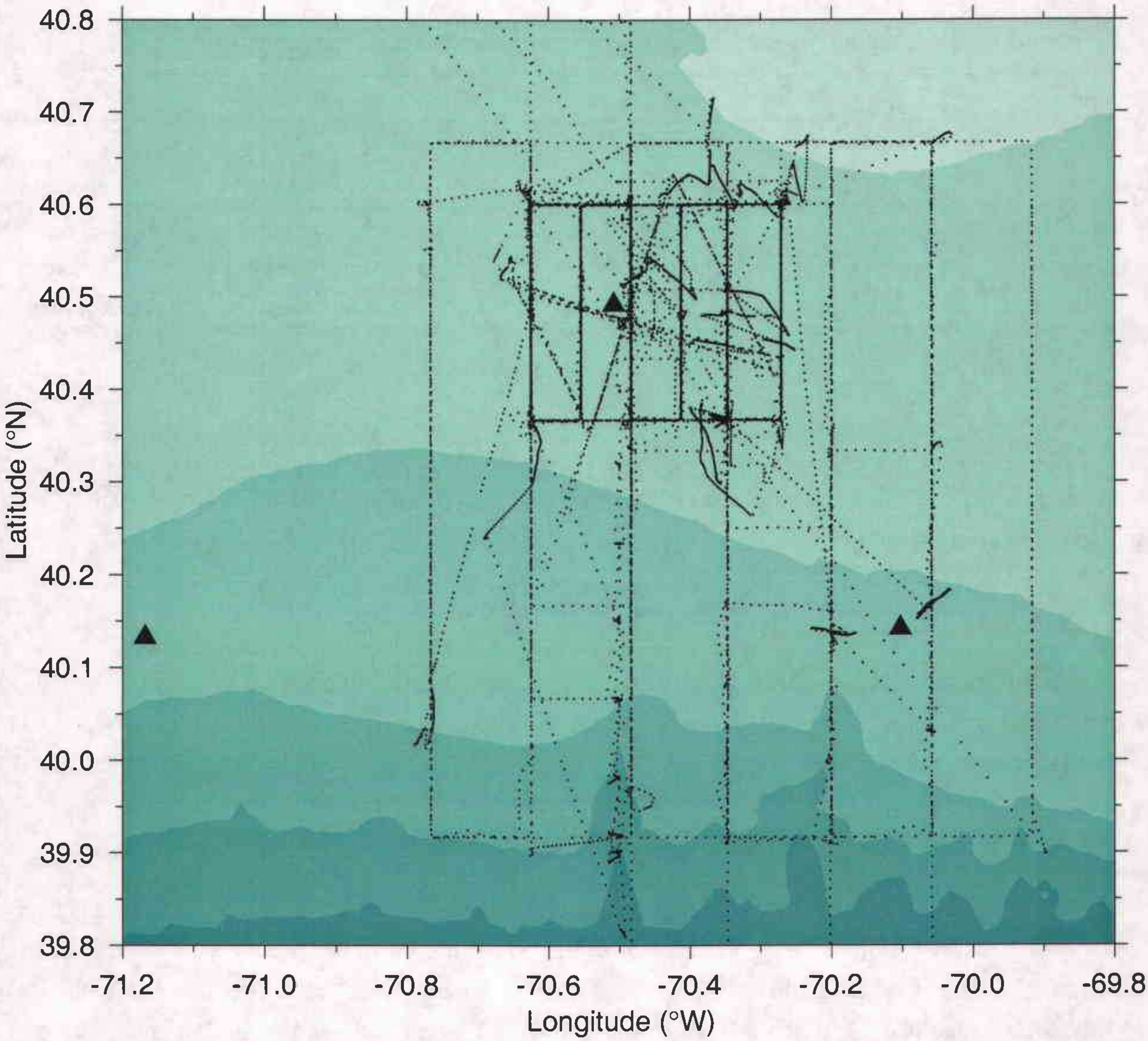

Fig. 8. Data sets used in the tidal estimation: shipboard ADCP (small dots) and moorings (filled triangles). The blue shading denotes the 50, 100, 200, 500, and 1000 m isobaths.

As in Pierce (1998), we take a similar approach but normalize u and v by x_c/H, where x_c is the x-distance from the observation to the coast and the y-axis points towards 270°T, approximately alongshore. The Battisti and Clarke (1982) model solutions for u and v contain these terms as well, a first-order approximation for the way a tidal Kelvin wave is modified by depth changes.

The surface-fitting polynomials take the form:

$$m_1 + m_2x + m_3y + m_4xy + m_5x^2 + m_6y^2 + \ldots \quad (2)$$

We expand b_i, c_i in these and then solve (1) for each velocity component u and v. Tidal ellipse parameters are then calculated from u, v using standard methods, e.g. Rosenfeld (1987). The number of terms of (2) which can be included and successfully determined will in general vary depending on the structure and quality of the data. We use the diagnostics provided by the singular value decomposition (SVD) to help determine how many unknown terms we are able to solve for (e.g. Press *et al.*, 1992). In our case, we use the first four terms (bilinear) of the sequence (2) for $M2$ and $K1$ and only the first term (constant) for the other constituents. Some experimentation with adding higher degree terms led to non-physical solutions which were also difficult for the solution machinery to produce (solution was rank-deficient).

Different from Candela *et al.* (1992), we estimate uncertainties for each of our data sources prior to the least-squares calculation. These uncertainties are used to weight the different data sets appropriately and they help determine resulting model uncertainties. For a 5-min shipboard ADCP depth-averaged velocity, we assume *apriori* uncertainties of ±1 cm/s when bottom-tracking is available and ±3 cm/s when it is not. For hourly depth-averaged current meter data we use ±1 cm/s.

Results

As expected, the $M2$ (12.42 hour) tidal component is the dominant one; 72% of the total tidal variance is contained here. The size of the $M2$ varies strongly across the region, with semi-major axes of 30 cm/s at the northeast corner of our survey region but decreasing to 2 cm/s in the southwest corner (Figure 9a). The rapid increase in tidal currents towards the northeast is consistent with previous observations; tidal currents continue to increase to the east of our region, reaching a maximum of about 100 cm/s in the vicinity of Georges Bank (Moody *et al.*, 1984). The ellipses are relatively circular in our region, indicated by the similarity in size of the semi-major and semi-minor axes (Figure 9a). The standard errors from the least-squares calculation for the semi-major/minor axes vary from 1–3 cm/s.

The $K1$ (23.93 hour) component, with 16% of the tidal variance, has semi-major axes which vary from 14 cm/s at the northeast corner to 2 cm/s at the southwest (Figure 10a). The eccentricity is more pronounced than in the $M2$ case, particularly in the northeast corner.

When tidal ellipses are relatively circular, determining orientation and other angular information is more difficult. We only present angular results where standard errors are less than 20° (Figures 9b and 10b). $M2$ orientation does not vary too much, while the $K1$ has an increasingly alongshore orientation moving onto the shelf.

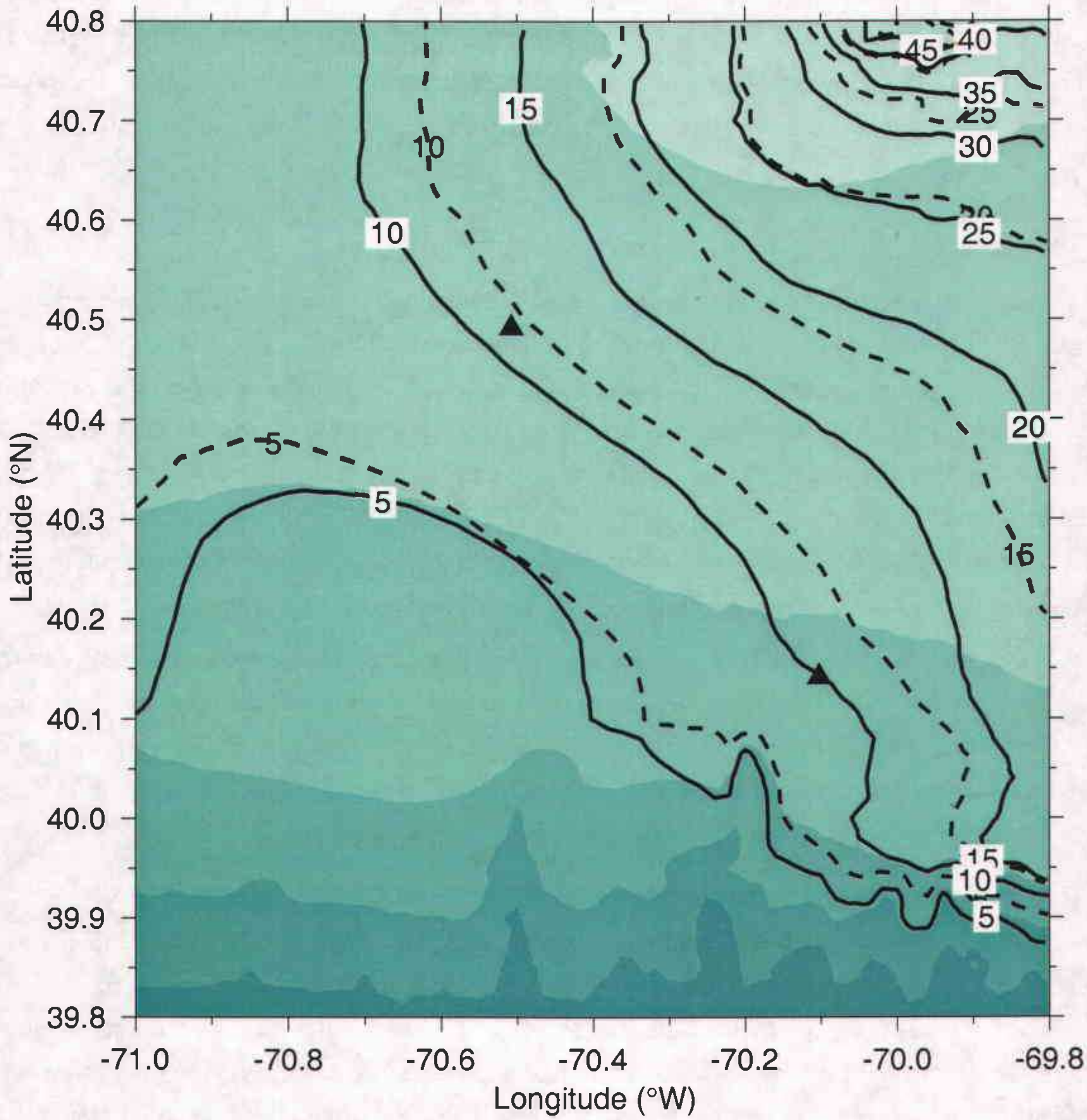

Fig. 9a. *M*2 tidal ellipse semi-major (solid) and semi-minor axes (dashed), cm/s.

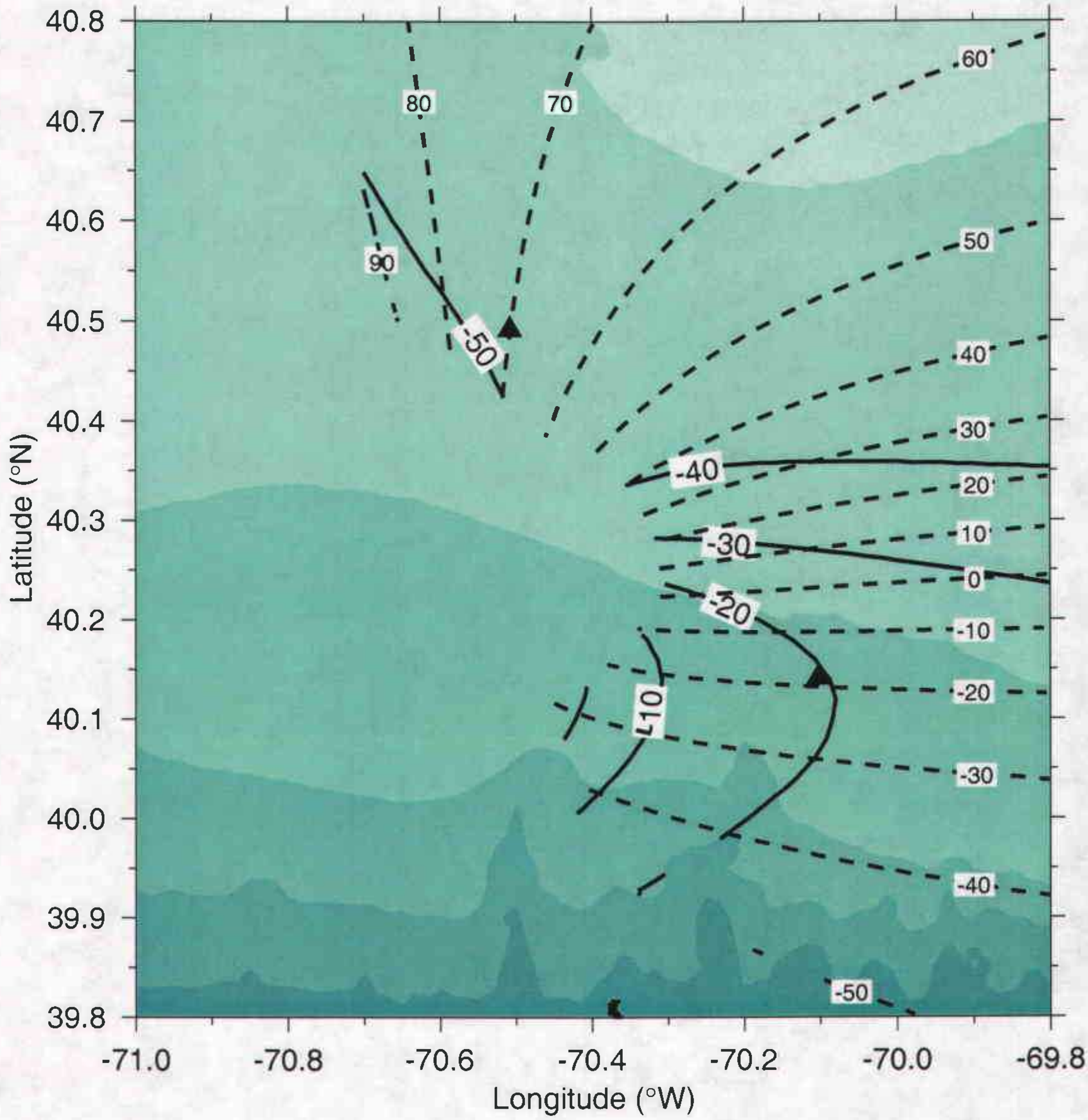

Fig. 9b. $M2$ tidal ellipse orientation (solid) and relative phase (dashed), °CW from alongshore. The rotation of the tidal ellipse is CW. Contours are only shown where the standard error is less than 20°.

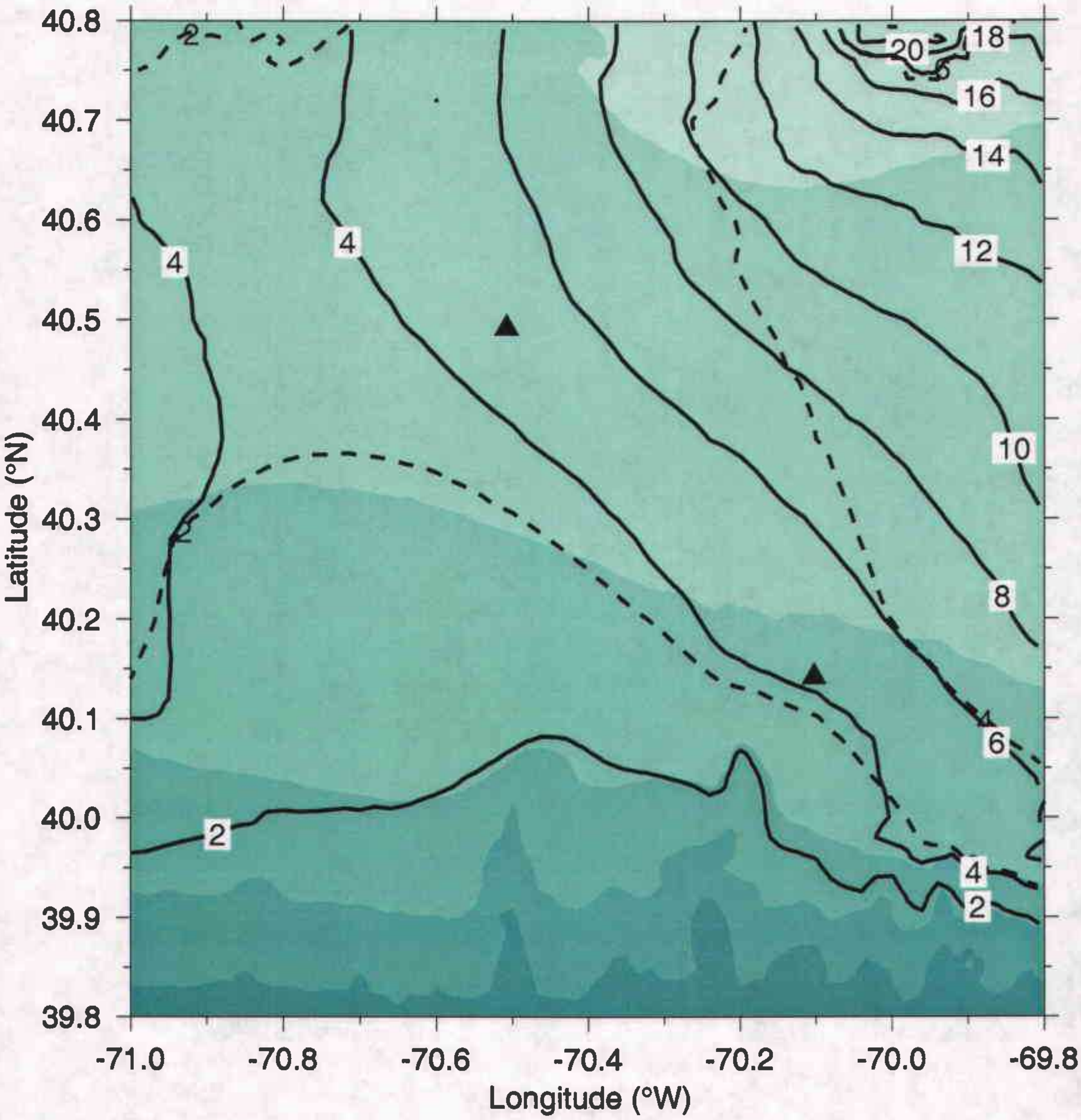

Fig. 10a. *K*1 tidal ellipse semi-major (solid) and semi-minor axes (dashed), cm/s.

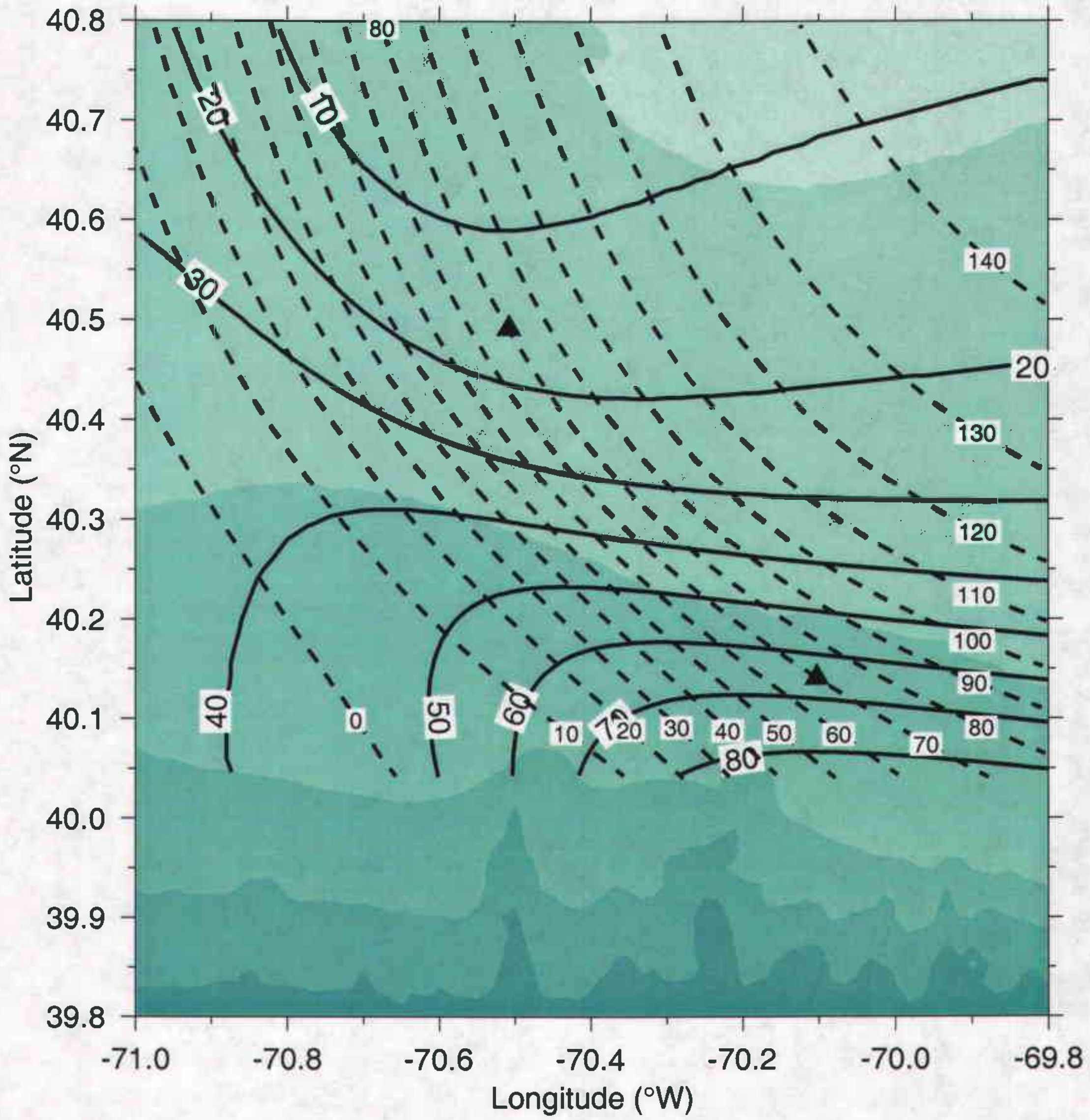

Fig. 10b. $K1$ tidal ellipse orientation (solid) and relative phase (dashed), °CW from alongshore. The rotation of the tidal ellipse is CW. Contours are only shown where the standard error is less than 20°.

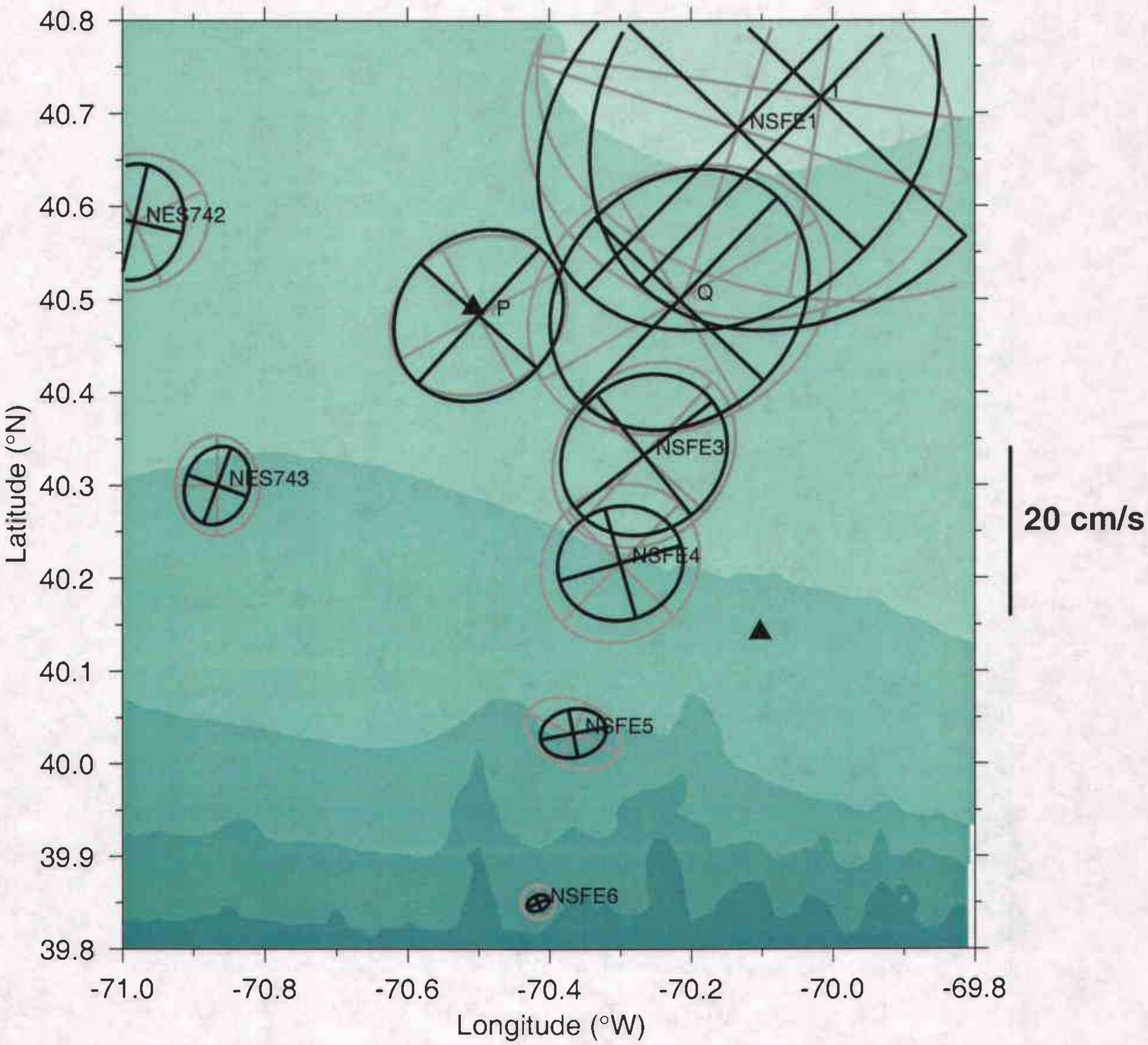

Fig. 11. *M*2 tidal ellipse sizes and orientations from the Moody *et al.* (1984) atlas (grayshade) and the present study (solid).

Results for the other three tidal constituents are much smaller, as expected for this region (these constituents were assumed to be spatially constant by the model):

Name	Period (hours)	% tidal variance	Semi-major(minor) axes (cm/s)	Orientation (°CW from alongshore)	Phase (°CW)
N2	12.66	7	3.2(3.0)	-18	13
O1	25.82	4	2.8(1.8)	40	48
S2	12.00	1	1.6(0.9)	51	16

All of our tidal results are generally consistent with the available tidal analyses of historical current meter records as compiled in the Moody *et al.* (1984) atlas. Among the comparisons shown in Figure 11, the *M*2 semi-major results have a 2 cm/s rms difference from Moody *et al.* (1984) results. This level of uncertainty is consistent with the error level predicted by the least-squares machinery (1–3 cm/s), which is a good check that our model and assumptions are reasonable.

DATA PRESENTATION

Maps

Maps of ADCP vectors at approximately 10 m increments are presented for E9608 (pp. 31-75) and E9704 (pp. 131-165). The 4-m depth bins selected are the closest available ones to the depths of the SeaSoar property maps (5, 15, 25, ... dbar) in O'Malley *et al.* (1998). Each vector is a 2 km horizontal spatial average of either the observed (grayshade) or subtidal (solid) velocity. Each map is labeled at the top with a survey name and time period (UTC). The blue shading denotes the 50, 100, 200, 500, and 1000 m isobaths.

Sections

Vertical sections of east and north subtidal velocity are shown for E9608 (pp. 77-116) and E9704 (pp. 167-215). For contouring, we use a Barnes objective analysis scheme with 3 iterations (Daley, 1991). The horizontal (vertical) grid spacings are 2 km (4 m), and the successive smoothing length scales are 5 km (10 m), 3.2 km (6.3 m), and 2 km (4 m). Velocity contour units are cm/s, and positive regions are shaded. Each page includes the time period (UTC) and a small map showing the location of the section.

Soliton sections

During E9608 on 28 August 1996, approximately 24 hours was devoted to special SeaSoar/ADCP sampling aimed at capturing internal solitary wave packets (solitons) as they propagated through the region. During this period, the ADCP ensemble averaging time was set to just 10 s, yielding high spatial resolution horizontally (60 m) but with larger inherent short-term uncertainty (±6 cm/s). Sections of observed velocities during this special period appear on pp. 117-129.

The data described here are publicly available from either the online version of this report (*http://diana.oce.orst.edu/cmoweb/adcp/*) or from the National Oceanographic Data Center Joint Archive for Shipboard ADCP (JASADCP). The JASADCP is accessible through the web at *http://ilikai.soest.hawaii.edu/sadcp/*.

ACKNOWLEDGMENTS

We thank the crew of the R/V *Endeavor* for superb work under difficult conditions, in a region with considerable ship traffic and fishing activity. We thank Marc Willis and the URI Marine Technicians for assistance with the adaptation and installation of the 307-kHz transducer borrowed from the R/V *Wecoma*. This work was supported by the Office of Naval Research Grant N00014-95-1-0382.

REFERENCES

Barth, J. A. and D. J. Bogucki, 1999: Spectral light absorption and attenuation measurements from a towed undulating vehicle. *Deep-Sea Res.*. [submitted.]

Barth, J. A., D. J. Bogucki, A. Y. Erofeev, and J. Simeon, 1999: SeaSoar spectral light absorption and attenuation observations during the Coastal Mixing and Optics experiment: R/V Endeavor cruises from 14-Aug to 1-Sep 1996 and 25-Apr to 15-May 1997, Data Rep., Coll. of Oceanic and Atm. Sci., Oregon State Univ. in preparation

Battisti, D. S. and A. J. Clarke, 1982: A simple method for estimating barotropic tidal currents on continental margins with specific application to the M2 tide off the Atlantic and Pacific coasts of the United States. *J. Phys. Oceanogr.*, **12**, 8-16.

Bowditch, N., 1977: *American Practical Navigator,* Defense Mapping Agency Hydrographic Center.

Boyd, T., M. D. Levine, and S. R. Gard, 1997: Mooring observations from the Mid-Atlantic Bight, July-September 1996, Data Rep. 164, Ref. 97-2, Coll. of Oceanic and Atm. Sci., Oregon State Univ.

Candela, J., R. C. Beardsley, and R. Limeburner, 1992: Separation of tidal and subtidal currents in ship-mounted acoustic doppler current profiler observations. *J. Geophys. Res.*, **97**, 769-788.

Daley, R., 1991: *Atmospheric data analysis,* Cambridge University Press.

Erofeev, A. Y., T. M. Dillon, J. A. Barth, and G. H. May, 1998: MicroSoar microstructure observations during the Coastal Mixing and Optics experiment: R/V Endeavor cruise from 25-Apr to 15-May 1997, Data Rep. 170, Ref. 98-3, Coll. of Oceanic and Atm. Sci., Oregon State Univ. Also available on-line at http://diana.oce.orst.edu/cmoweb/micro/main.html

Firing, E., J. Ranada, and P. Caldwell, 1995: *Processing ADCP data with the CODAS software system version 3.1, user's manual,* University of Hawaii. Manual and software available electronically at ftp://noio.soest.hawaii.edu/pub/codas3

Horn, W., 1960: Some recent approaches to tidal problems. *Int. Hydrogr. Rev.*, **38**, 28-105.

Joyce, T. M., 1989: On in situ "calibration" of shipboard ADCPs. *J. Atmos. Oceanic Technol.*, **6**, 169-172.

Kelley, D., 1995: *Gri - a program to make science graphs, user's manual,* Dalhousie University. Available on-line at http://phys.ocean.dal.ca/~kelley/gri/gri1.html

King, B. A. and E. B. Cooper, 1993: Comparison of ship's heading determined from an array of GPS antennae with heading from conventional gyrocompass measurements. *Deep-Sea Res.*, **40**, 2207-2216.

Kosro, P. M., 1985: Shipboard acoustic current profiling during the Coastal Ocean Dynamics Experiment., UCSD Ph.D. thesis, SIO Ref. No. 85-8, University of California, La Jolla, Ca..

Moody, J. A., B. Butman, R. C. Beardsley, W. S. Brown, P. Daifuku, J. D. Irish, D. A. Mayer, H. O. Mofjeld, B. Petrie, S. Ramp, P. Smith, and W. R. Wright, 1984: American continental shelf, Bulletin 1611, U.S. Geological Survey.

O'Malley, R., J. A. Barth, A. Y. Erofeev, J. Fleischbein, P. M. Kosro, and S. D. Pierce, 1998: SeaSoar CTD observations during the Coastal Mixing and Optics experiment: R/V Endeavor cruises from 14-Aug to 1-Sep 1996 and 25-Apr to 15-May 1997, Data Rep. 168, Ref. 98-1, Coll. of Oceanic and Atm. Sci., Oregon State Univ. Also available on-line at http://diana.oce.orst.edu/cmoweb/csr/main.html

Pierce, S. D., 1998: Equatorward jets and poleward undercurrents along the eastern boundary of the mid-latitude North Pacific, COAS Ph.D. thesis, Oregon State University, Corvallis, OR.

Press, W. H., S. A. Teukolsky, W. T. Vetterling, and B. P. Flannery, 1992: *Numerical Recipes, 2nd edition,* Cambridge University Press.

RDI, 1989: *Acoustic Doppler current profilers principles of operation: a practical primer,* RD Instruments, San Diego, Ca..

Rosenfeld, L. K., 1987: Tidal Band Current Variability Over the Northern California Continental Shelf. *WHOI Tech. Report*, **87-11**.

Trump, C. L. and G. O. Marmorino, 1997: Calibrating a gyrocompass using ADCP and DGPS data. *J. Atmos. Oceanic Technol.*, **14**, 211-214.

Wilson, D. and A. Leetmaa, 1988: Acoustic doppler current profiling in the equatorial Pacific in 1984. *J. Geophys. Res.*, **93**, 13947-13966.

E9608 observed and subtidal velocity vectors at standard depths

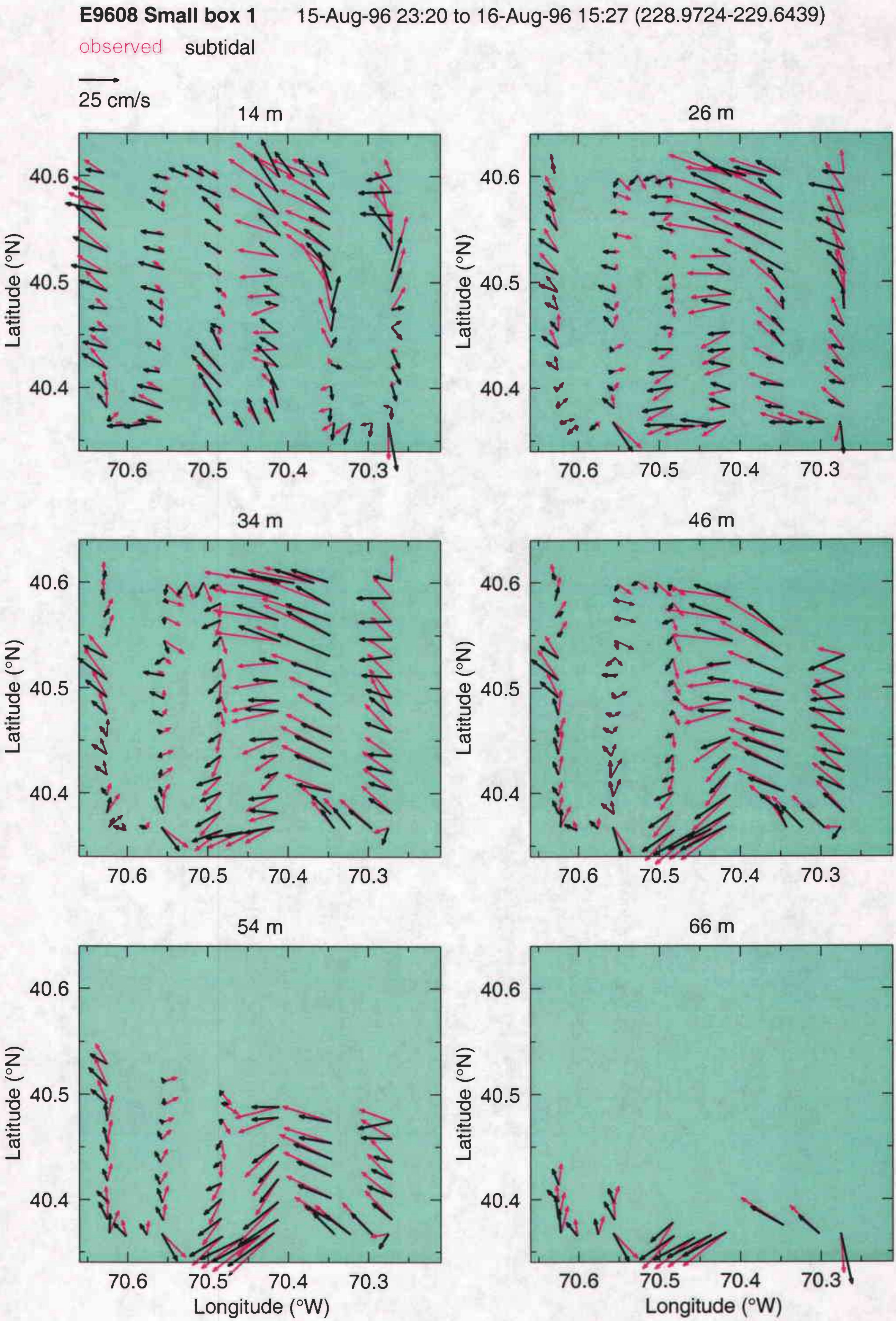
E9608 Small box 1
15-Aug-96 23:20 to 16-Aug-96 15:27 (228.9724-229.6439)
observed
subtidal
25 cm/s
14 m
26 m
34 m
46 m
54 m
66 m
40.6
40.5
40.4
Latitude (°N)
70.6
70.5
70.4
70.3
Longitude (°W)

E9608 Big box 1

14 m ADCP, 17-Aug-96 01:59 to 18-Aug-96 09:07 (230.0833-231.3804)

observed

subtidal

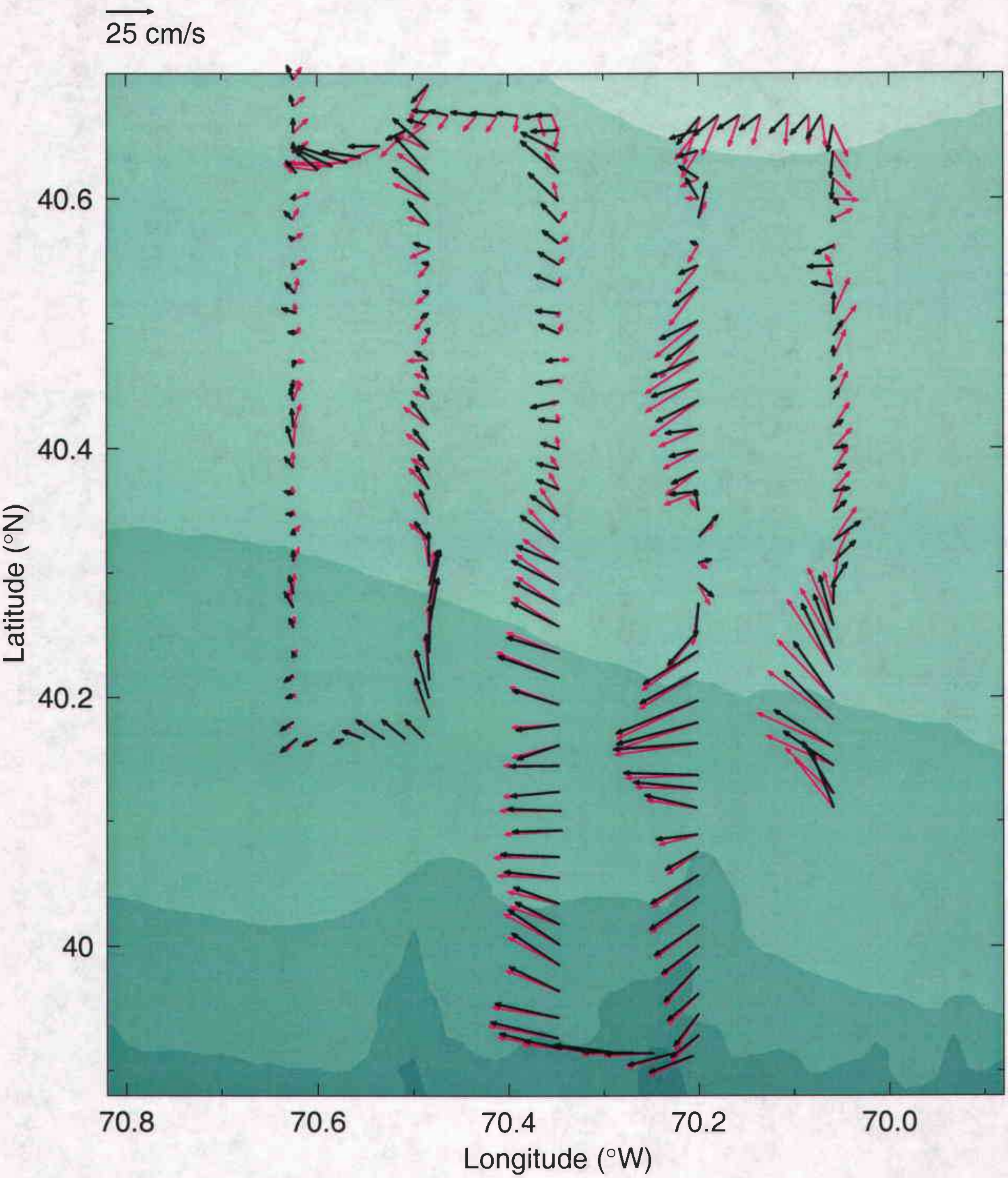

E9608 Big box 1

26 m ADCP, 17-Aug-96 01:59 to 18-Aug-96 09:07 (230.0833-231.3804)

observed

subtidal

25 cm/s

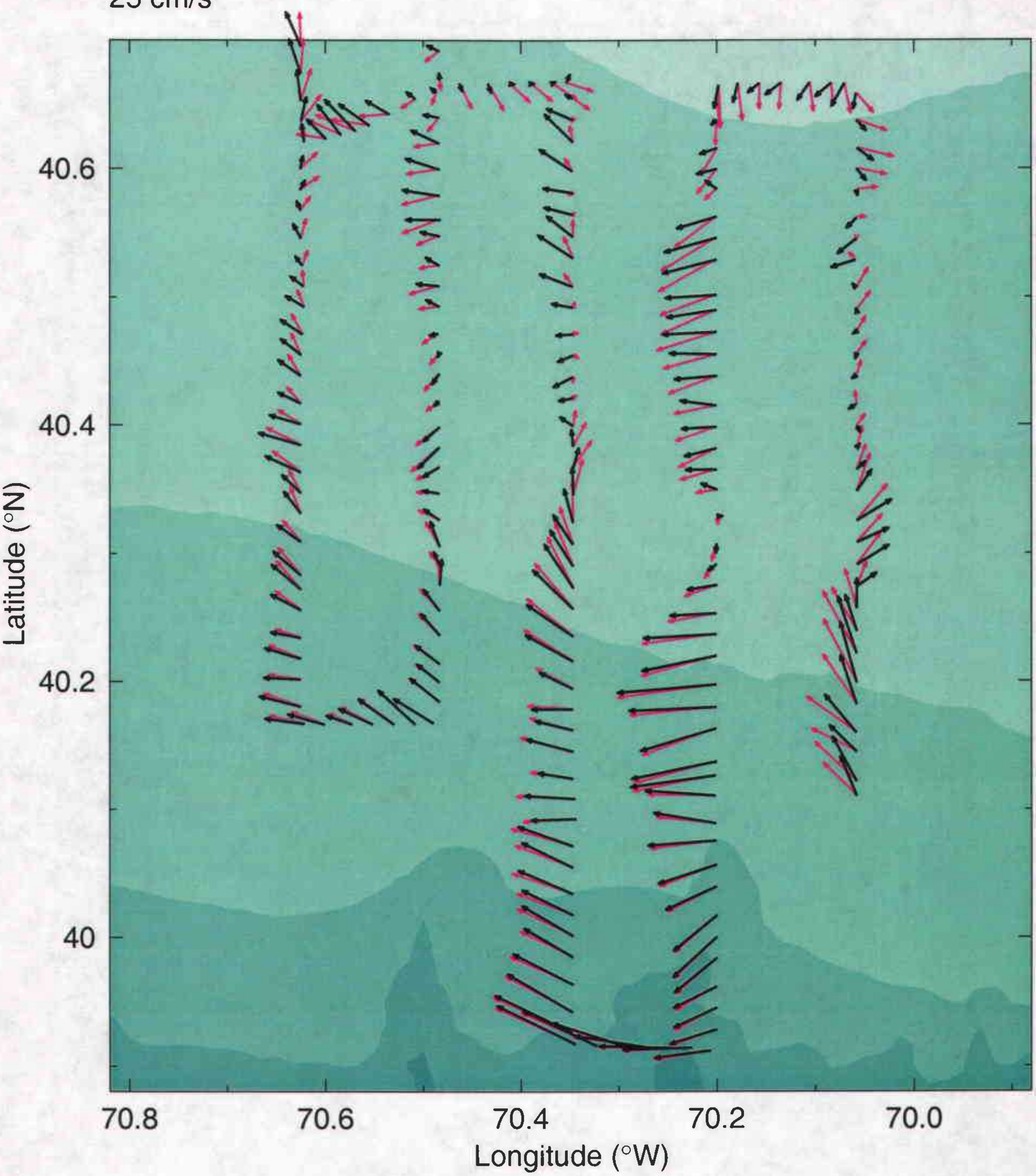

E9608 Big box 1

34 m ADCP, 17-Aug-96 01:59 to 18-Aug-96 09:07 (230.0833-231.3804)

observed

subtidal

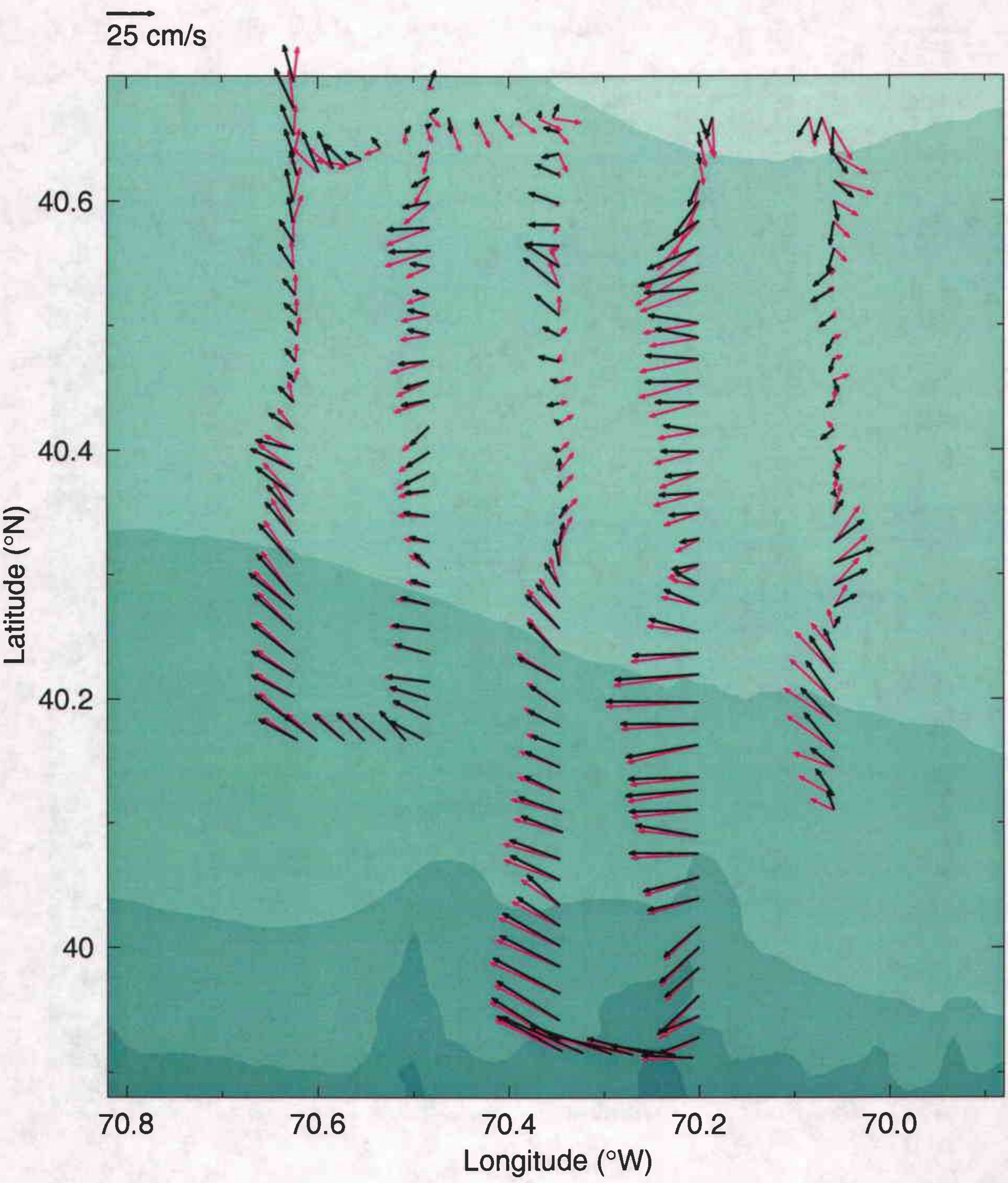

E9608 Big box 1

46 m ADCP, 17-Aug-96 01:59 to 18-Aug-96 09:07 (230.0833-231.3804)

observed

subtidal

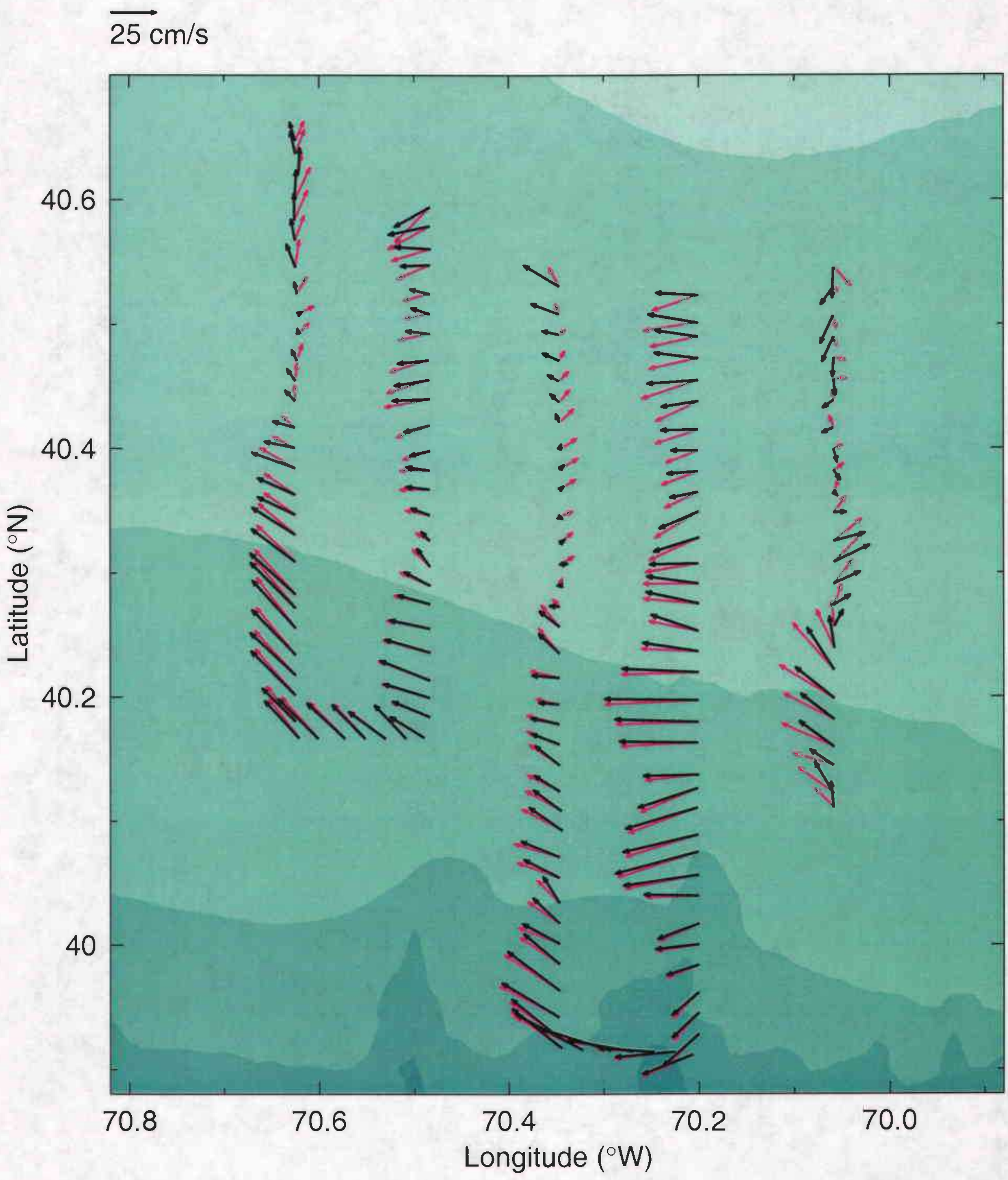

E9608 Big box 1

54 m ADCP, 17-Aug-96 01:59 to 18-Aug-96 09:07 (230.0833-231.3804)

observed

subtidal

25 cm/s

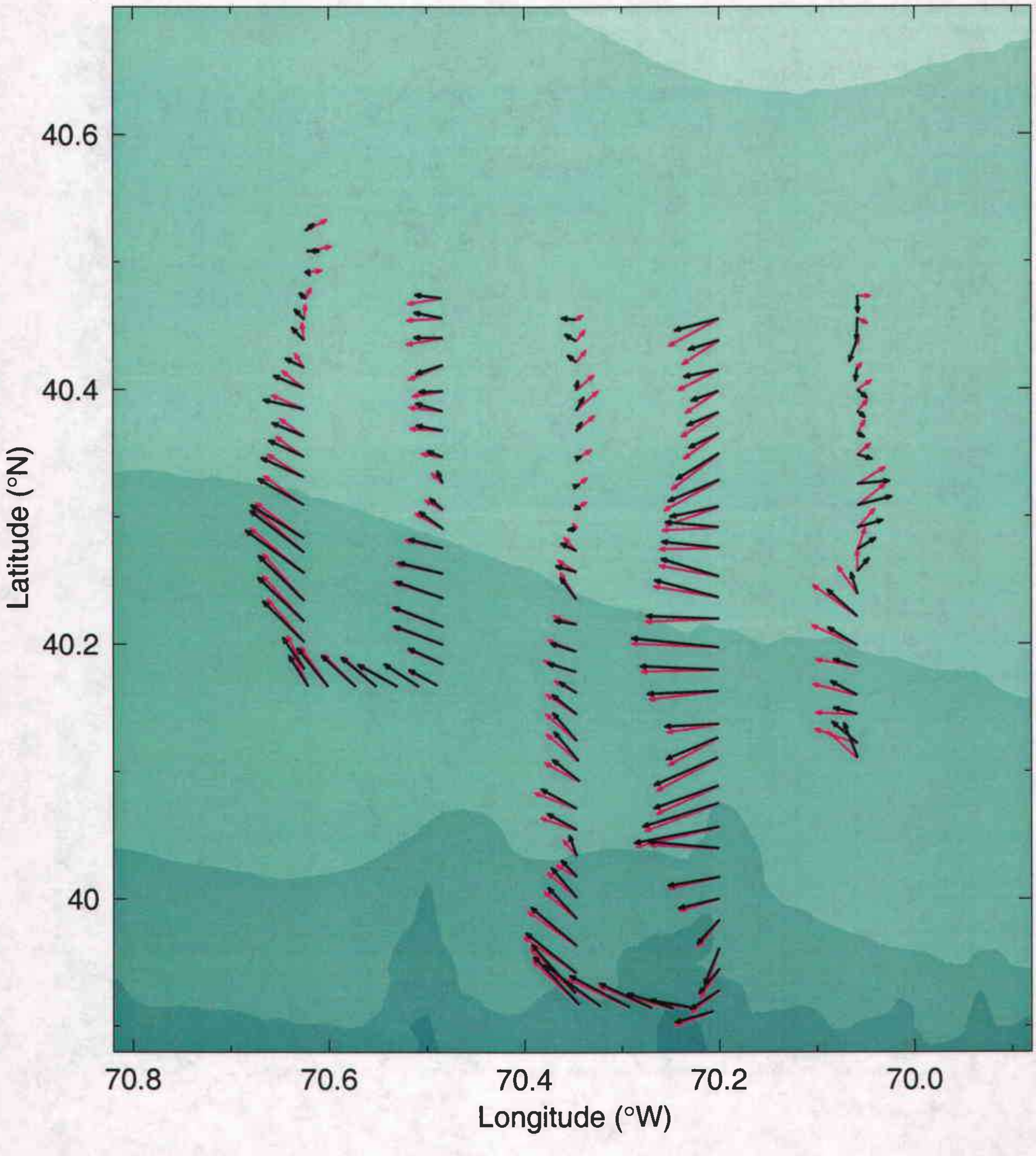

E9608 Big box 1

66 m ADCP, 17-Aug-96 01:59 to 18-Aug-96 09:07 (230.0833-231.3804)

observed

subtidal

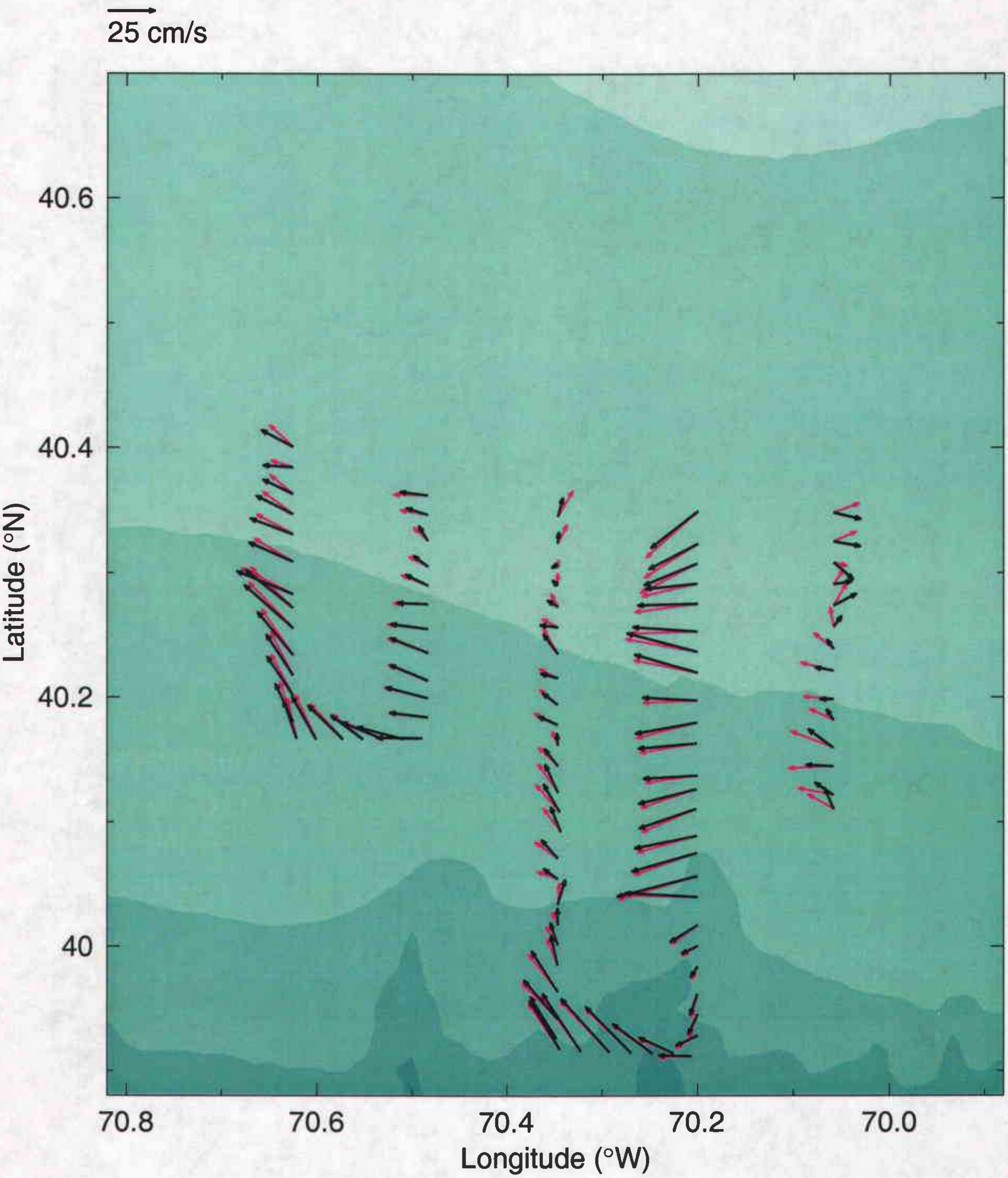

E9608 Big box 1

74 m ADCP, 17-Aug-96 01:59 to 18-Aug-96 09:07 (230.0833-231.3804)

observed

subtidal

25 cm/s

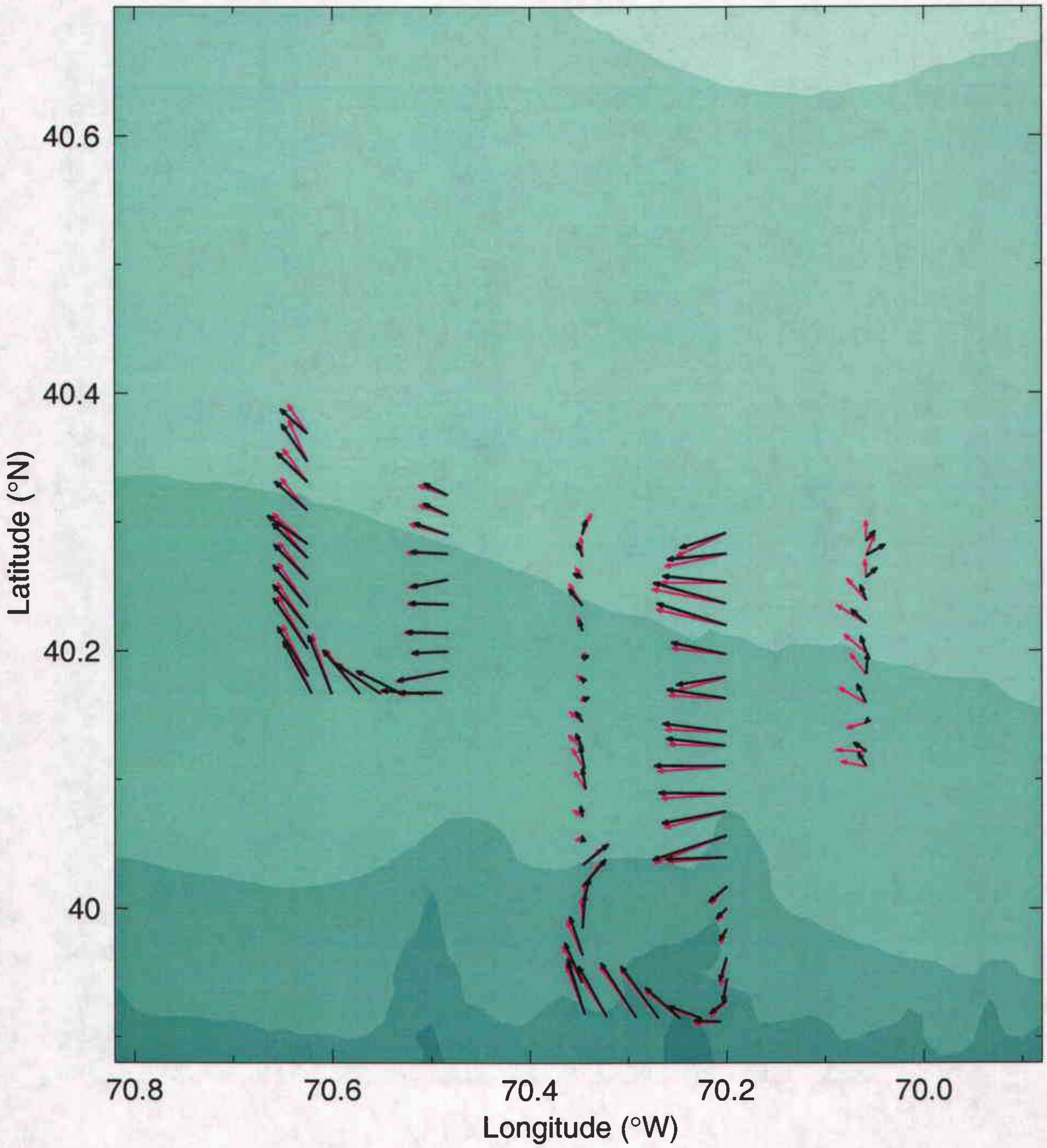

E9608 Big box 1

86 m ADCP, 17-Aug-96 01:59 to 18-Aug-96 09:07 (230.0833-231.3804)

observed

subtidal

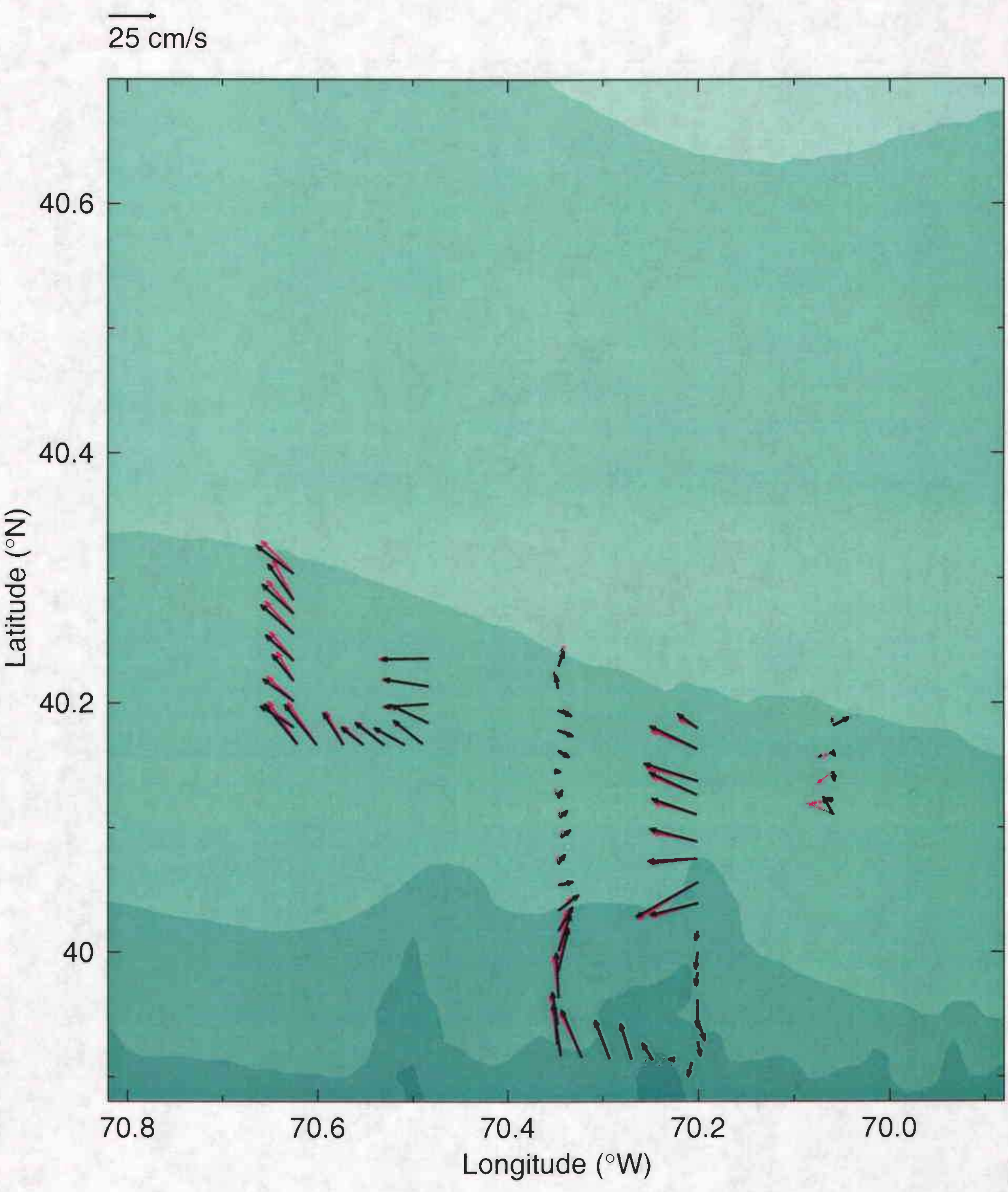

E9608 Big box 1

94 m ADCP, 17-Aug-96 01:59 to 18-Aug-96 09:07 (230.0833-231.3804)

observed

subtidal

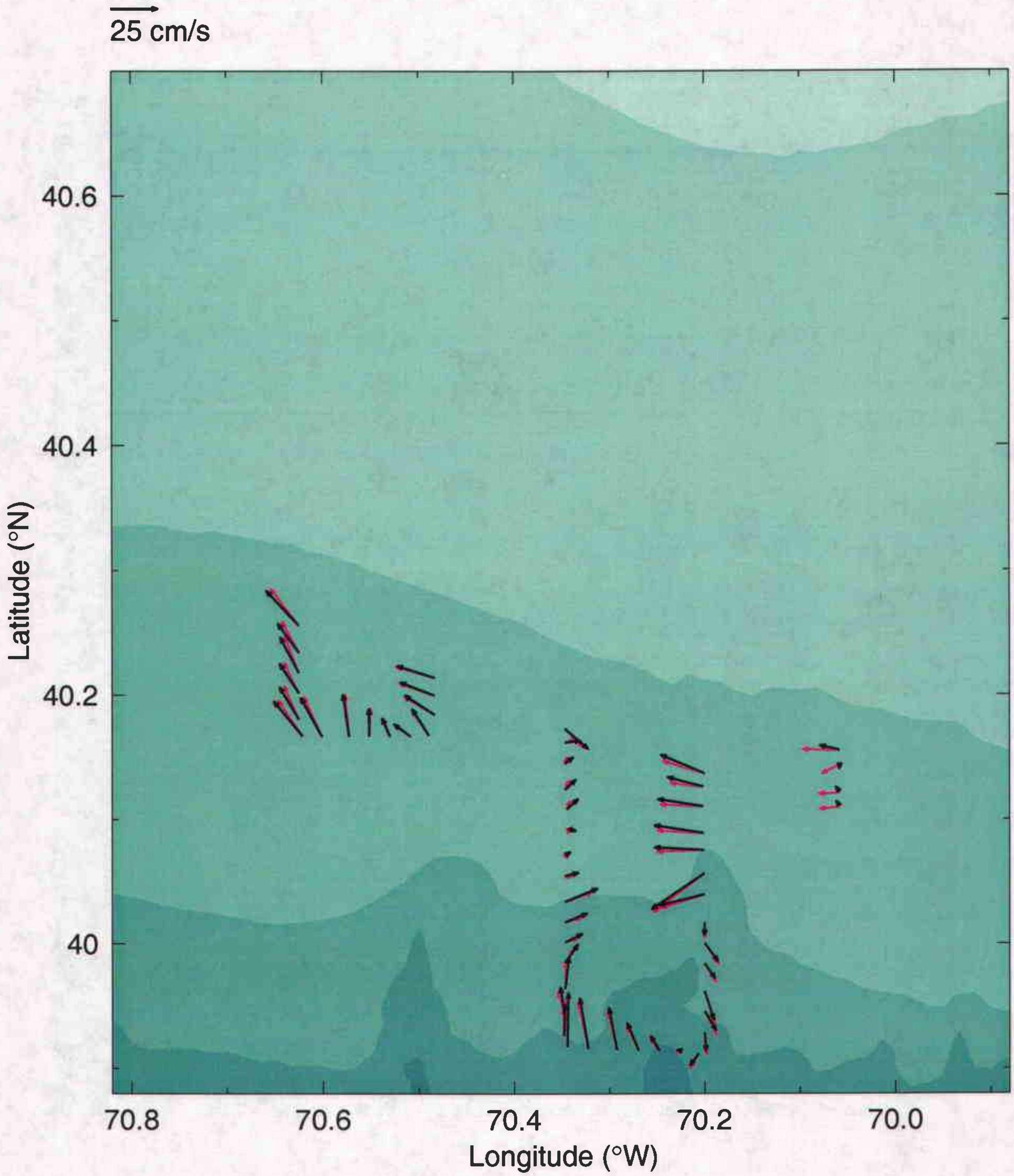

E9608 Big box 1

106 m ADCP, 17-Aug-96 01:59 to 18-Aug-96 09:07 (230.0833-231.3804)

observed

subtidal

25 cm/s

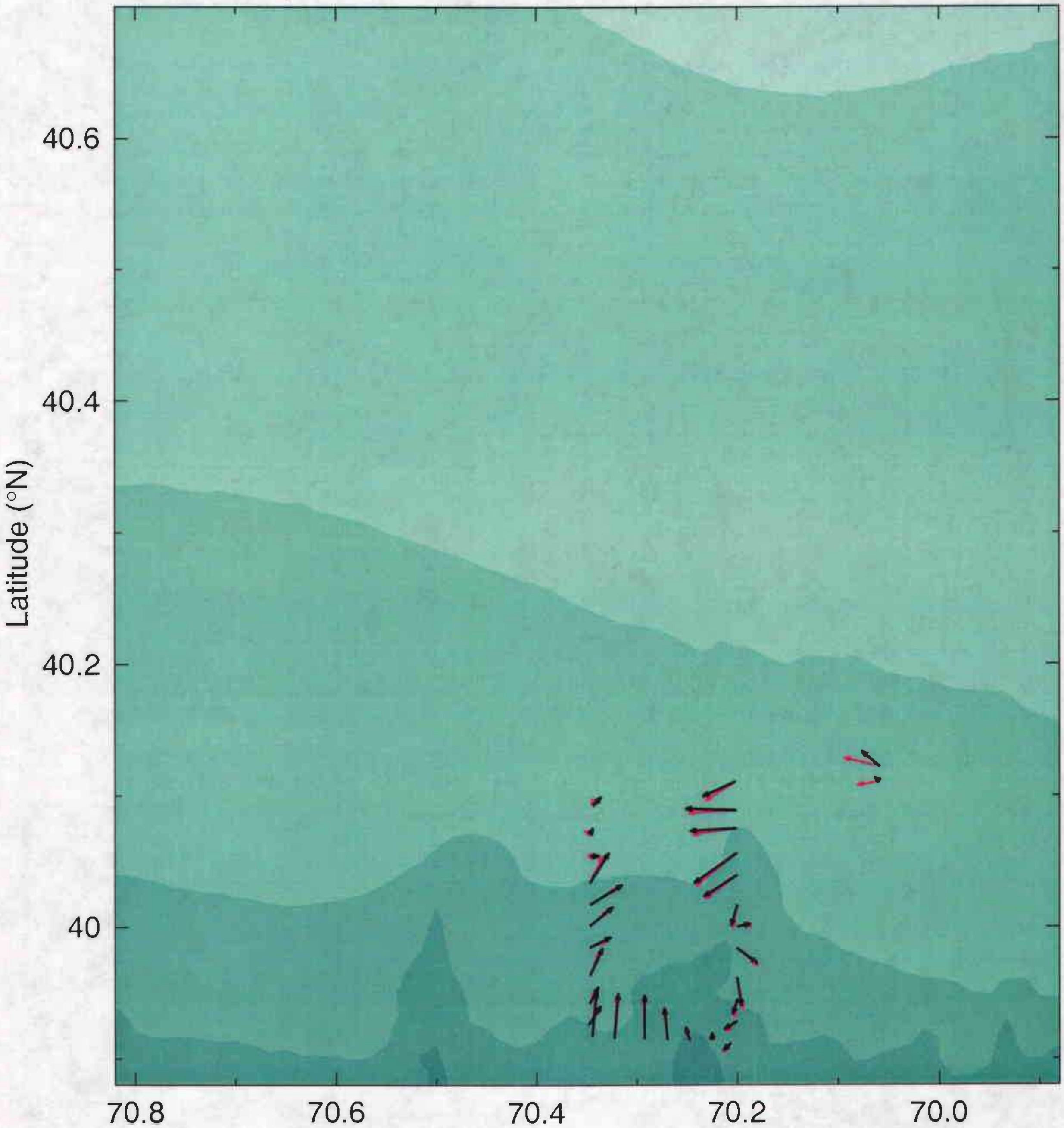

E9608 Small box 2 18-Aug-96 09:35 to 19-Aug-96 03:08 (231.3995-232.1310)

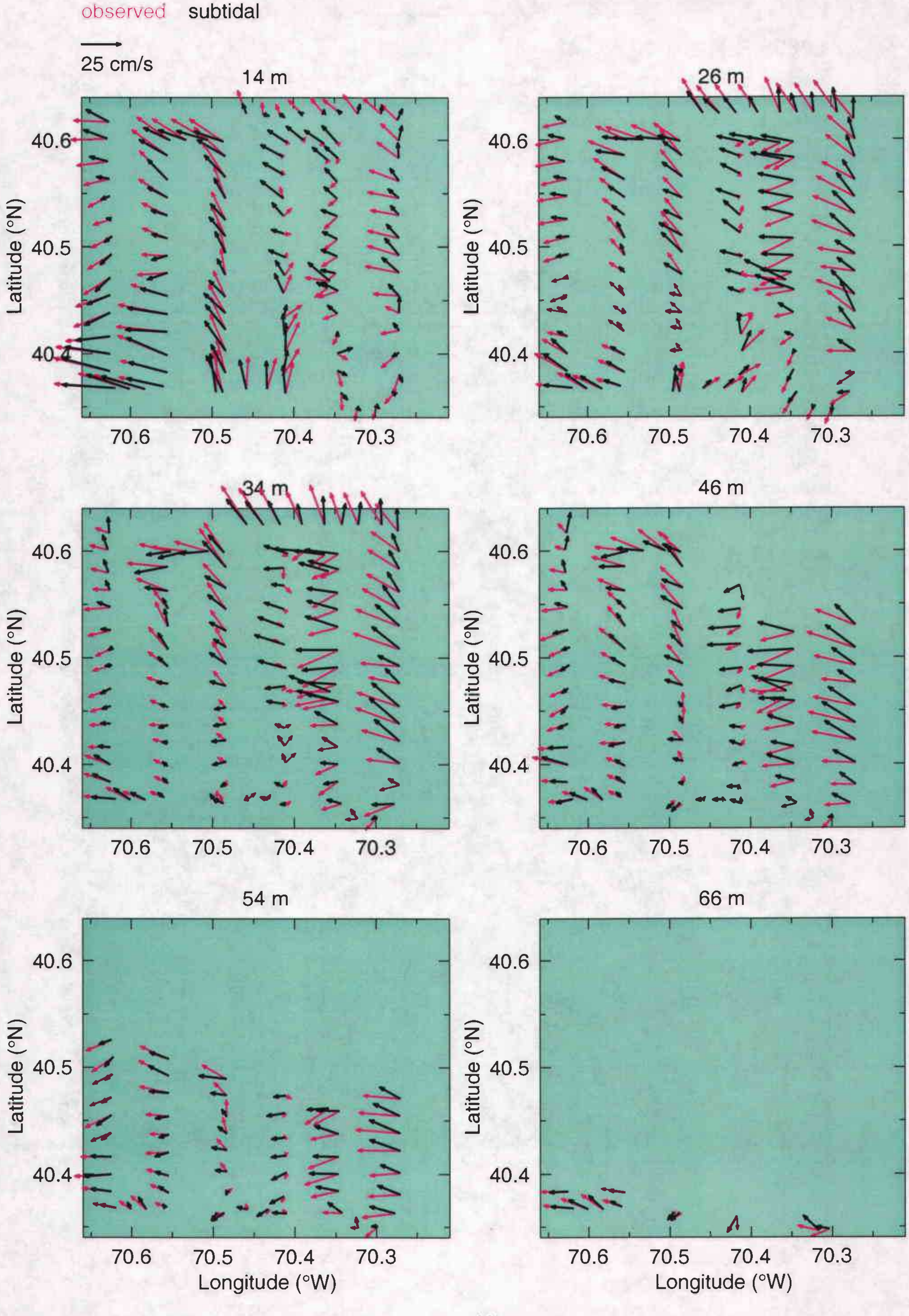

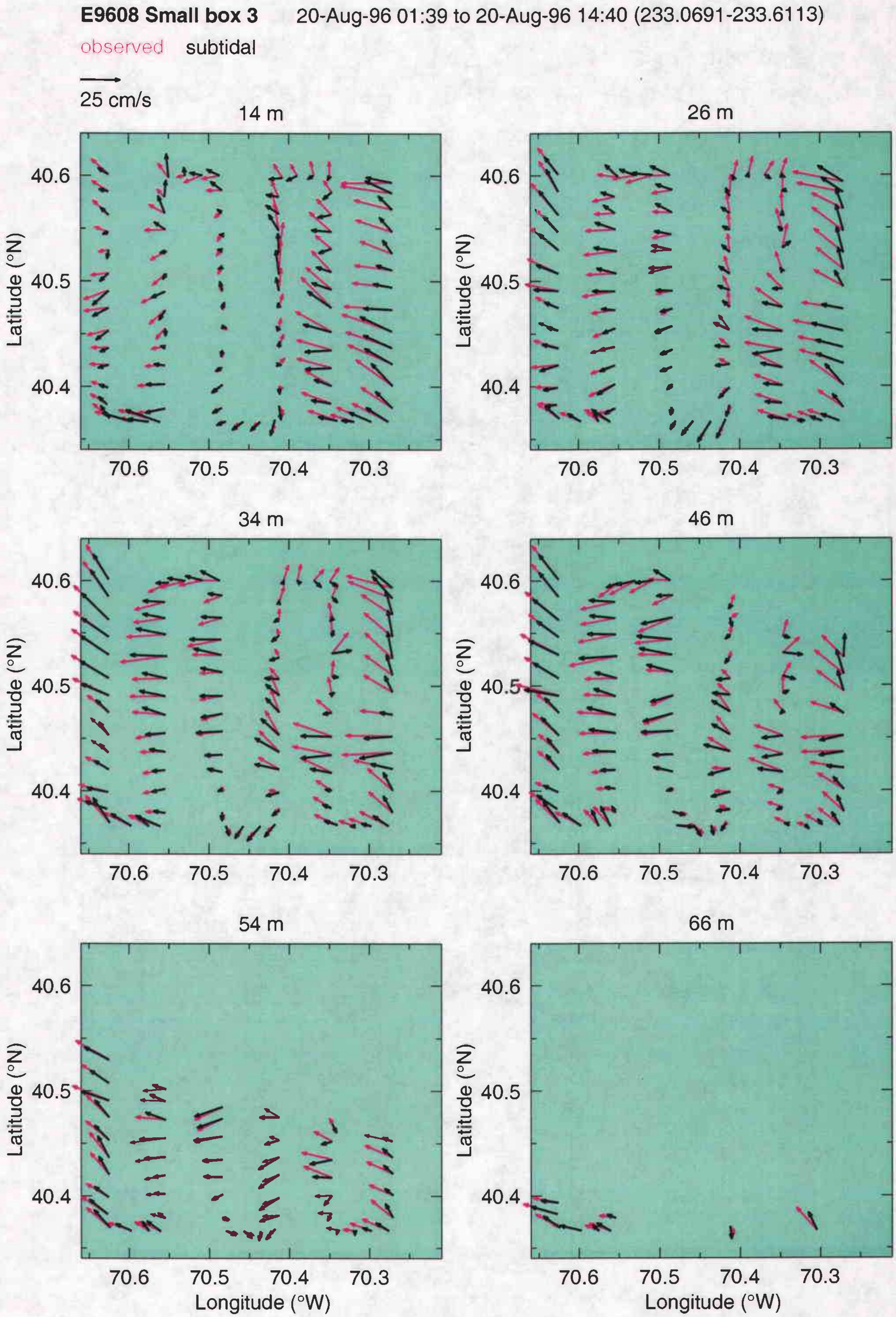
E9608 Small box 3
20-Aug-96 01:39 to 20-Aug-96 14:40 (233.0691-233.6113)
observed
subtidal
25 cm/s
14 m
26 m
34 m
46 m
54 m
66 m
Latitude (°N)
40.6
40.5
40.4
70.6
70.5
70.4
70.3
Longitude (°W)

E9608 Big box 2

14 m ADCP, 20-Aug-96 17:03 to 21-Aug-96 21:58 (233.7107-234.9158)

observed

subtidal

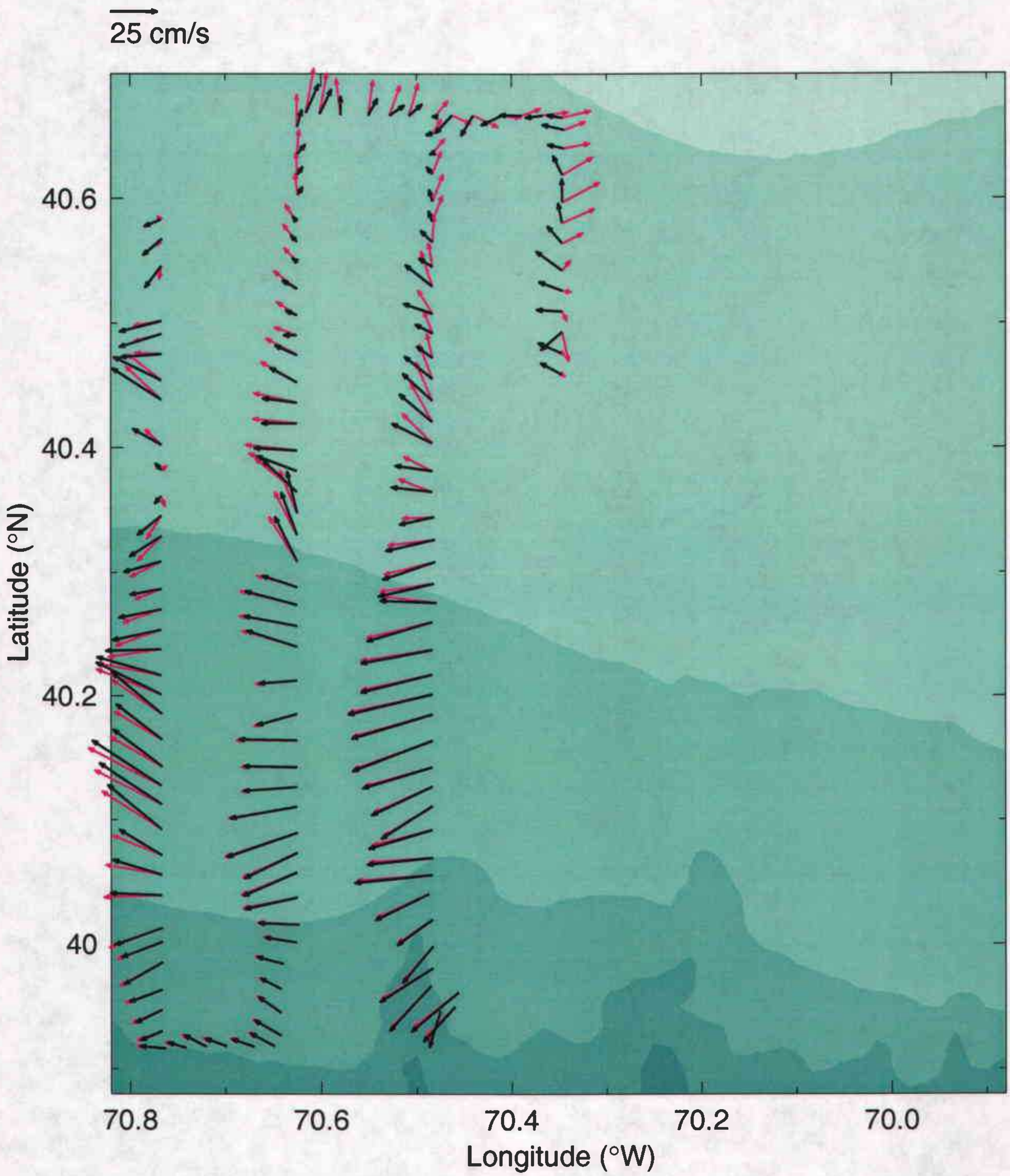

E9608 Big box 2

26 m ADCP, 20-Aug-96 17:03 to 21-Aug-96 21:58 (233.7107-234.9158)

observed

subtidal

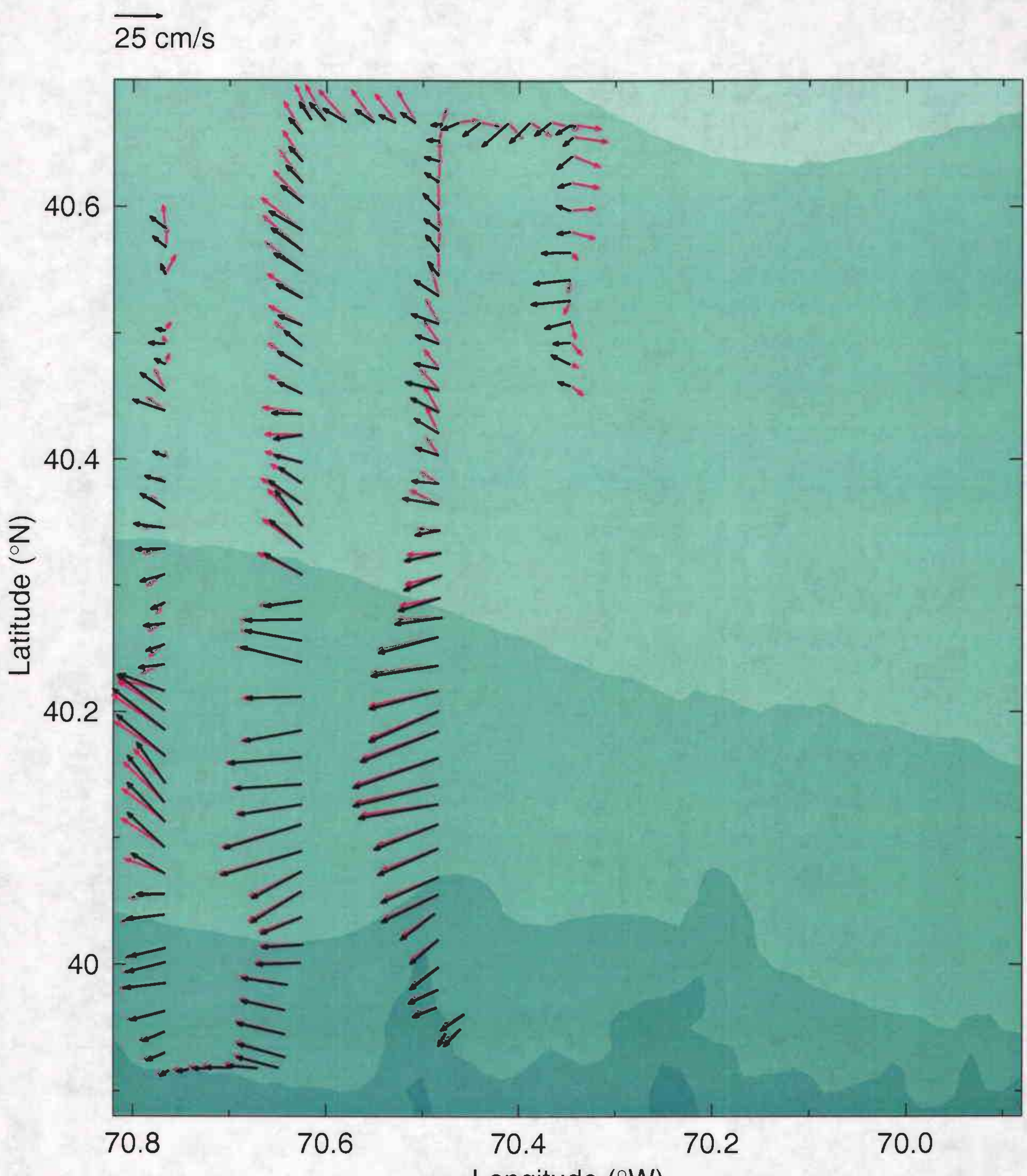

E9608 Big box 2

34 m ADCP, 20-Aug-96 17:03 to 21-Aug-96 21:58 (233.7107-234.9158)

observed

subtidal

25 cm/s

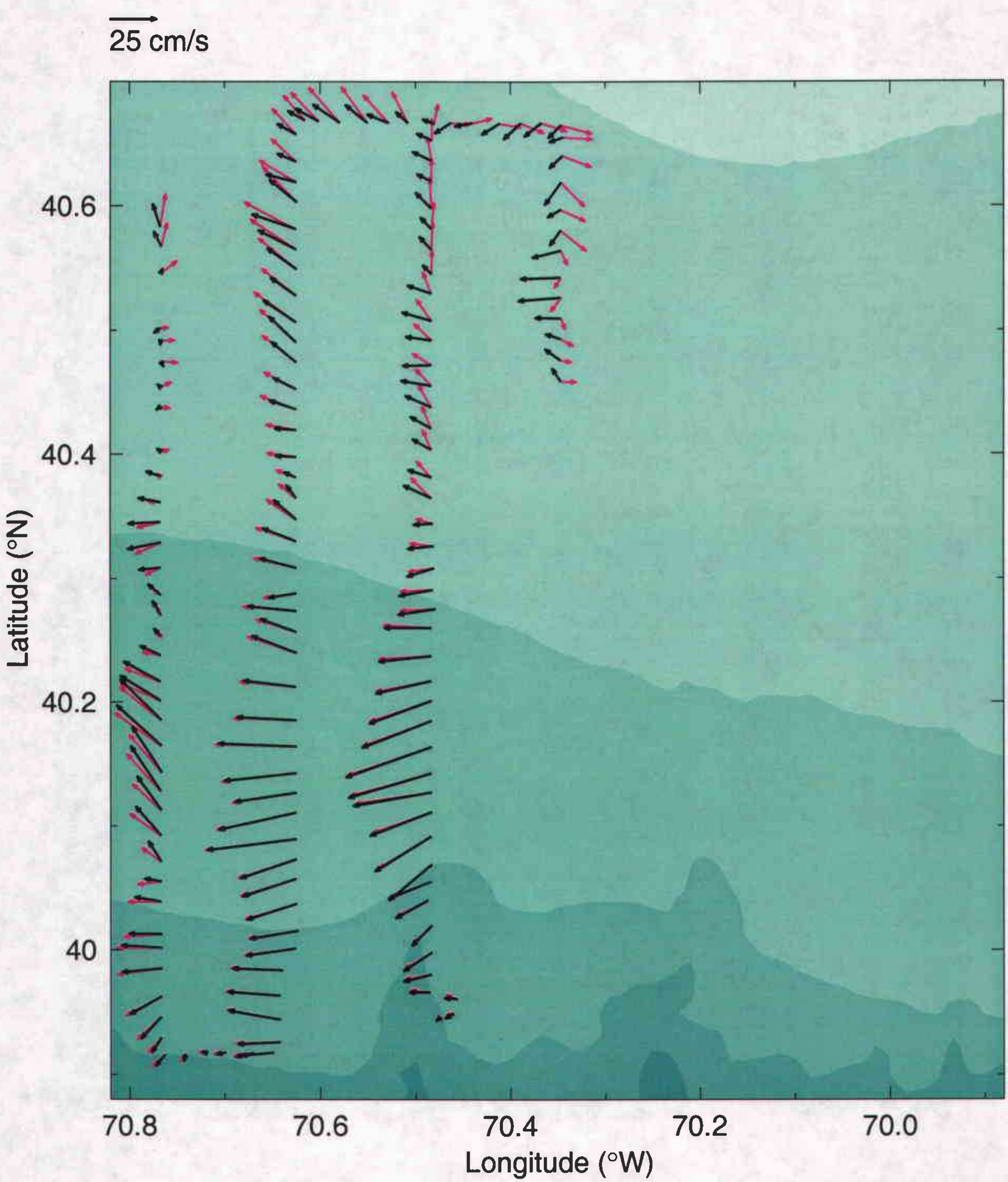

E9608 Big box 2

46 m ADCP, 20-Aug-96 17:03 to 21-Aug-96 21:58 (233.7107-234.9158)

observed

subtidal

25 cm/s

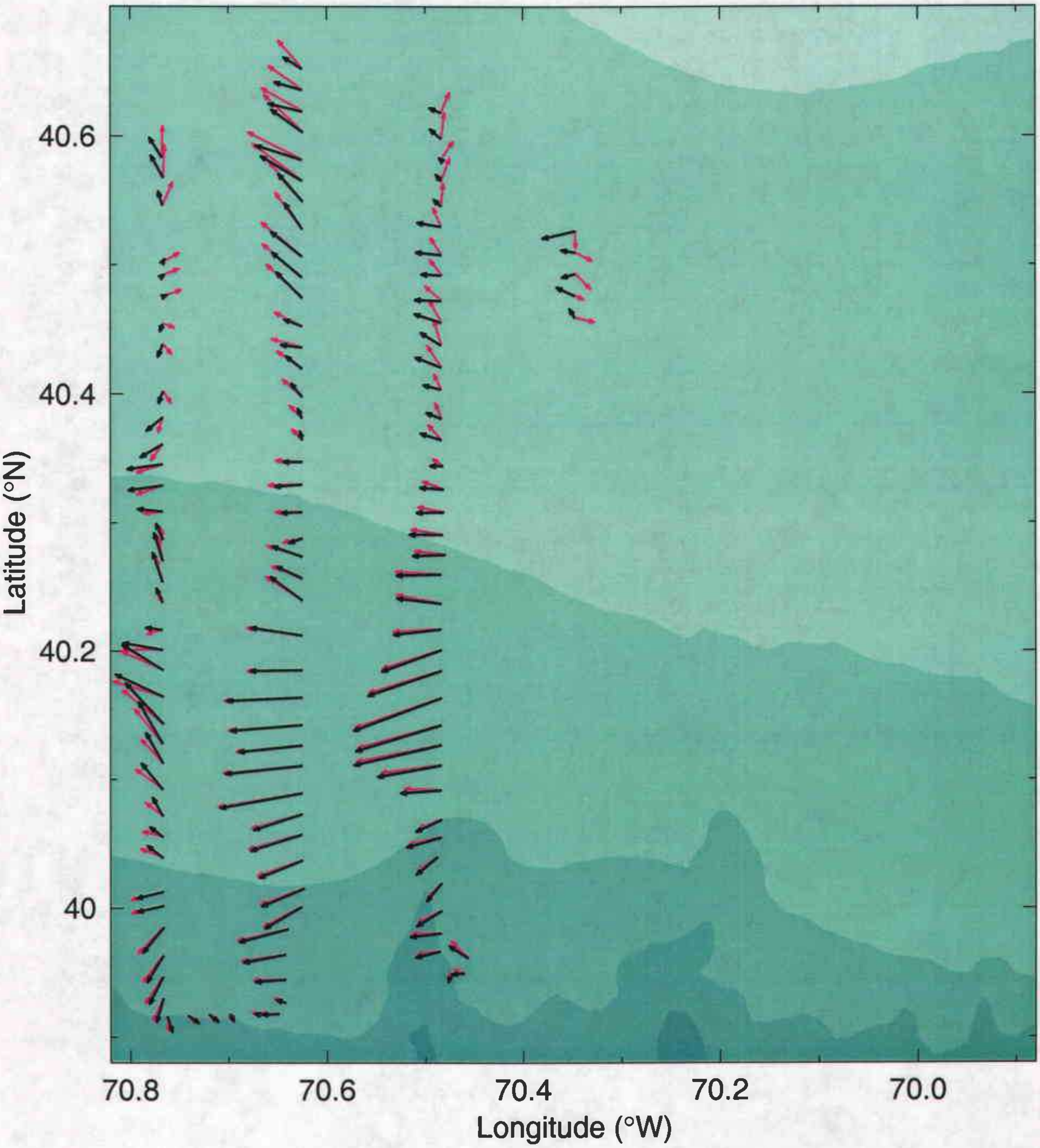

E9608 Big box 2

54 m ADCP, 20-Aug-96 17:03 to 21-Aug-96 21:58 (233.7107-234.9158)

observed

subtidal

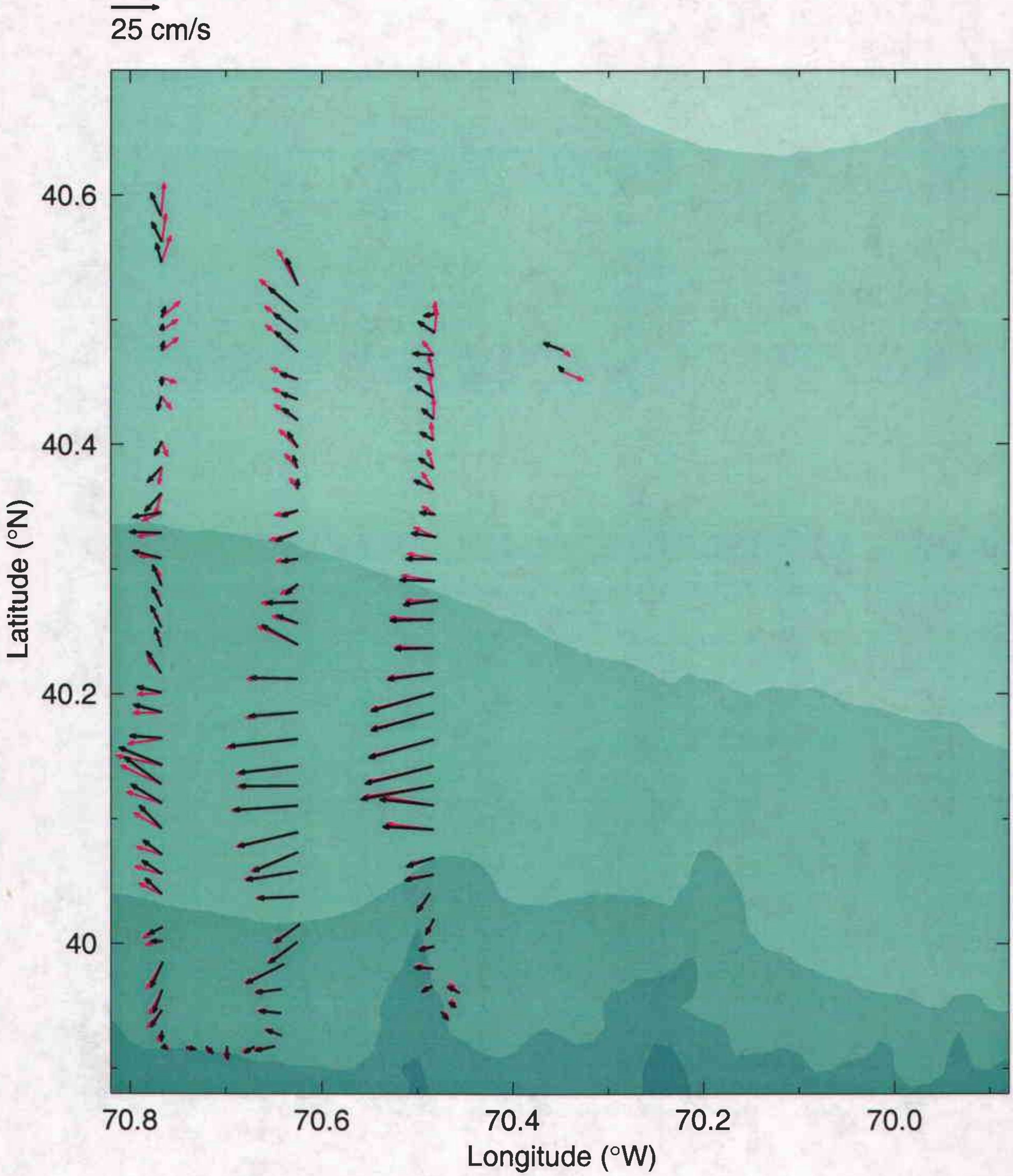

E9608 Big box 2

66 m ADCP, 20-Aug-96 17:03 to 21-Aug-96 21:58 (233.7107-234.9158)

observed

subtidal

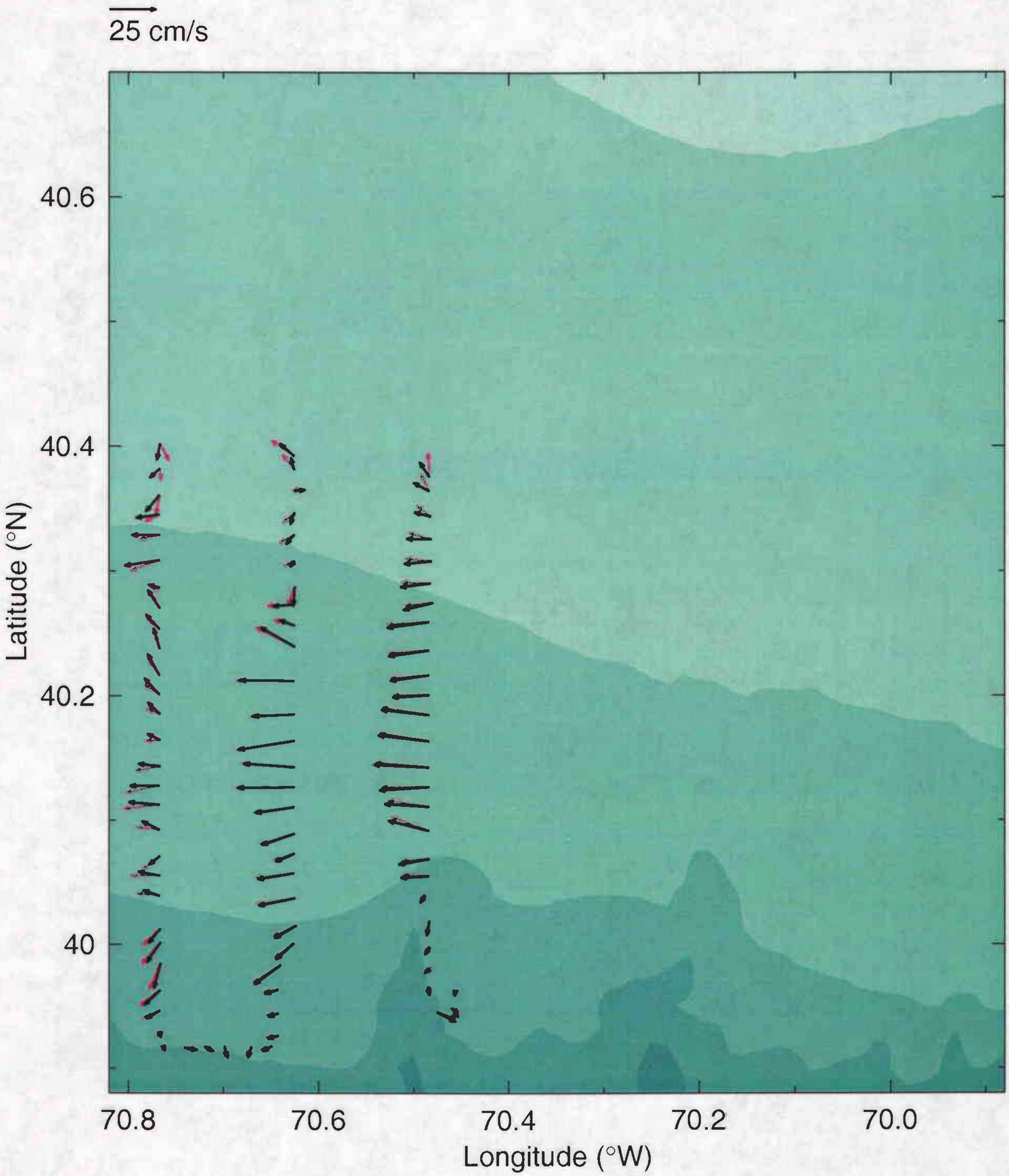

E9608 Big box 2

74 m ADCP, 20-Aug-96 17:03 to 21-Aug-96 21:58 (233.7107-234.9158)

observed

subtidal

25 cm/s

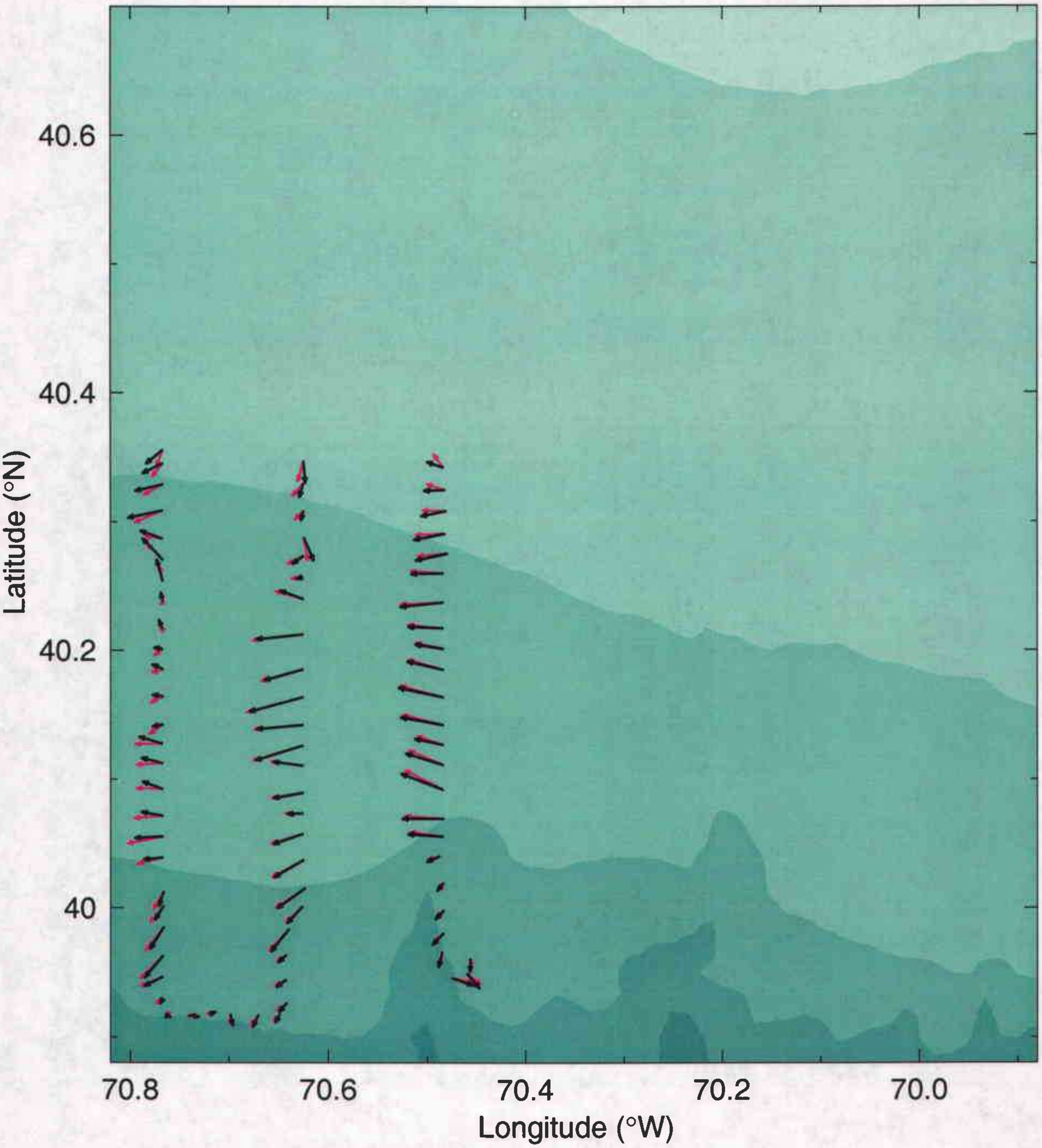

E9608 Big box 2

86 m ADCP, 20-Aug-96 17:03 to 21-Aug-96 21:58 (233.7107-234.9158)

observed

subtidal

25 cm/s

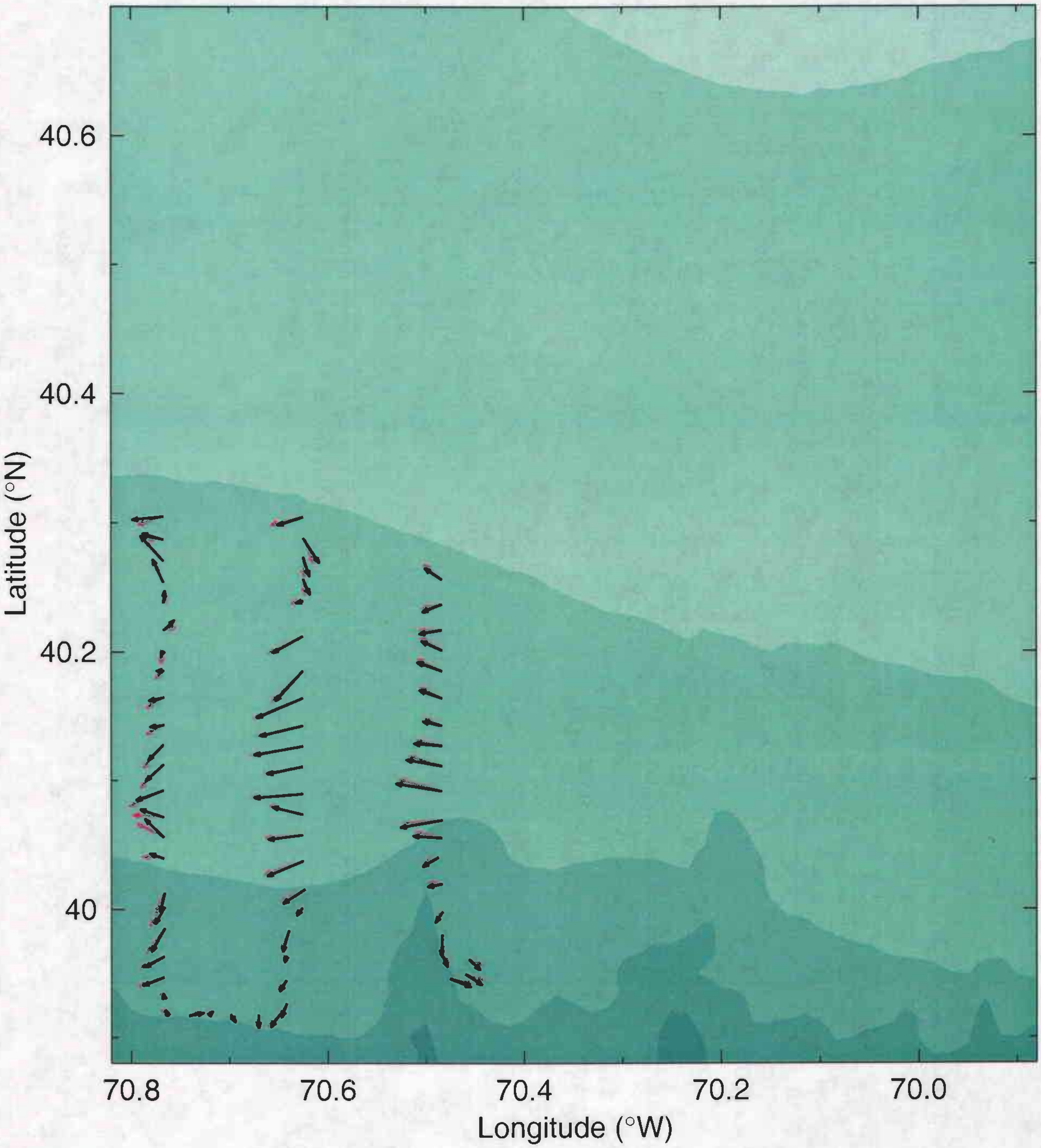

E9608 Big box 2

94 m ADCP, 20-Aug-96 17:03 to 21-Aug-96 21:58 (233.7107-234.9158)

observed

subtidal

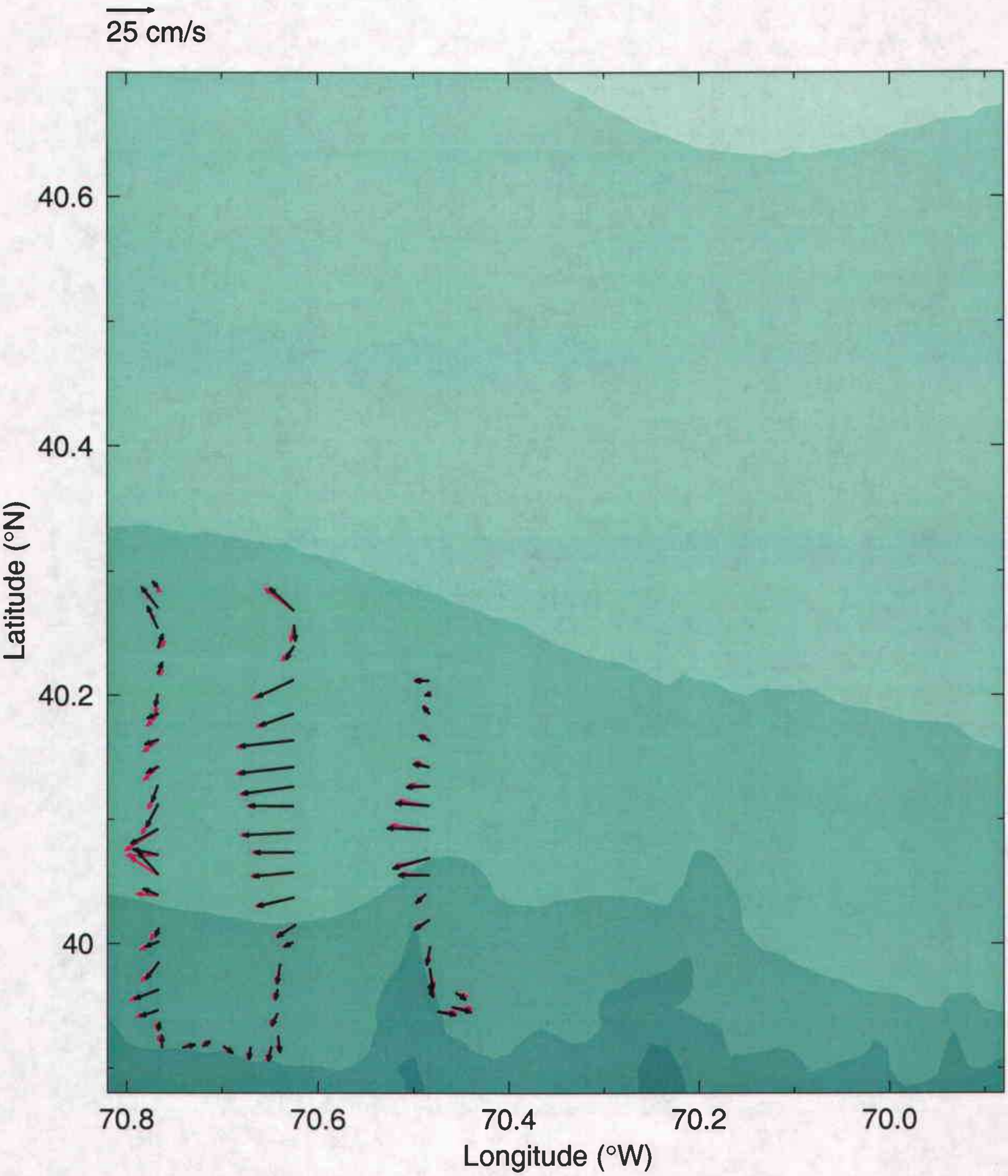

E9608 Big box 2

106 m ADCP, 20-Aug-96 17:03 to 21-Aug-96 21:58 (233.7107-234.9158)

observed

subtidal

25 cm/s

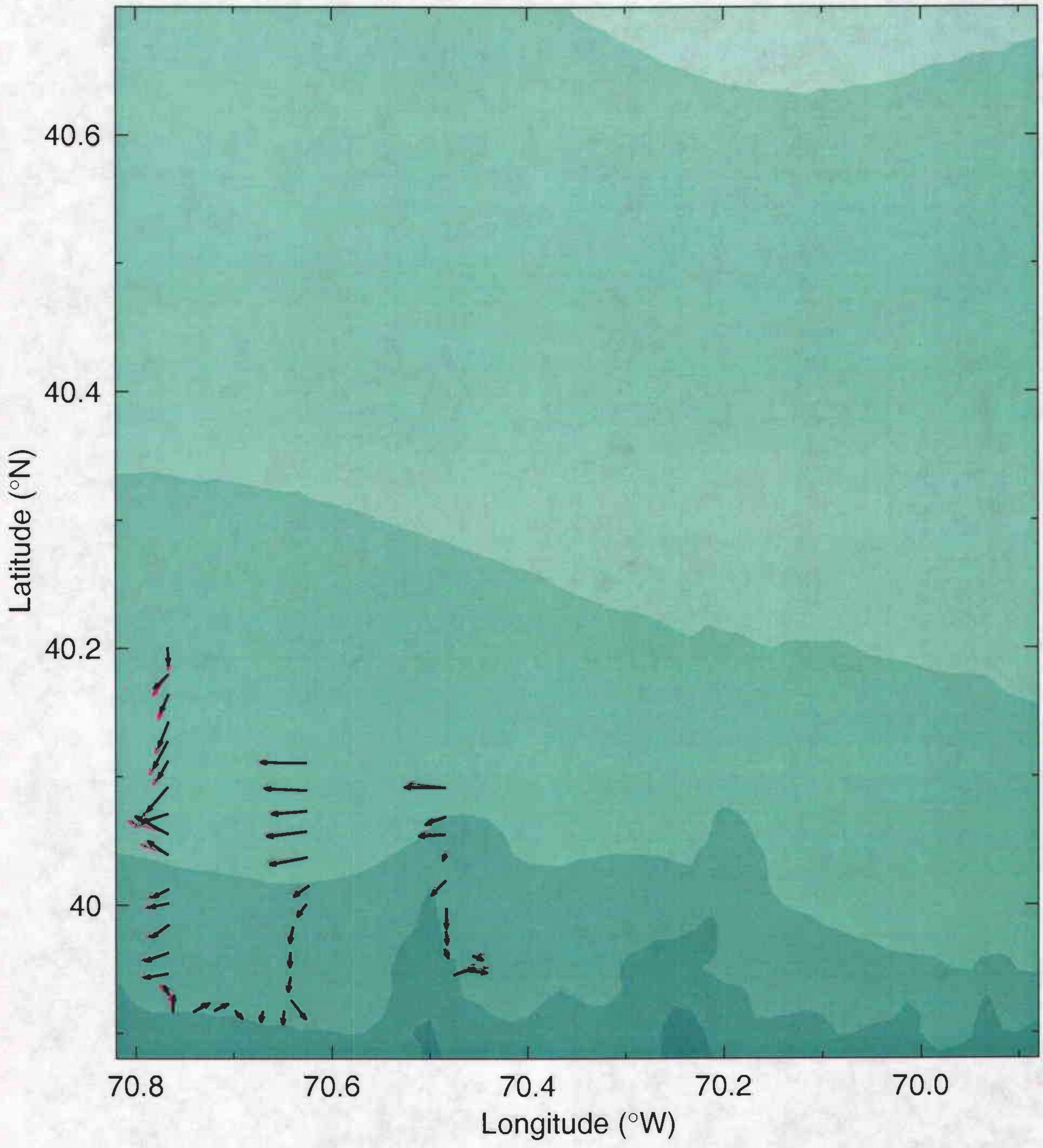

E9608 Small box 4 24-Aug-96 20:01 to 25-Aug-96 11:34 (237.8345-238.4826)

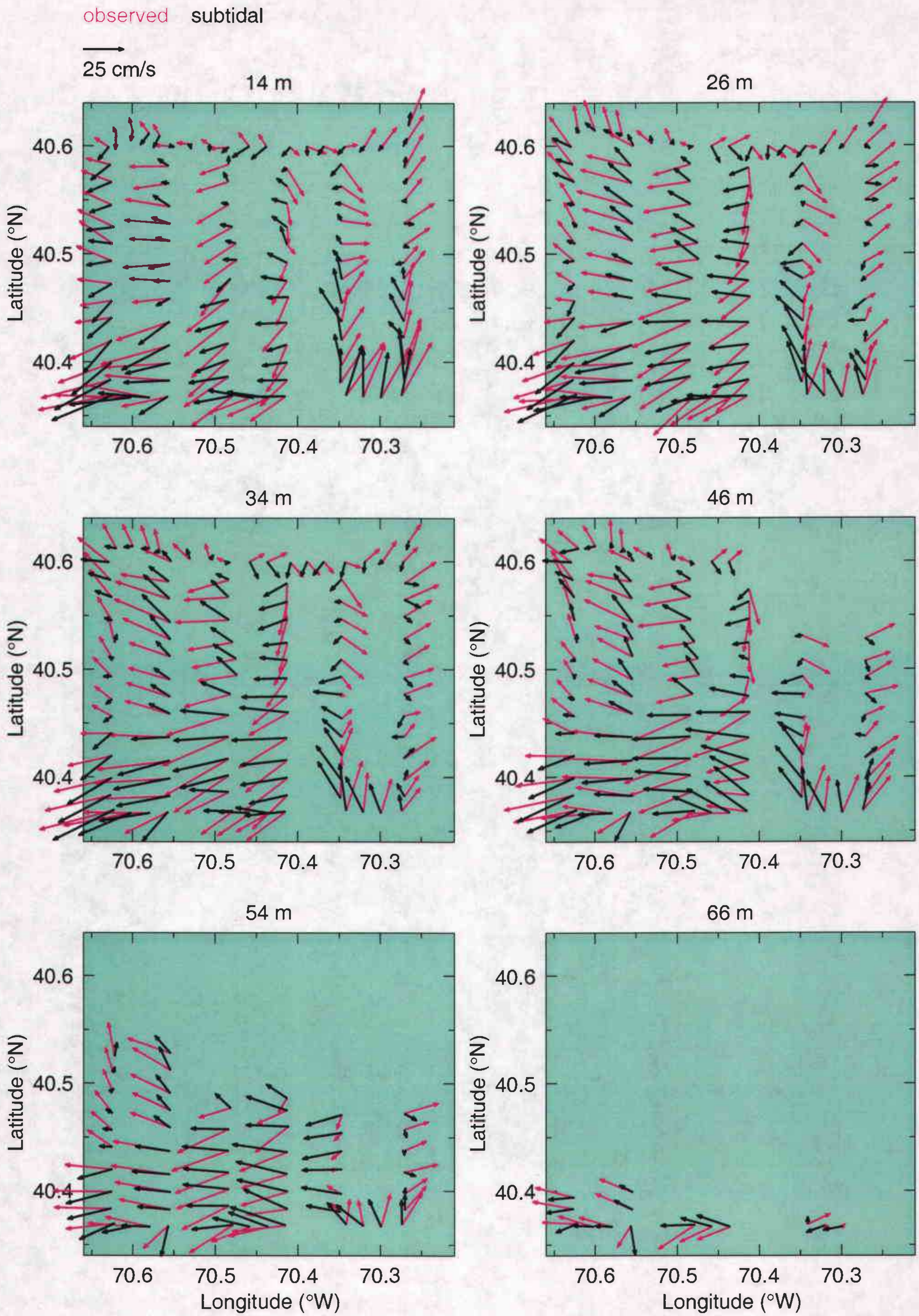

E9608 Small box 5 25-Aug-96 11:34 to 26-Aug-96 03:11 (238.4826-239.1331)

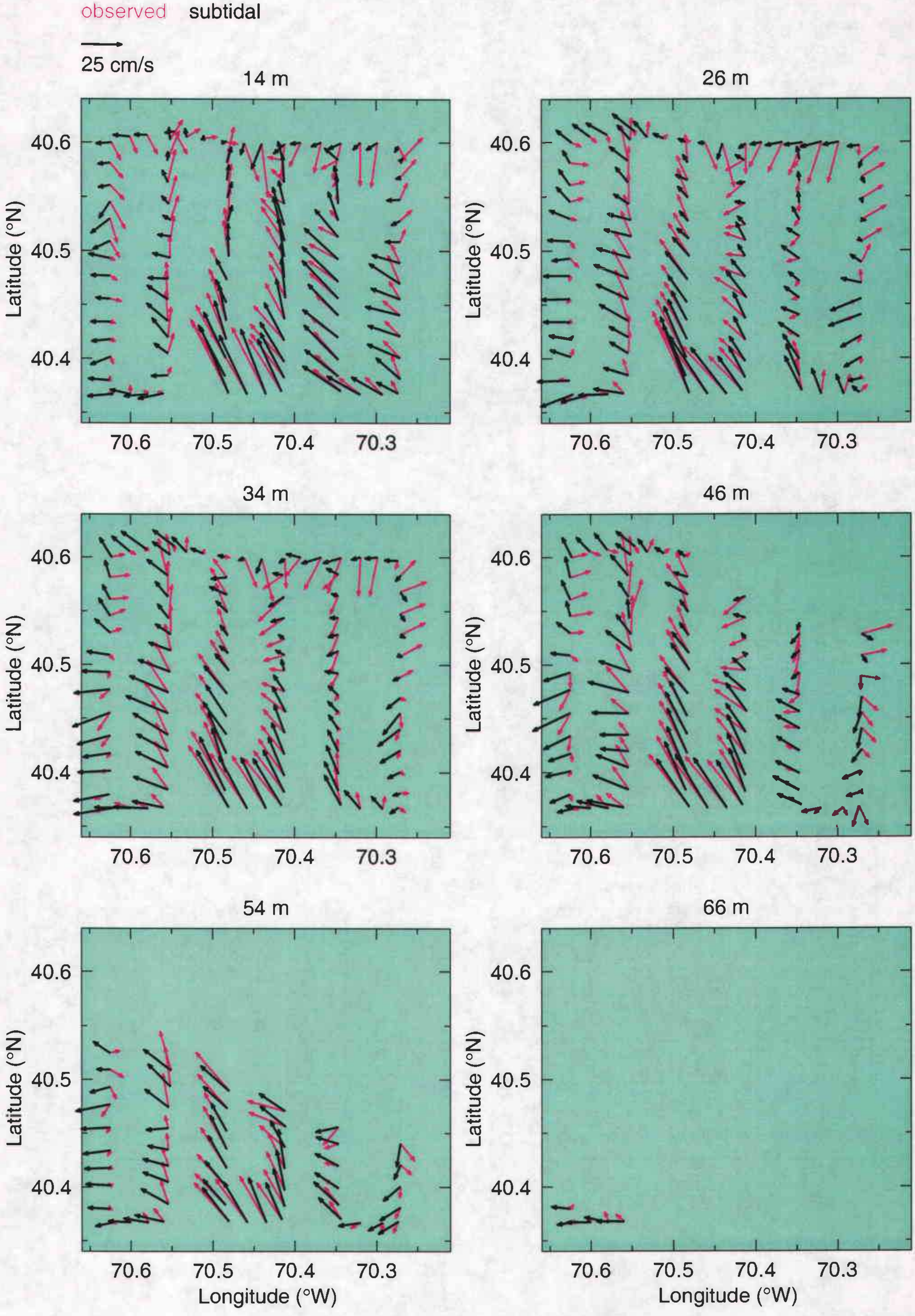

E9608 Small box 6 26-Aug-96 03:11 to 26-Aug-96 16:53 (239.1331-239.7038)

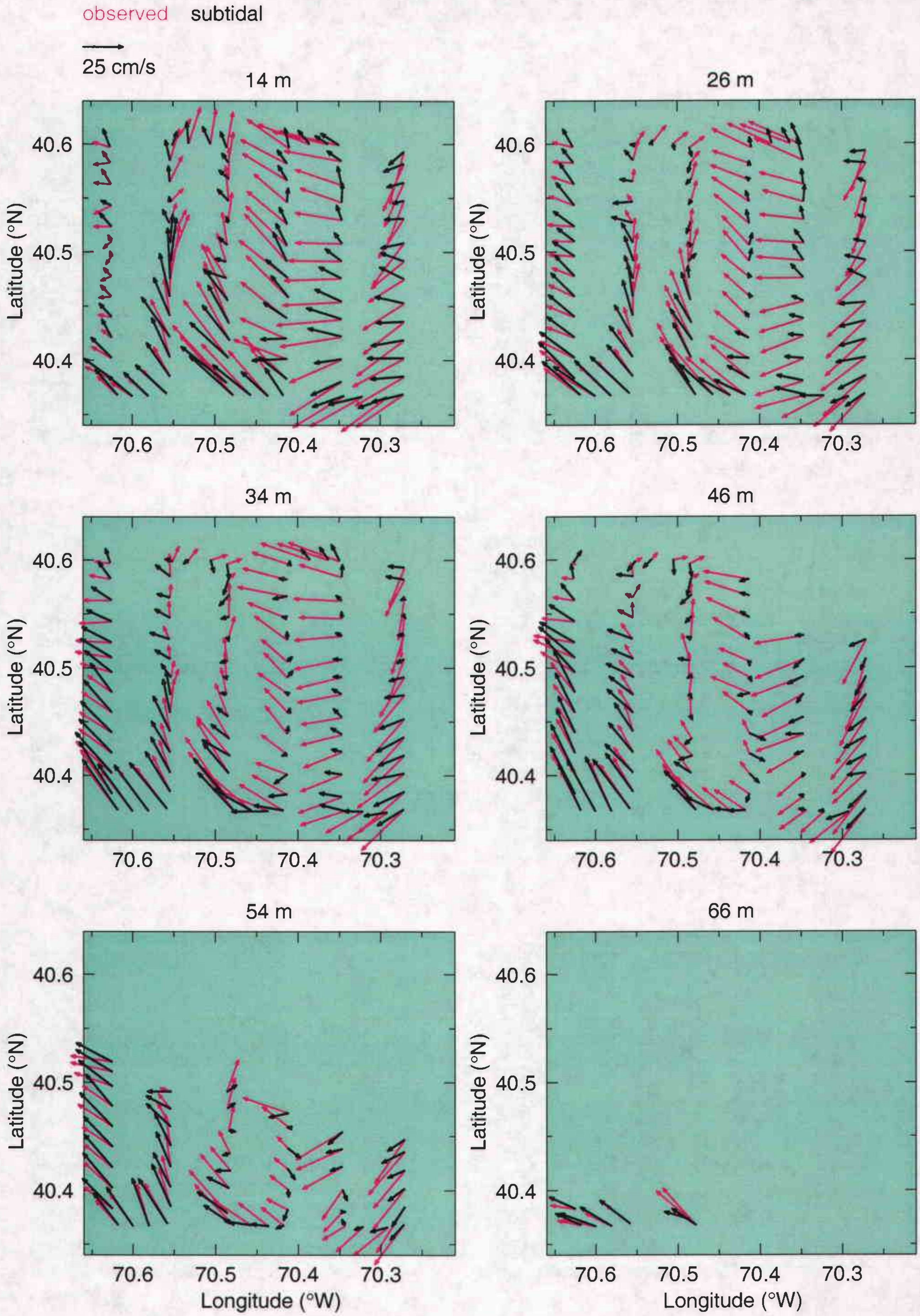

E9608 Butterfly 1 26-Aug-96 23:59 to 27-Aug-96 11:12 (239.9998-240.4669)

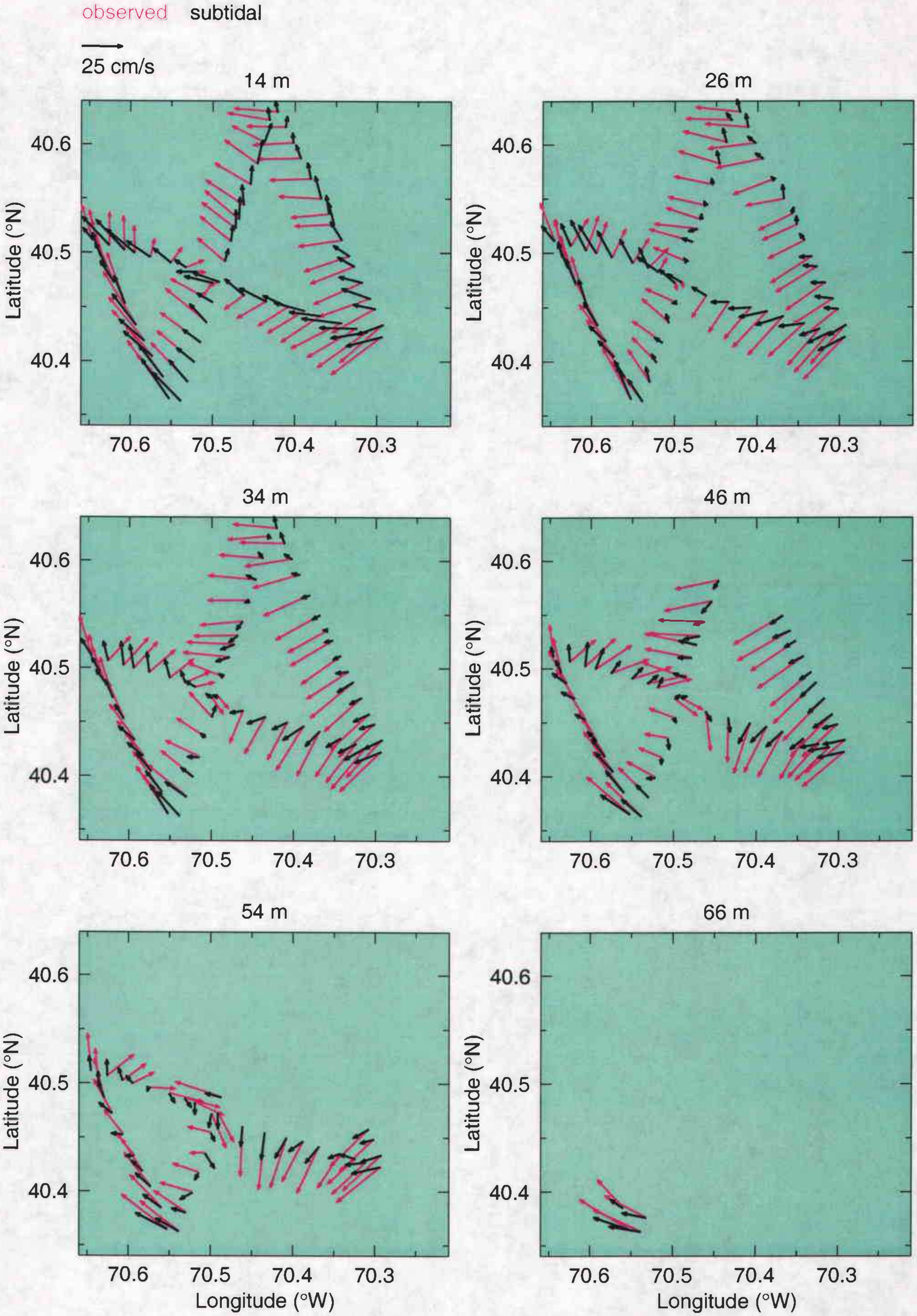

E9608 Butterfly 2 27-Aug-96 11:12 to 27-Aug-96 21:28 (240.4669-240.8951)

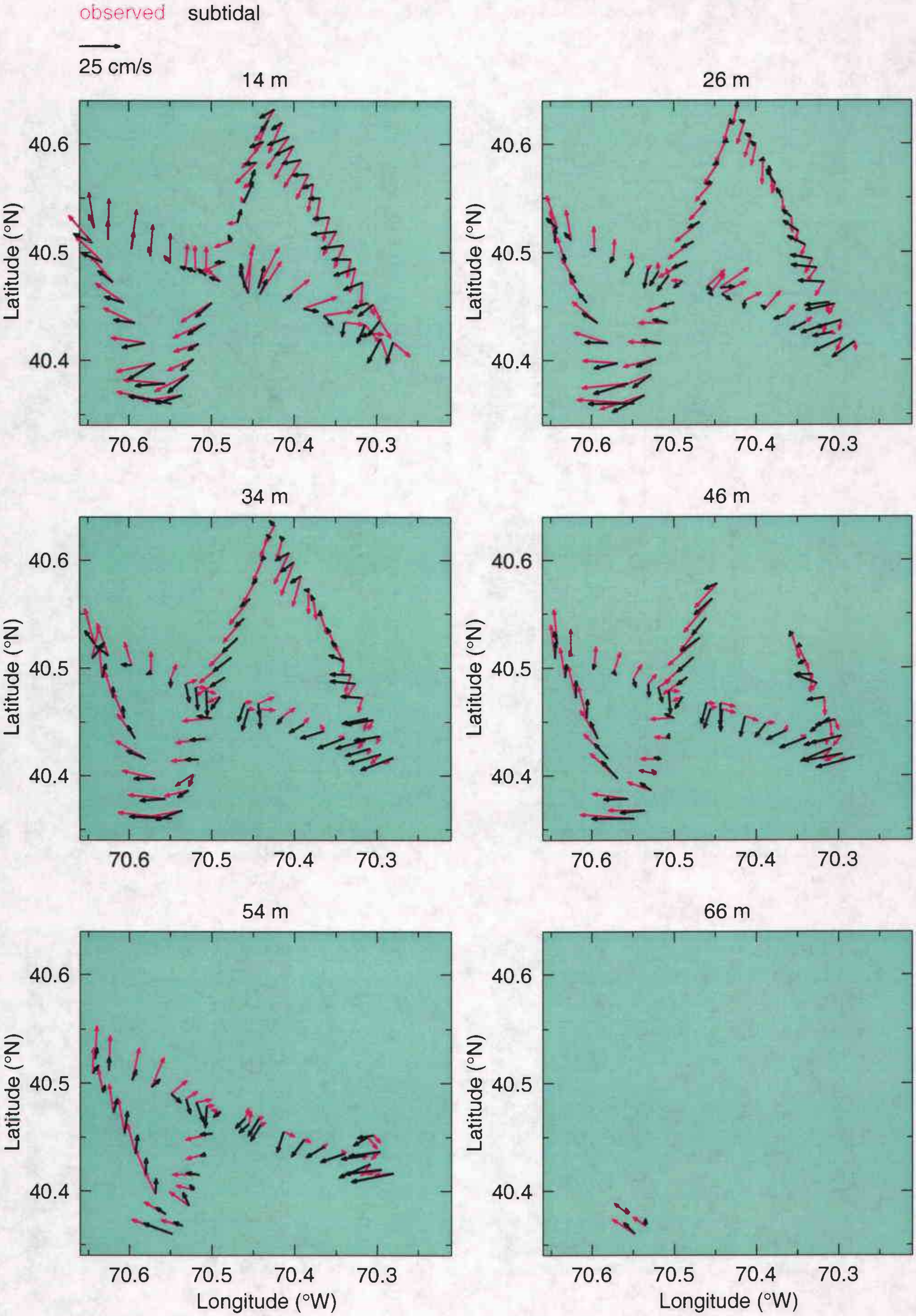

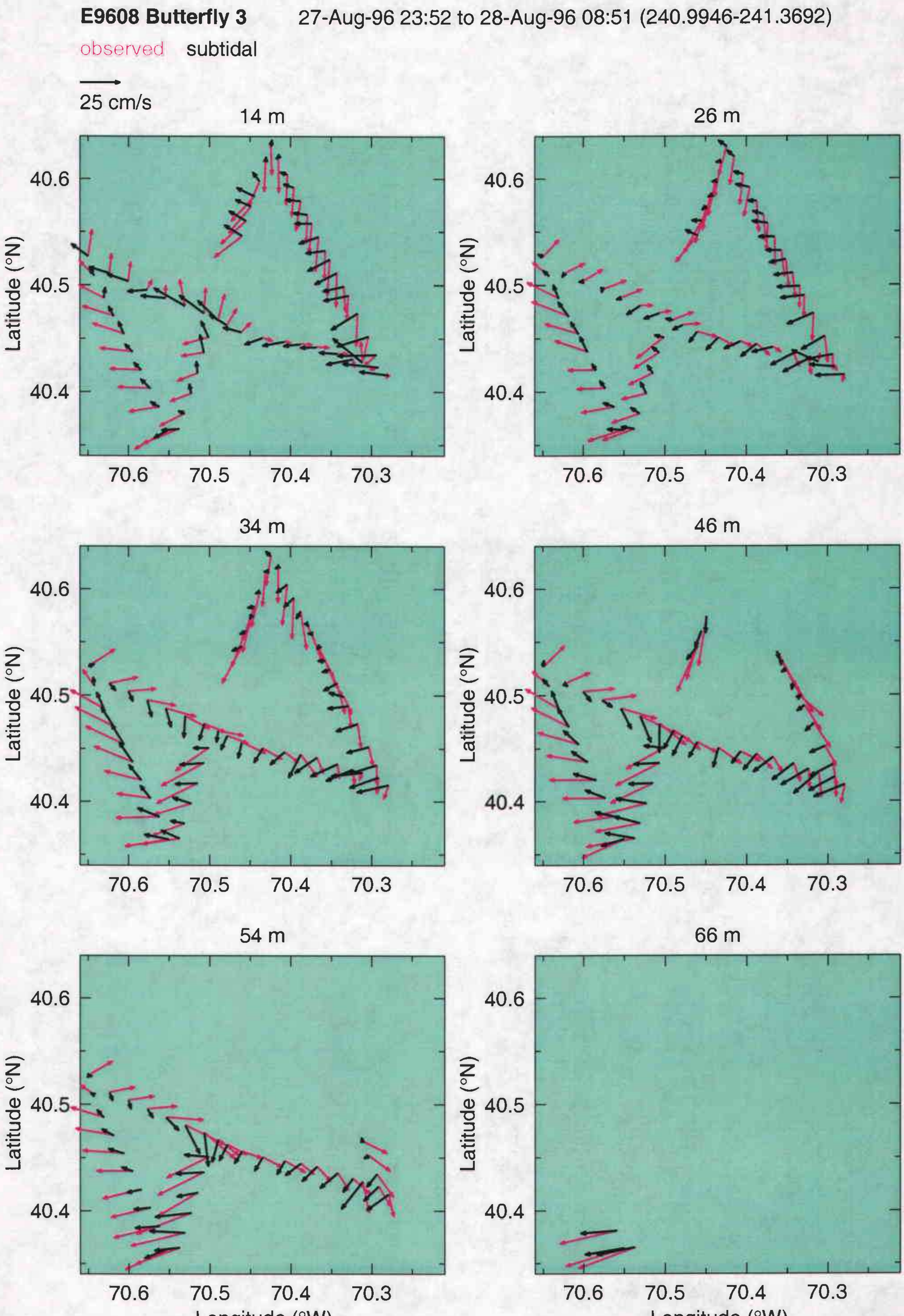
E9608 Butterfly 3
27-Aug-96 23:52 to 28-Aug-96 08:51 (240.9946-241.3692)
observed
subtidal
25 cm/s
14 m
26 m
34 m
46 m
54 m
66 m
Latitude (°N)
40.6
40.5
40.4
70.6
70.5
70.4
70.3
Longitude (°W)

E9608 Butterfly 4 28-Aug-96 09:41 to 28-Aug-96 17:09 (241.4038-241.7152)

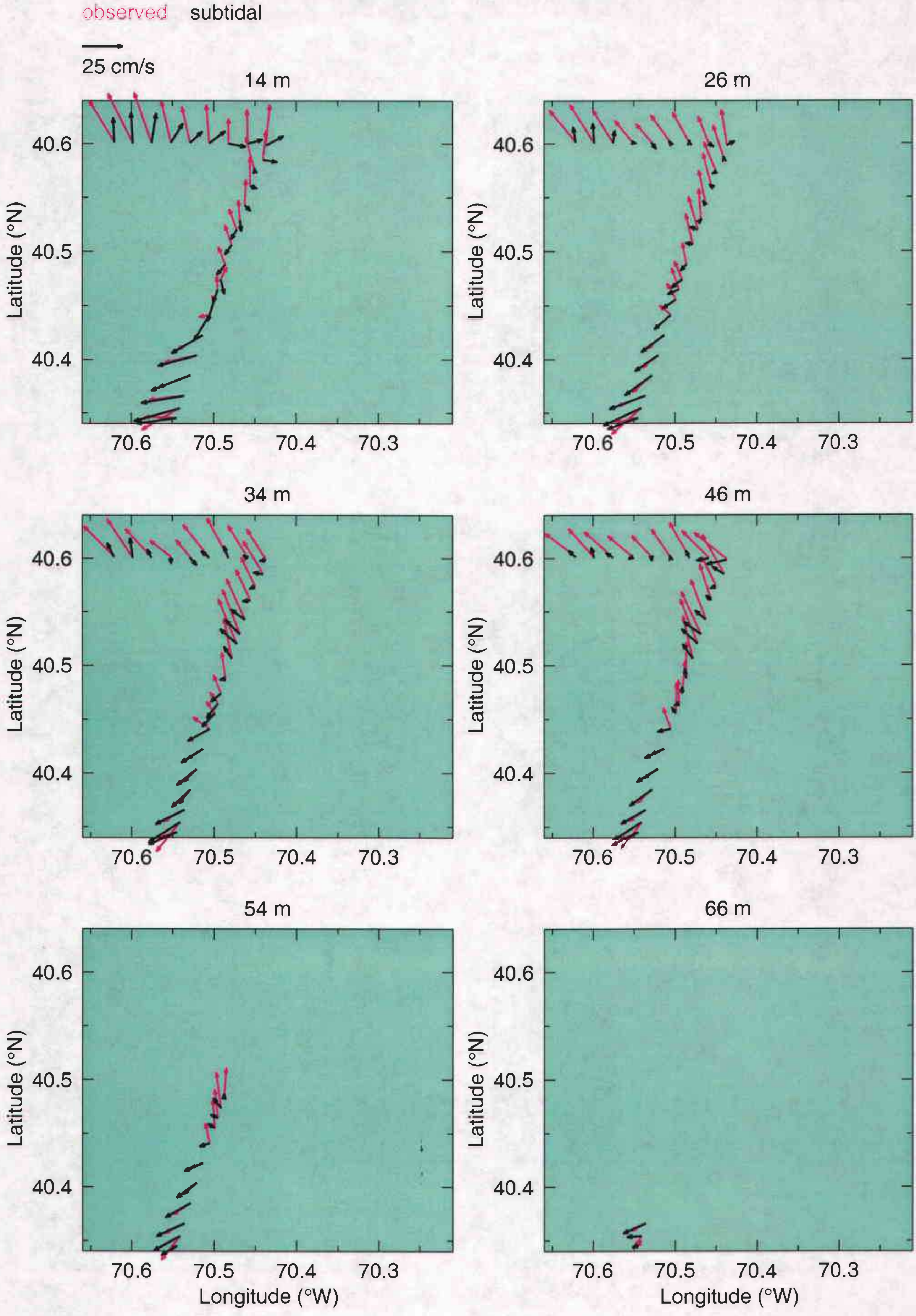

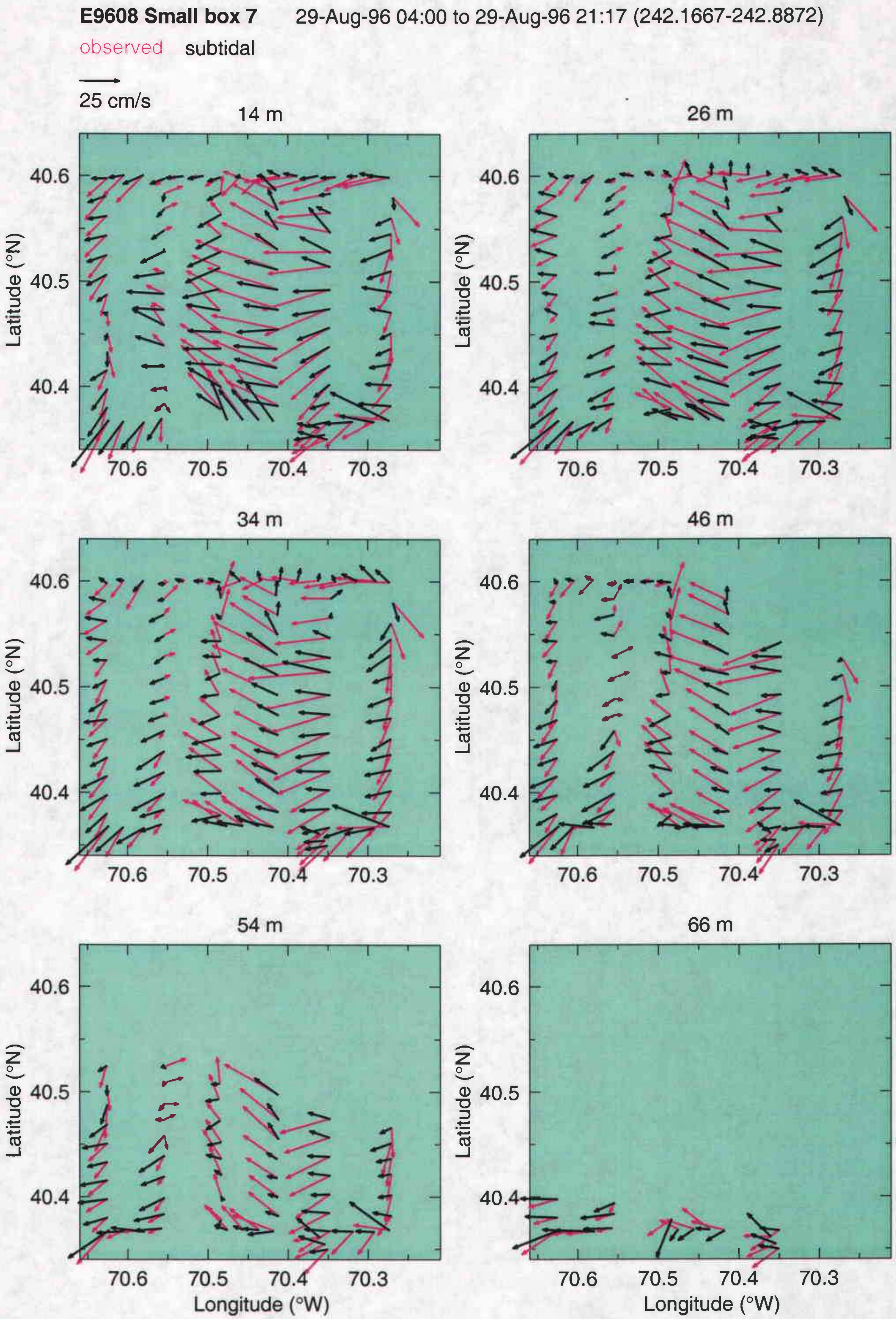
E9608 Small box 7
29-Aug-96 04:00 to 29-Aug-96 21:17 (242.1667-242.8872)
observed
subtidal
25 cm/s
14 m
26 m
34 m
46 m
54 m
66 m
Latitude (°N)
40.6
40.5
40.4
70.6
70.5
70.4
70.3
Longitude (°W)

E9608 Small box 8 29-Aug-96 21:17 to 30-Aug-96 12:10 (242.8872-243.5076)

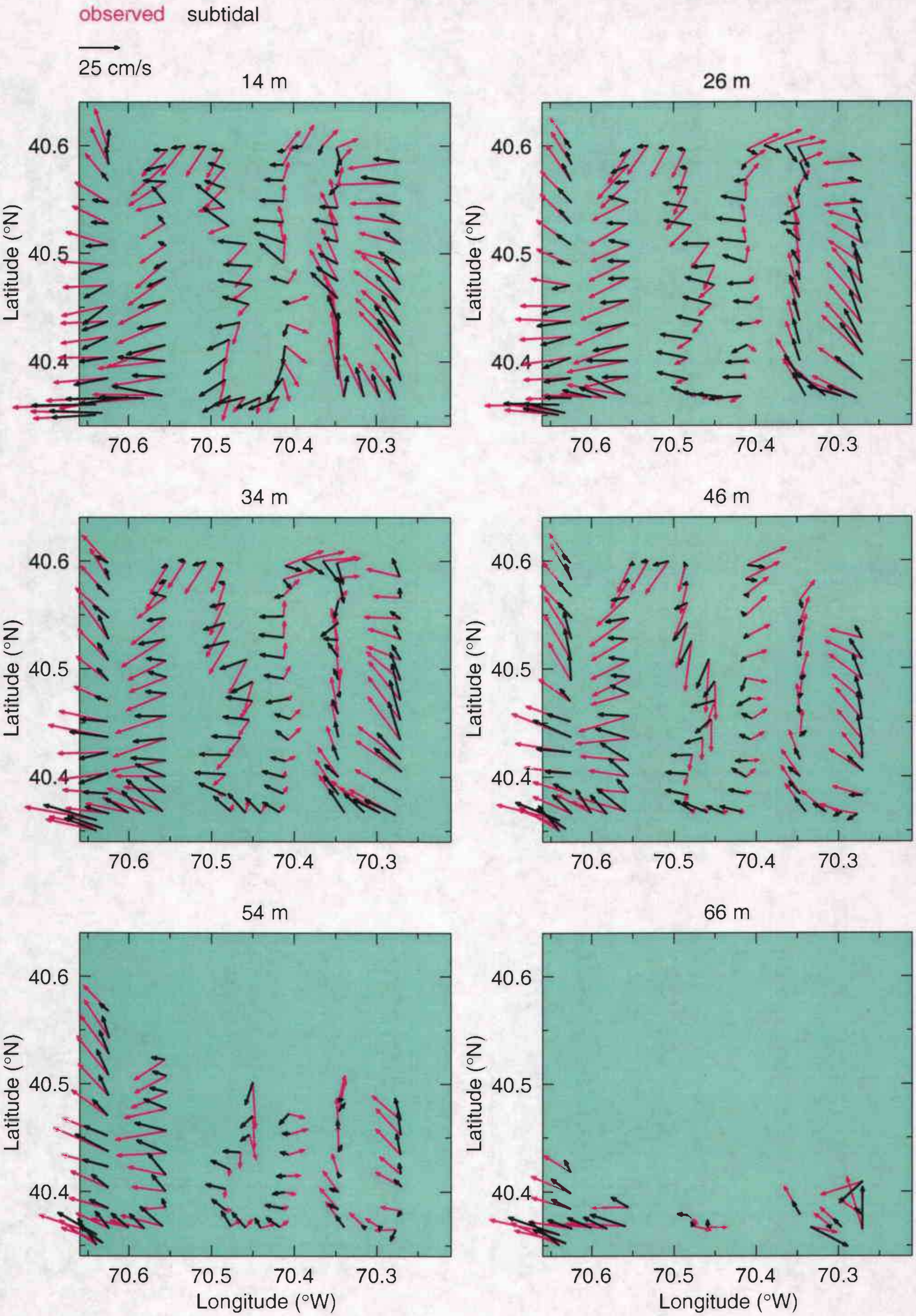

E9608 Small box 9 30-Aug-96 14:52 to 31-Aug-96 05:49 (243.6196-244.2424)

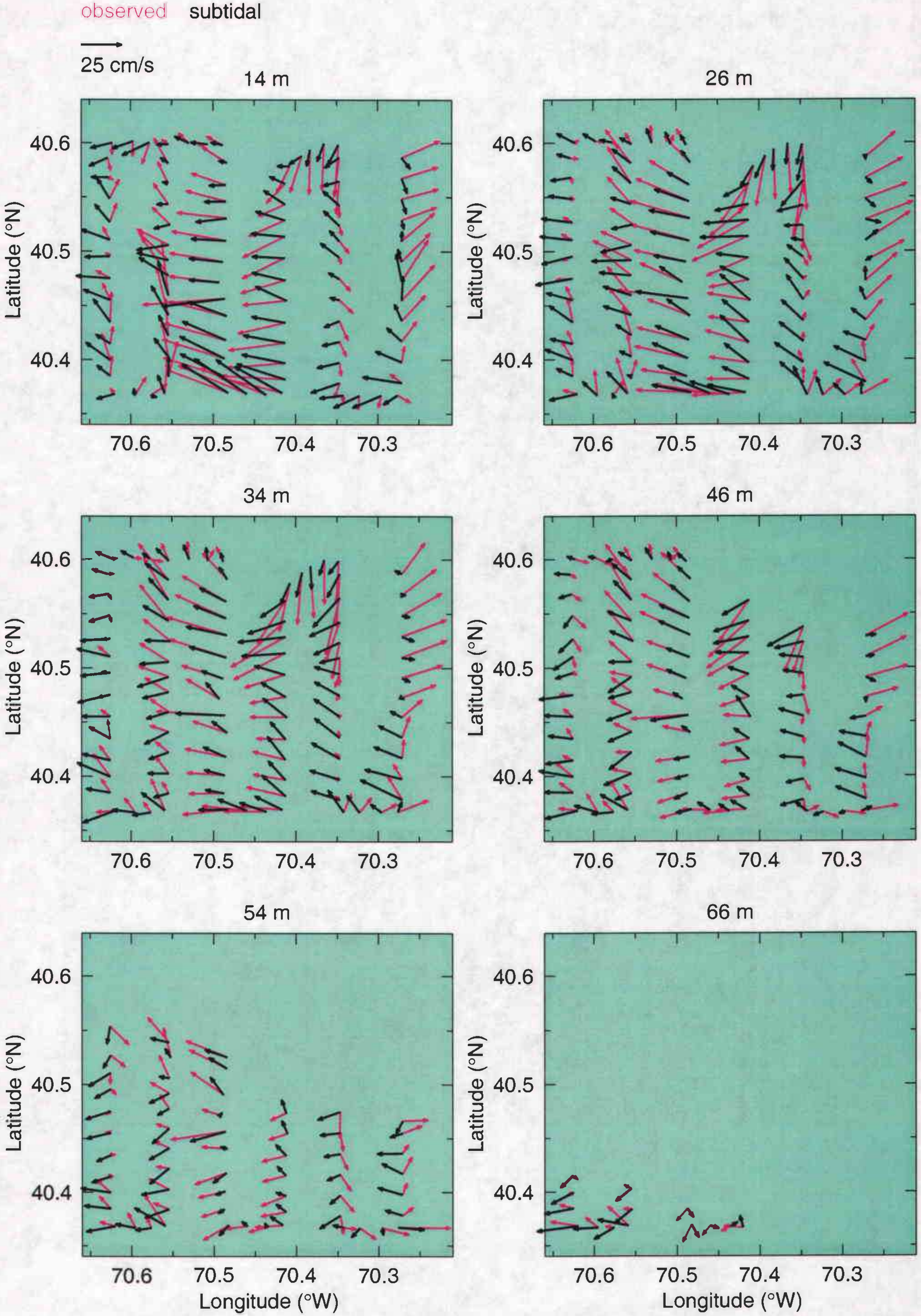

E9608 Big box 3

14 m ADCP, 31-Aug-96 05:49 to 01-Sep-96 11:08 (244.2424-245.4640)

observed

subtidal

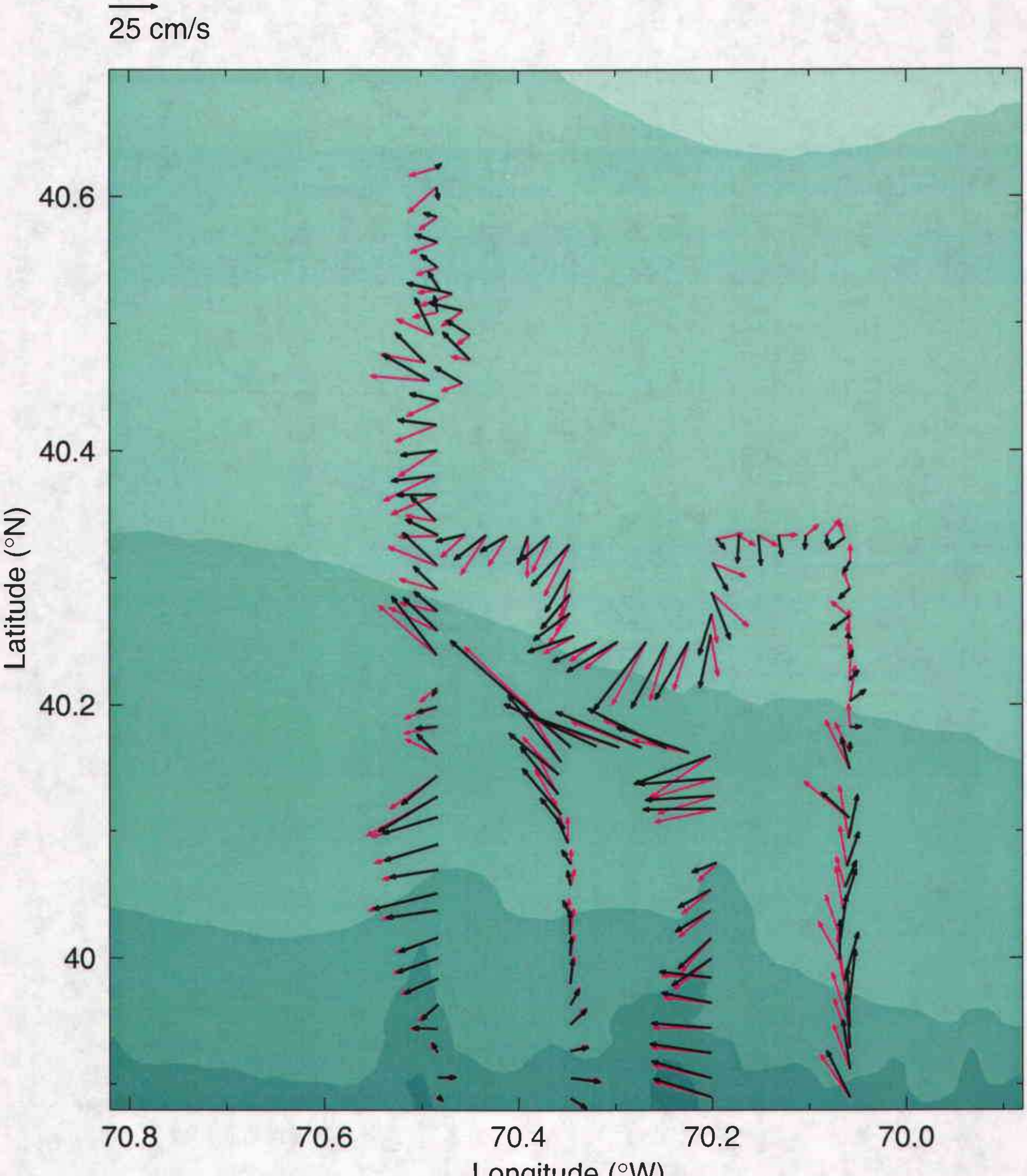

E9608 Big box 3

26 m ADCP, 31-Aug-96 05:49 to 01-Sep-96 11:08 (244.2424-245.4640)

observed

subtidal

25 cm/s

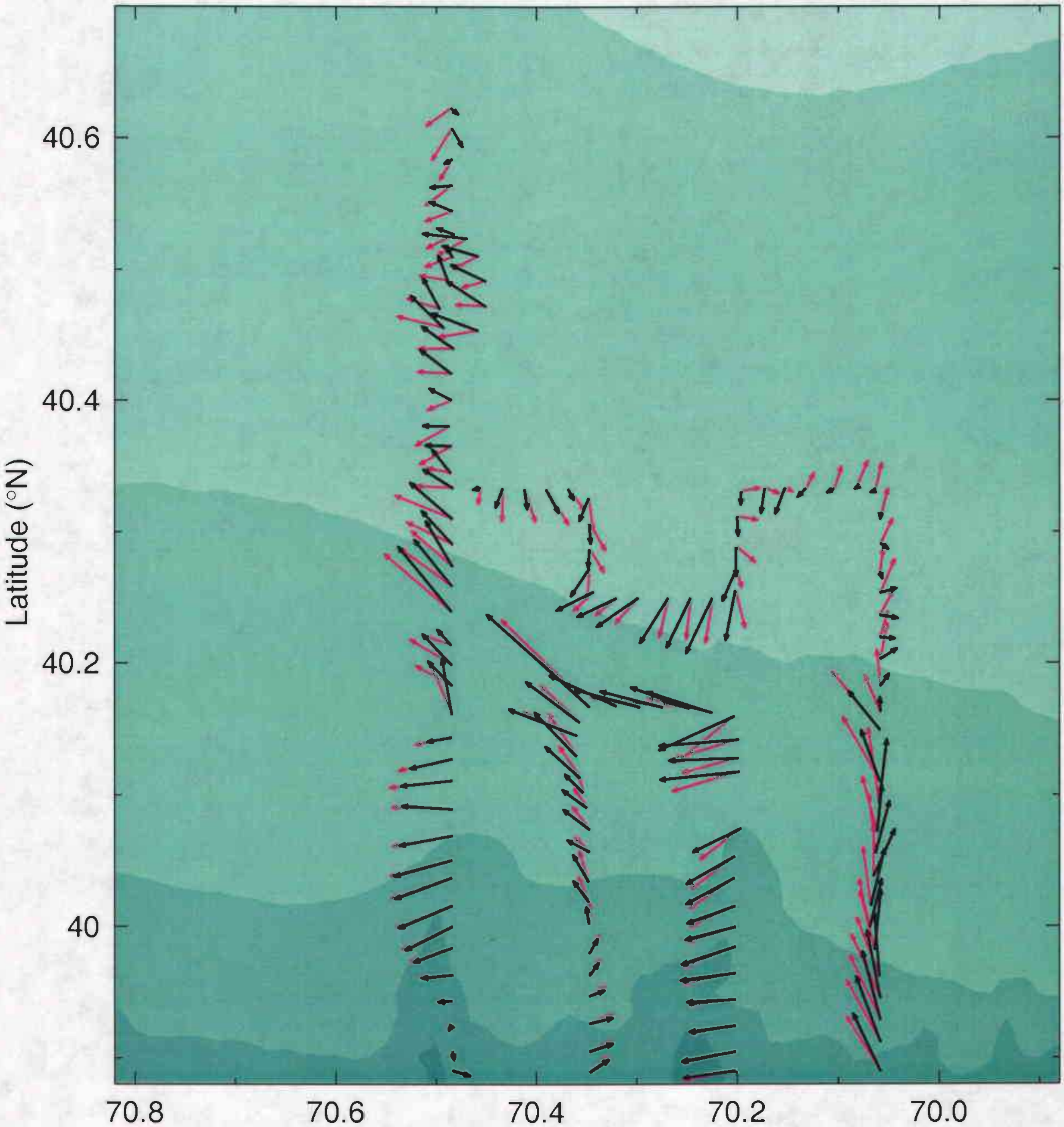

E9608 Big box 3

34 m ADCP, 31-Aug-96 05:49 to 01-Sep-96 11:08 (244.2424-245.4640)

observed

subtidal

25 cm/s

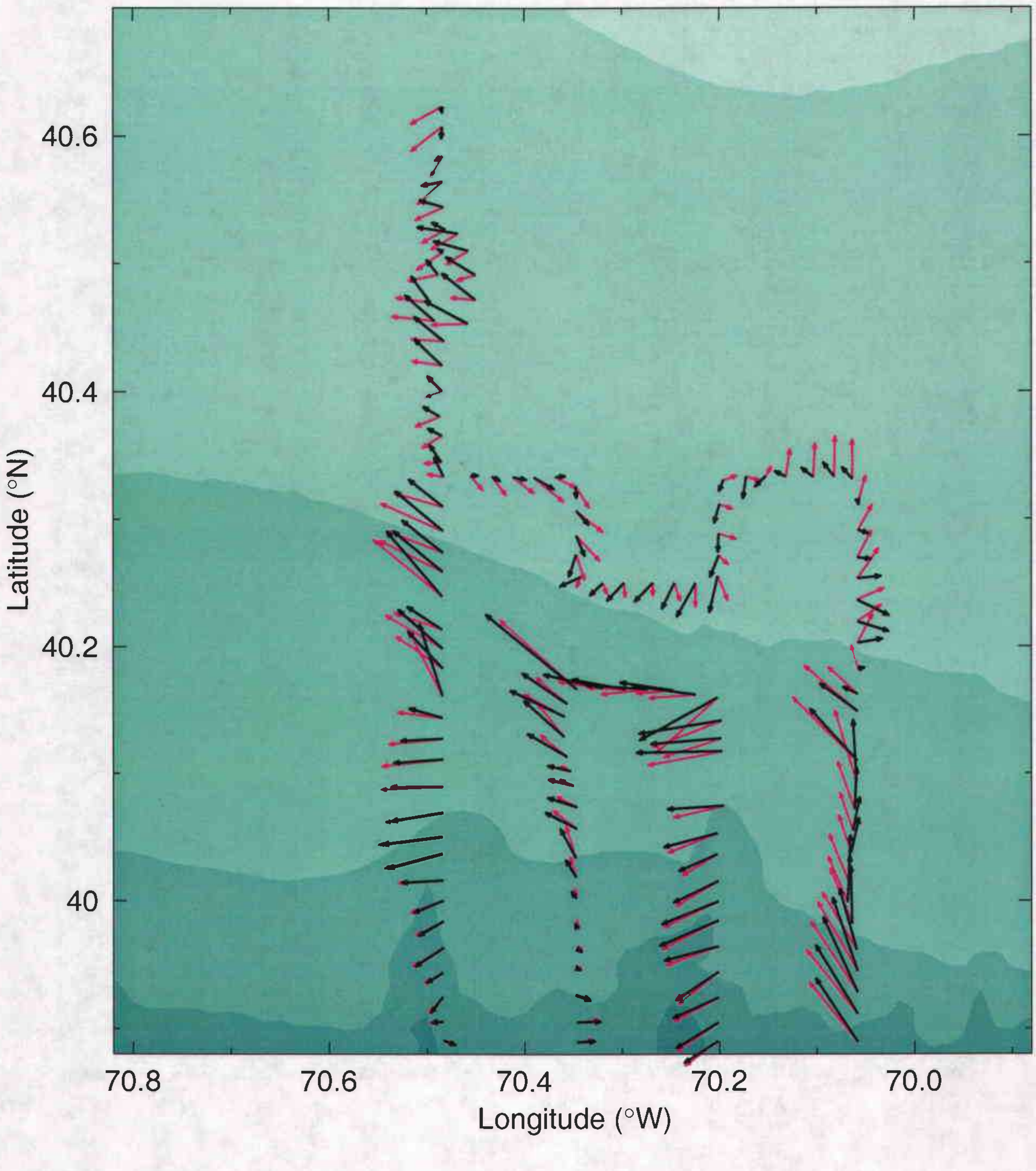

E9608 Big box 3

46 m ADCP, 31-Aug-96 05:49 to 01-Sep-96 11:08 (244.2424-245.4640)

observed

subtidal

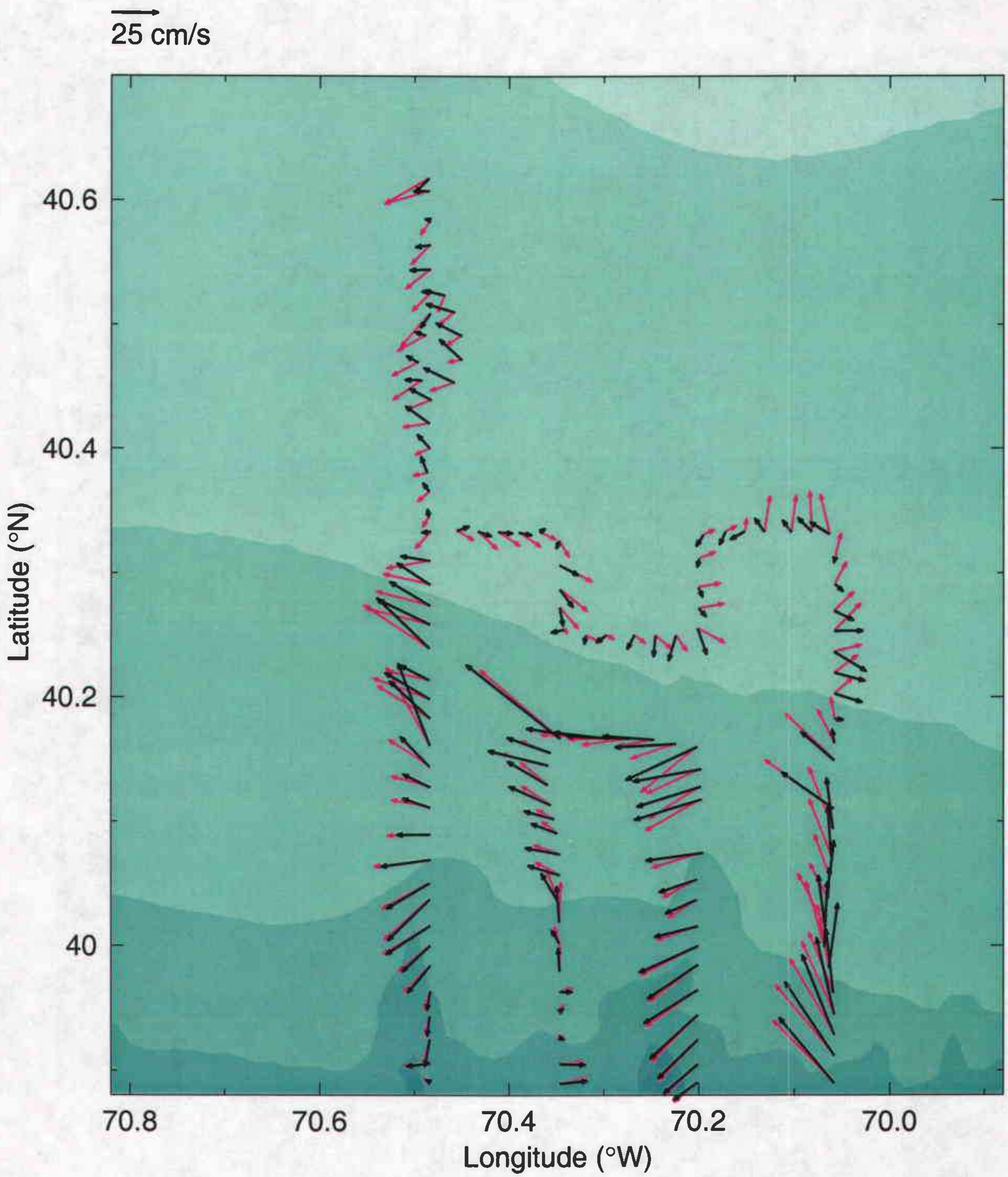

E9608 Big box 3

54 m ADCP, 31-Aug-96 05:49 to 01-Sep-96 11:08 (244.2424-245.4640)

observed

subtidal

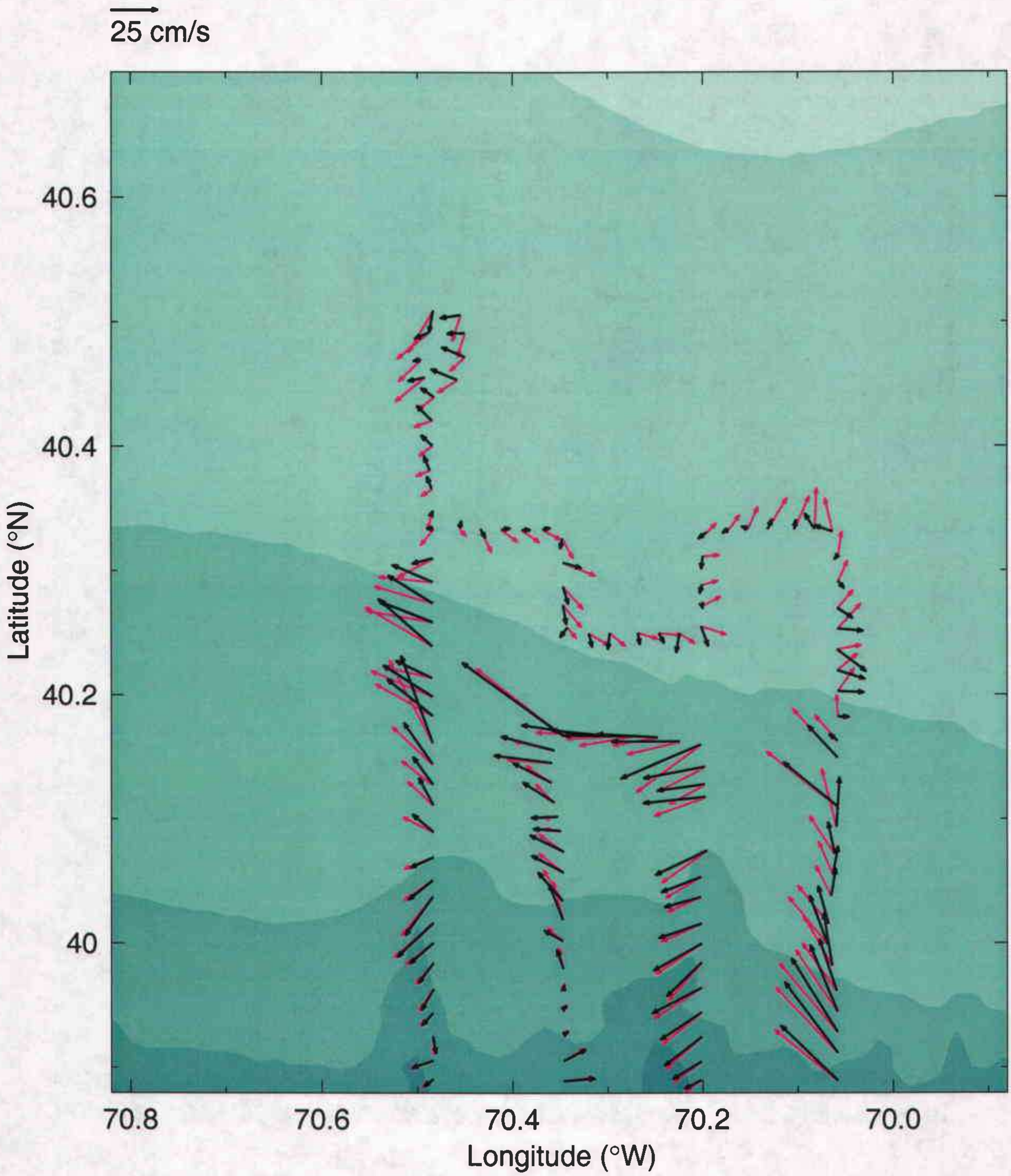

E9608 Big box 3

66 m ADCP, 31-Aug-96 05:49 to 01-Sep-96 11:08 (244.2424-245.4640)

observed

subtidal

25 cm/s

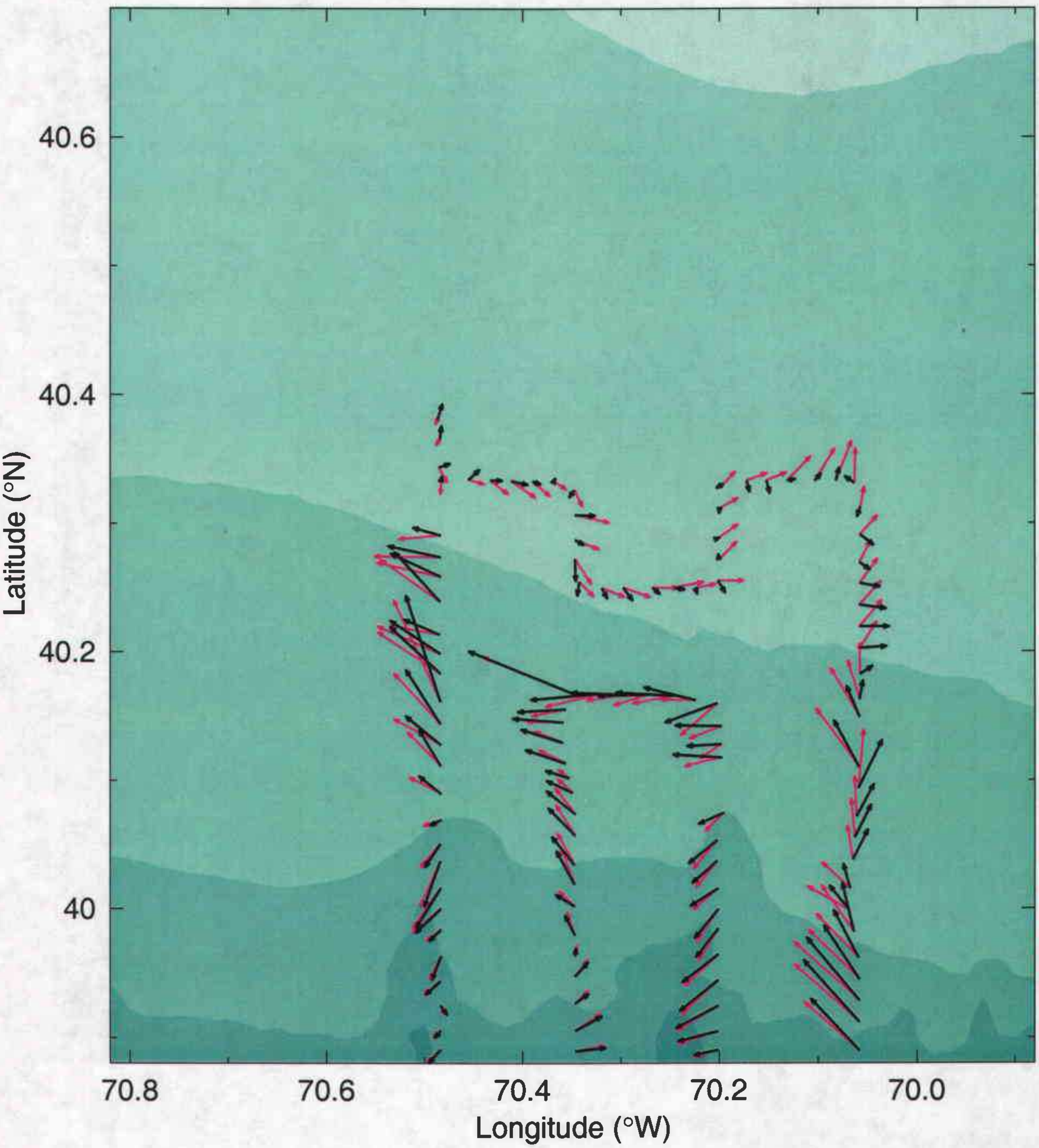

E9608 Big box 3

74 m ADCP, 31-Aug-96 05:49 to 01-Sep-96 11:08 (244.2424-245.4640)

observed

subtidal

25 cm/s

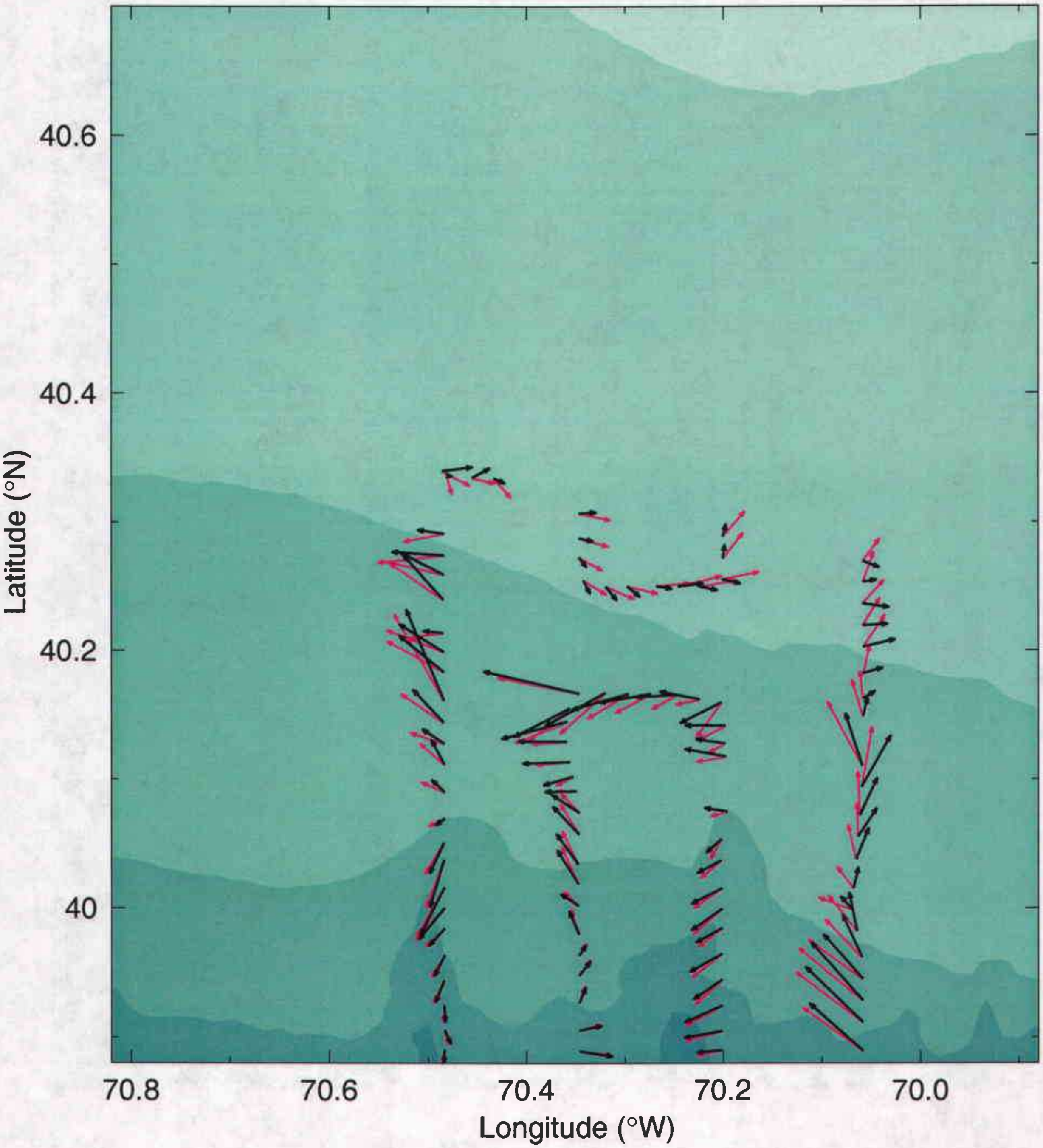

E9608 Big box 3

86 m ADCP, 31-Aug-96 05:49 to 01-Sep-96 11:08 (244.2424-245.4640)

observed

subtidal

25 cm/s

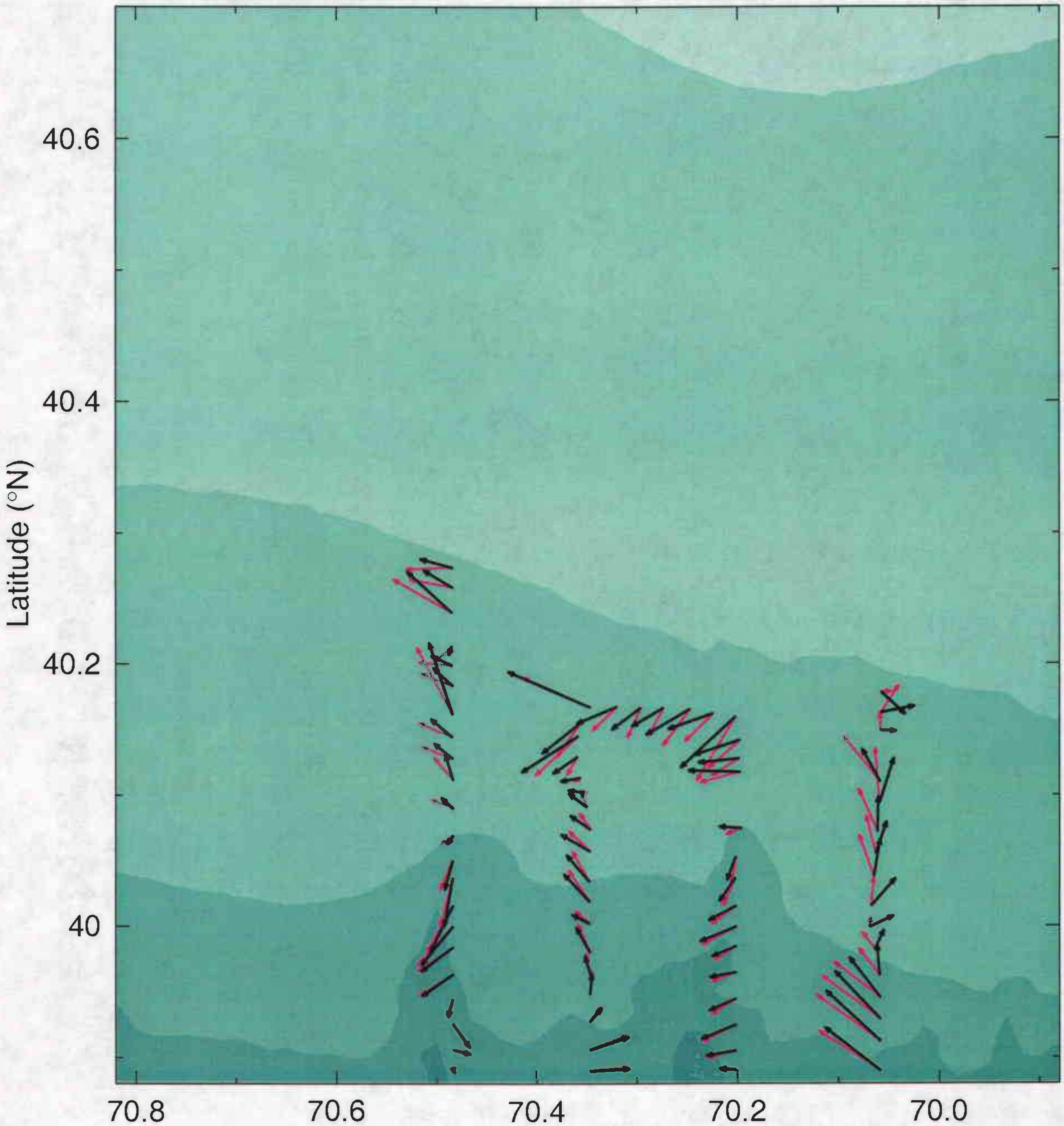

E9608 Big box 3

94 m ADCP, 31-Aug-96 05:49 to 01-Sep-96 11:08 (244.2424-245.4640)

observed

subtidal

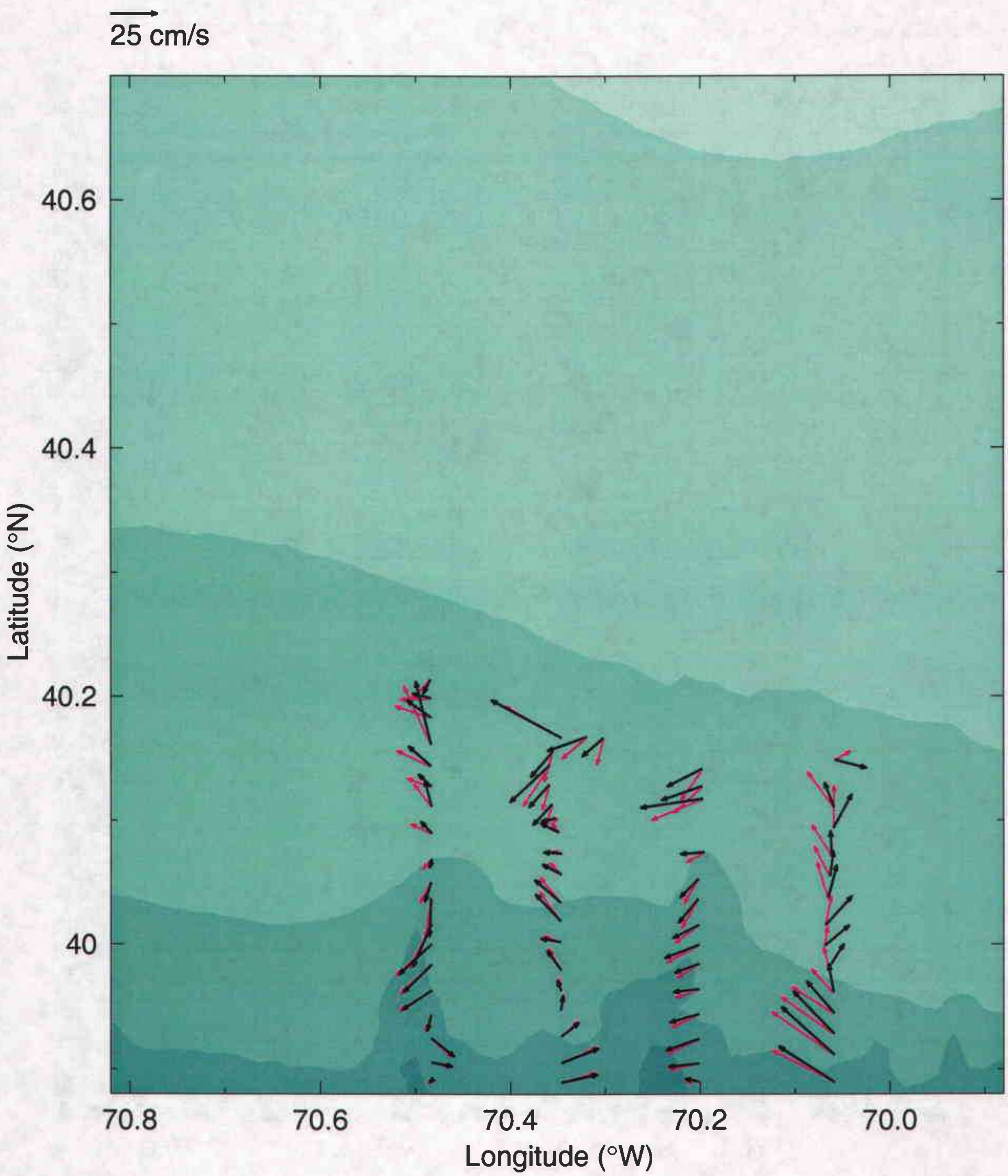

E9608 Big box 3

106 m ADCP, 31-Aug-96 05:49 to 01-Sep-96 11:08 (244.2424-245.4640)

observed

subtidal

25 cm/s

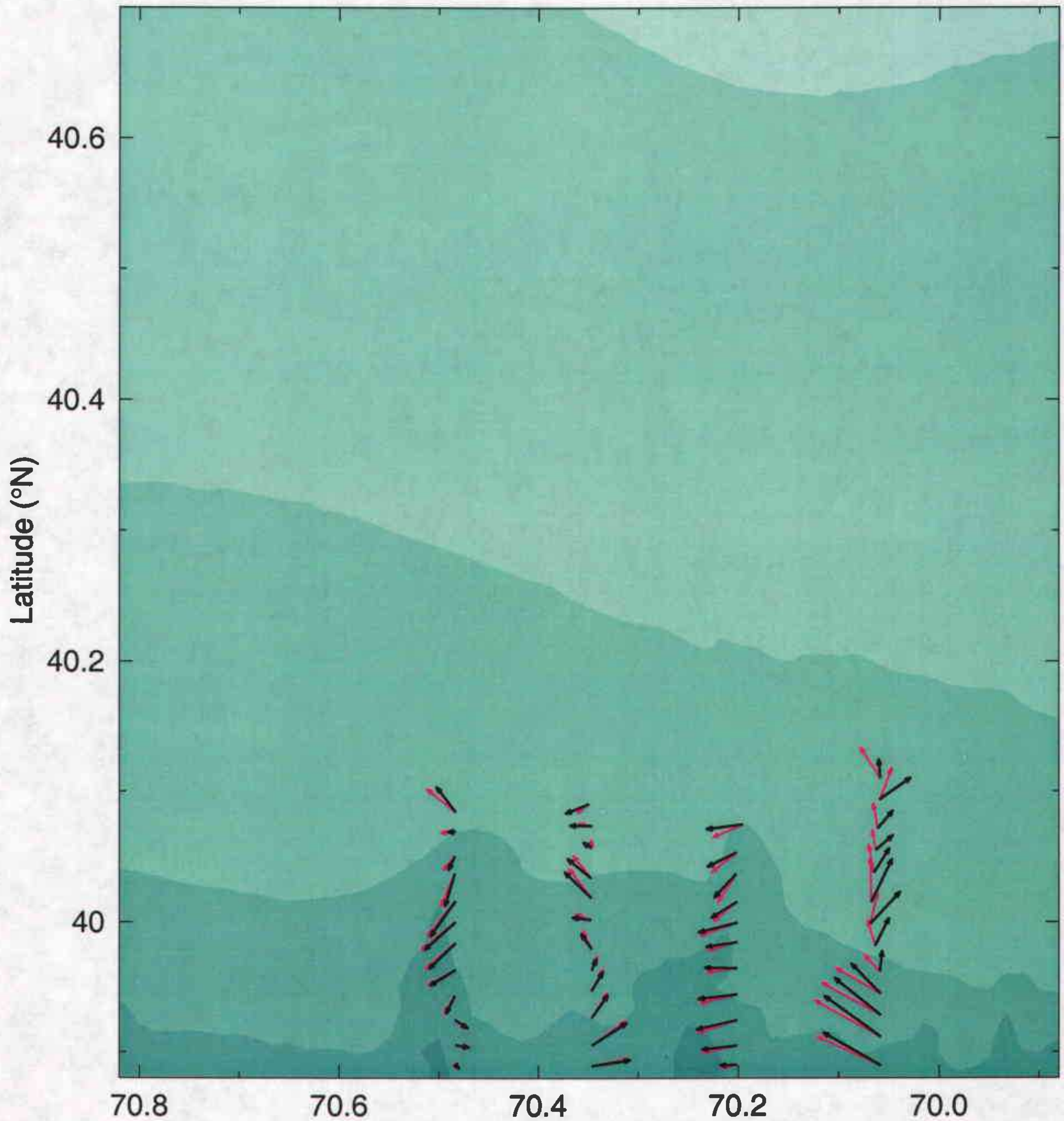

E9608 subtidal east and north velocity sections

E9608 Small Box 1

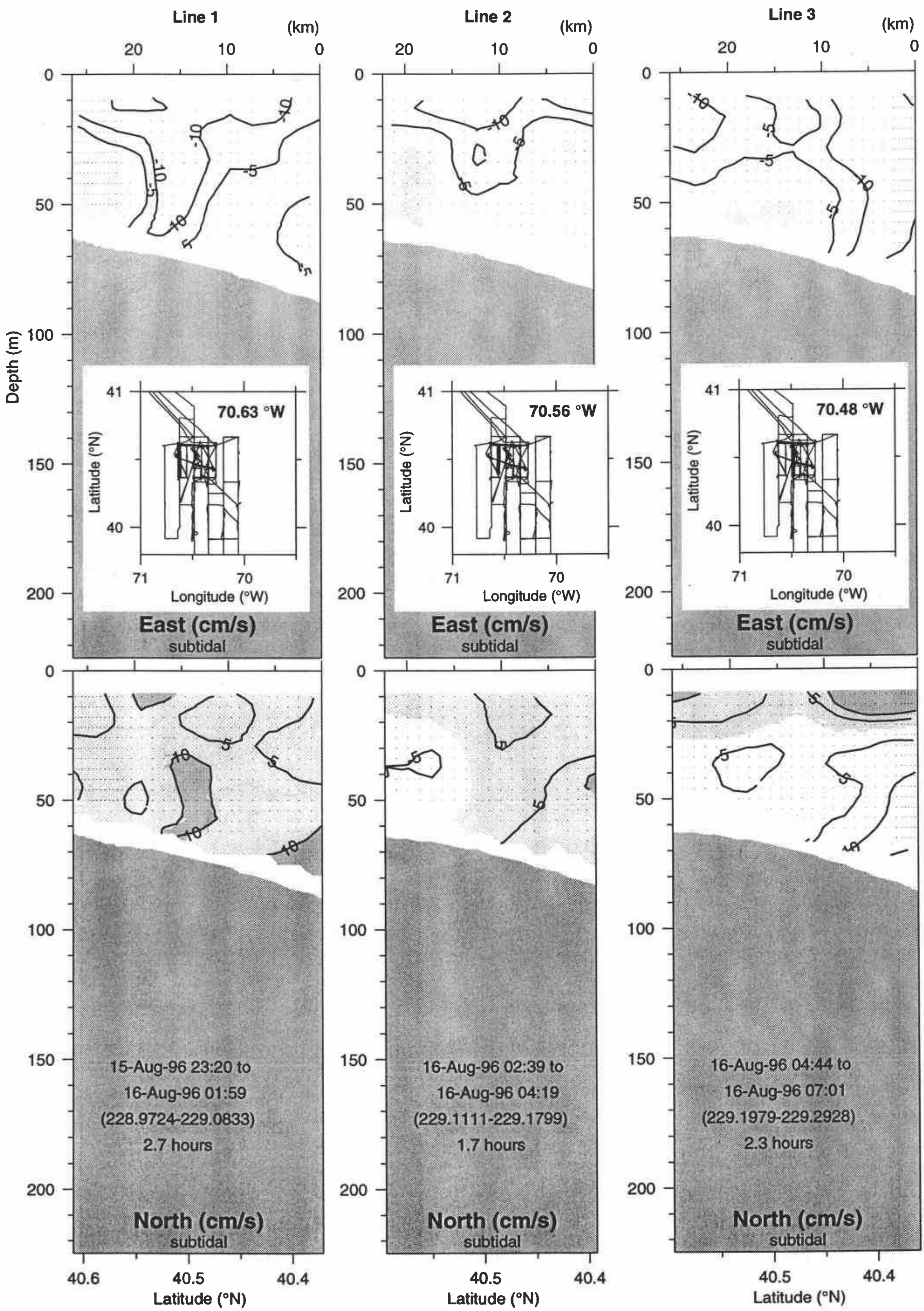

E9608 Small Box 1

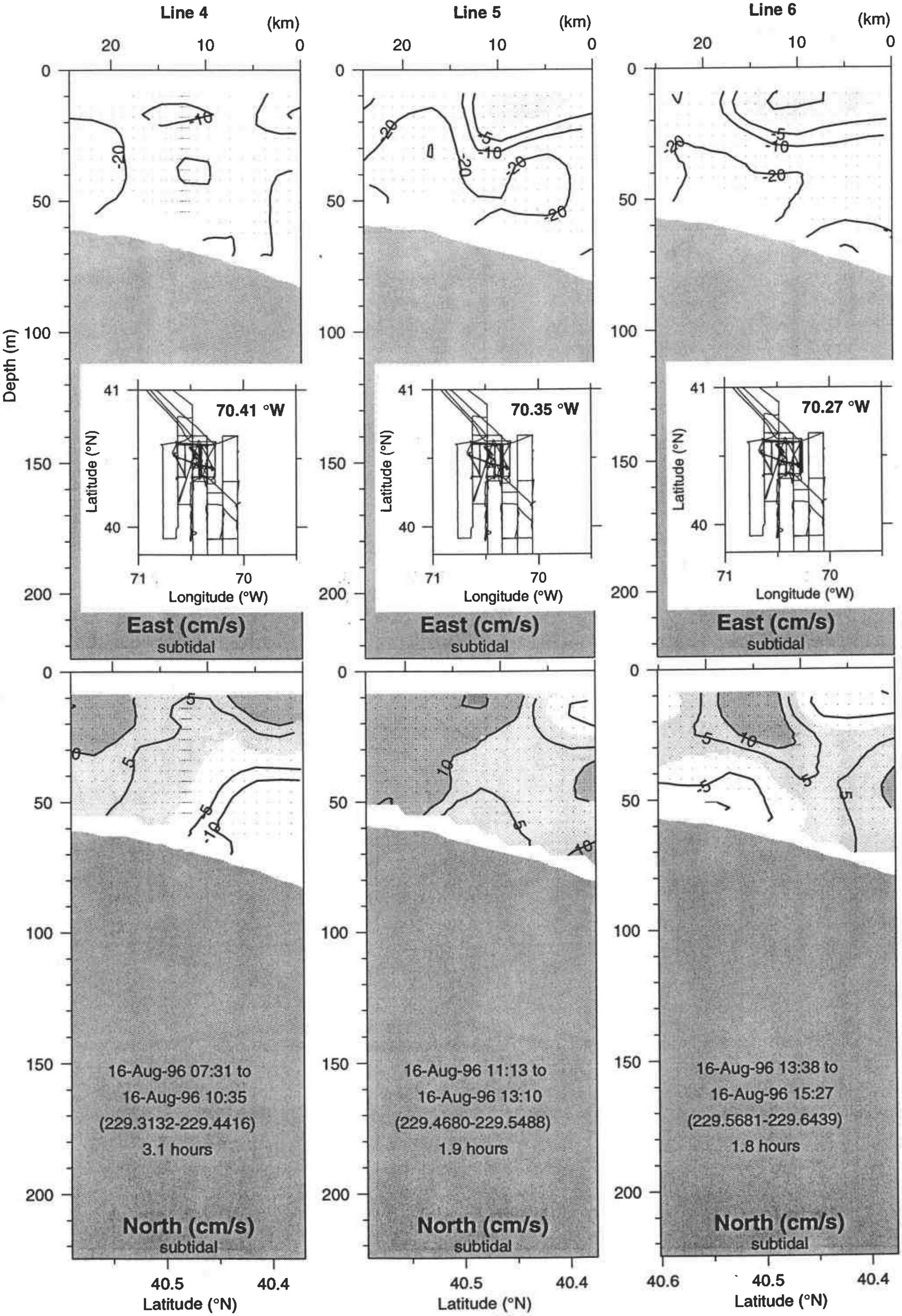

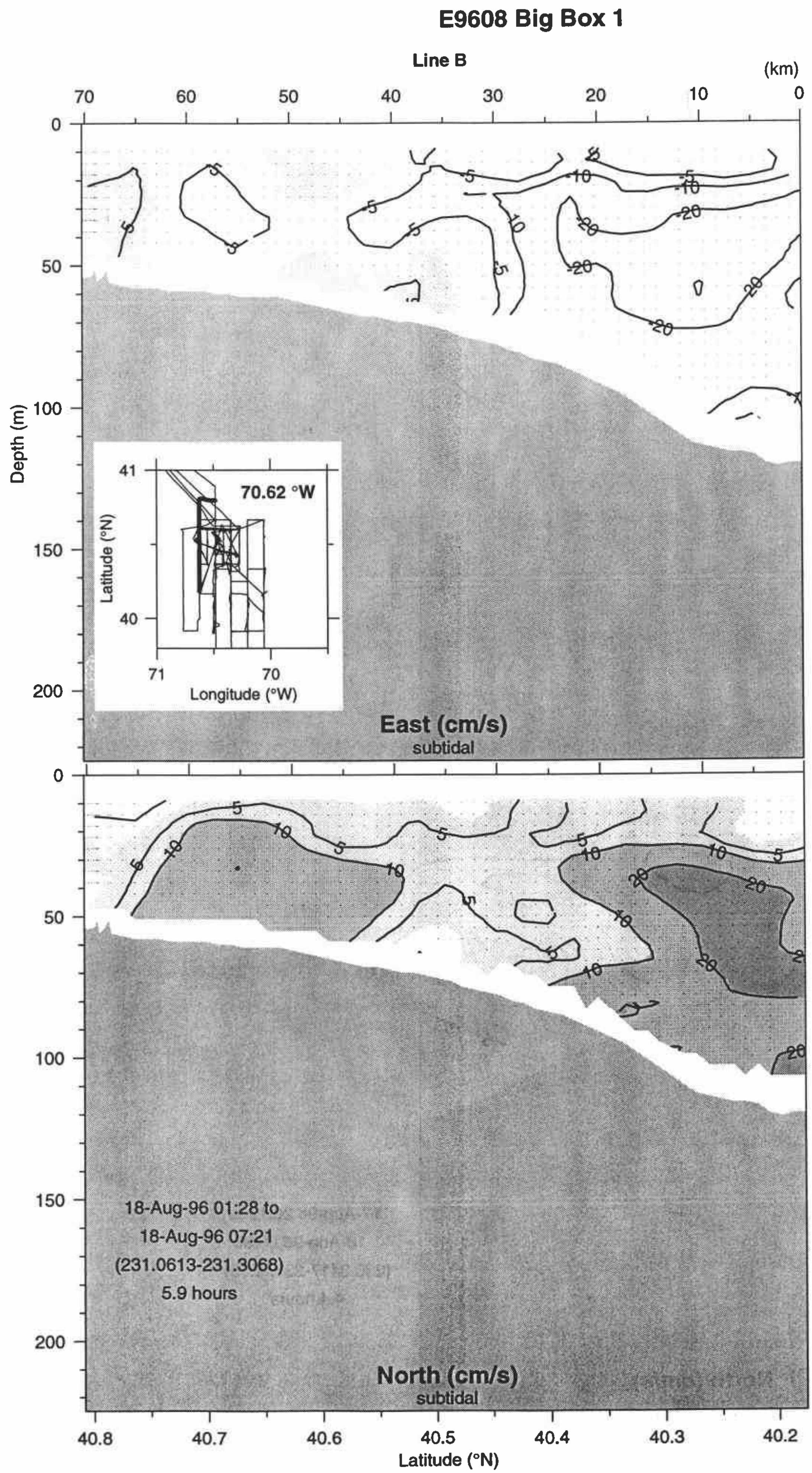
E9608 Big Box 1
Line B
(km)
70
60
50
40
30
20
10
0
Depth (m)
0
50
100
150
200
East (cm/s)
subtidal
70.62 °W
Latitude (°N)
41
40
71
70
Longitude (°W)
North (cm/s)
subtidal
18-Aug-96 01:28 to
18-Aug-96 07:21
(231.0613-231.3068)
5.9 hours
40.8
40.7
40.6
40.5
40.4
40.3
40.2
Latitude (°N)

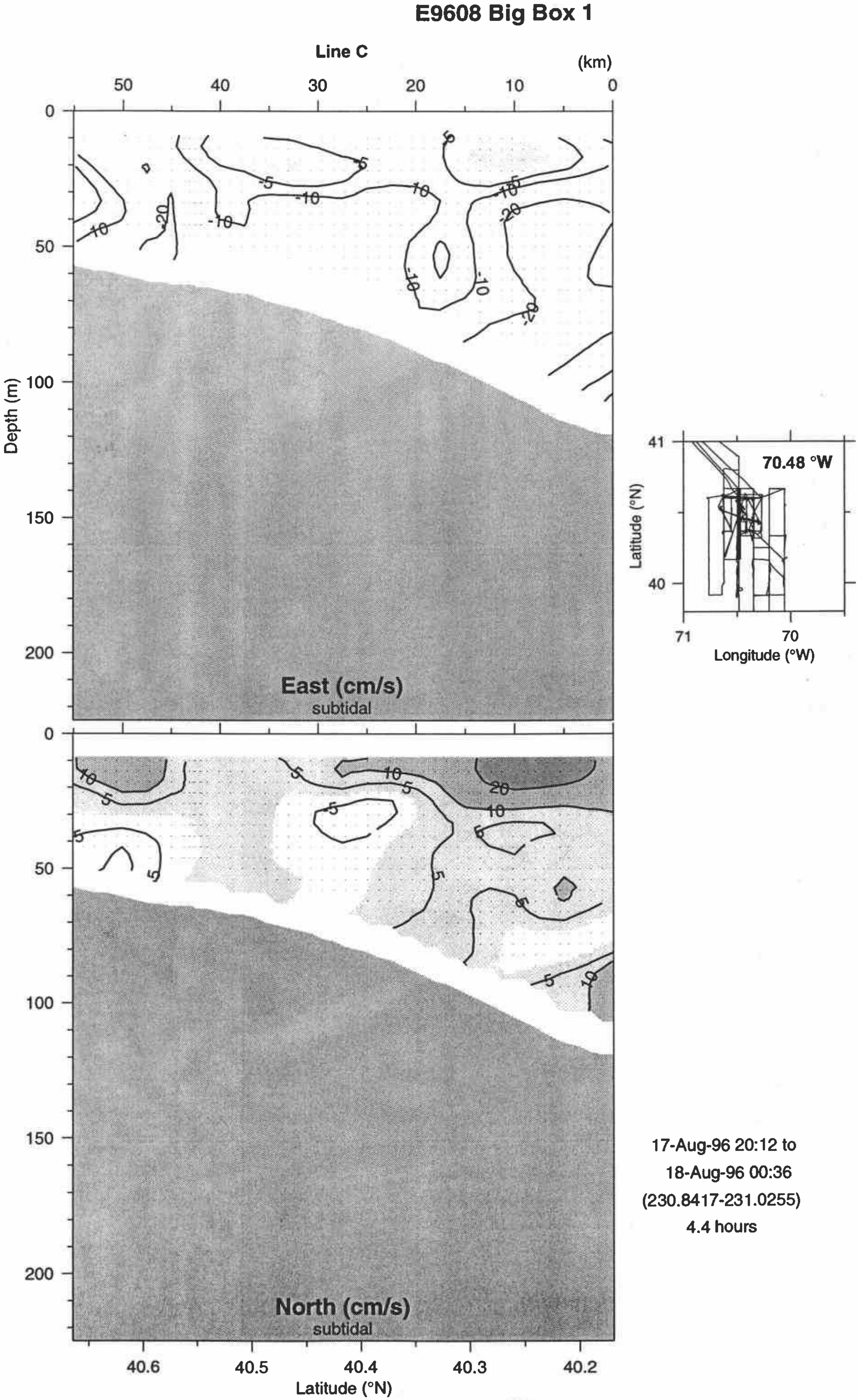

E9608 Big Box 1
Line C
(km)
50 40 30 20 10 0
Depth (m)
0 50 100 150 200
East (cm/s)
subtidal
North (cm/s)
subtidal
40.6 40.5 40.4 40.3 40.2
Latitude (°N)
41 40
Latitude (°N)
70.48 °W
71 70
Longitude (°W)
17-Aug-96 20:12 to
18-Aug-96 00:36
(230.8417-231.0255)
4.4 hours

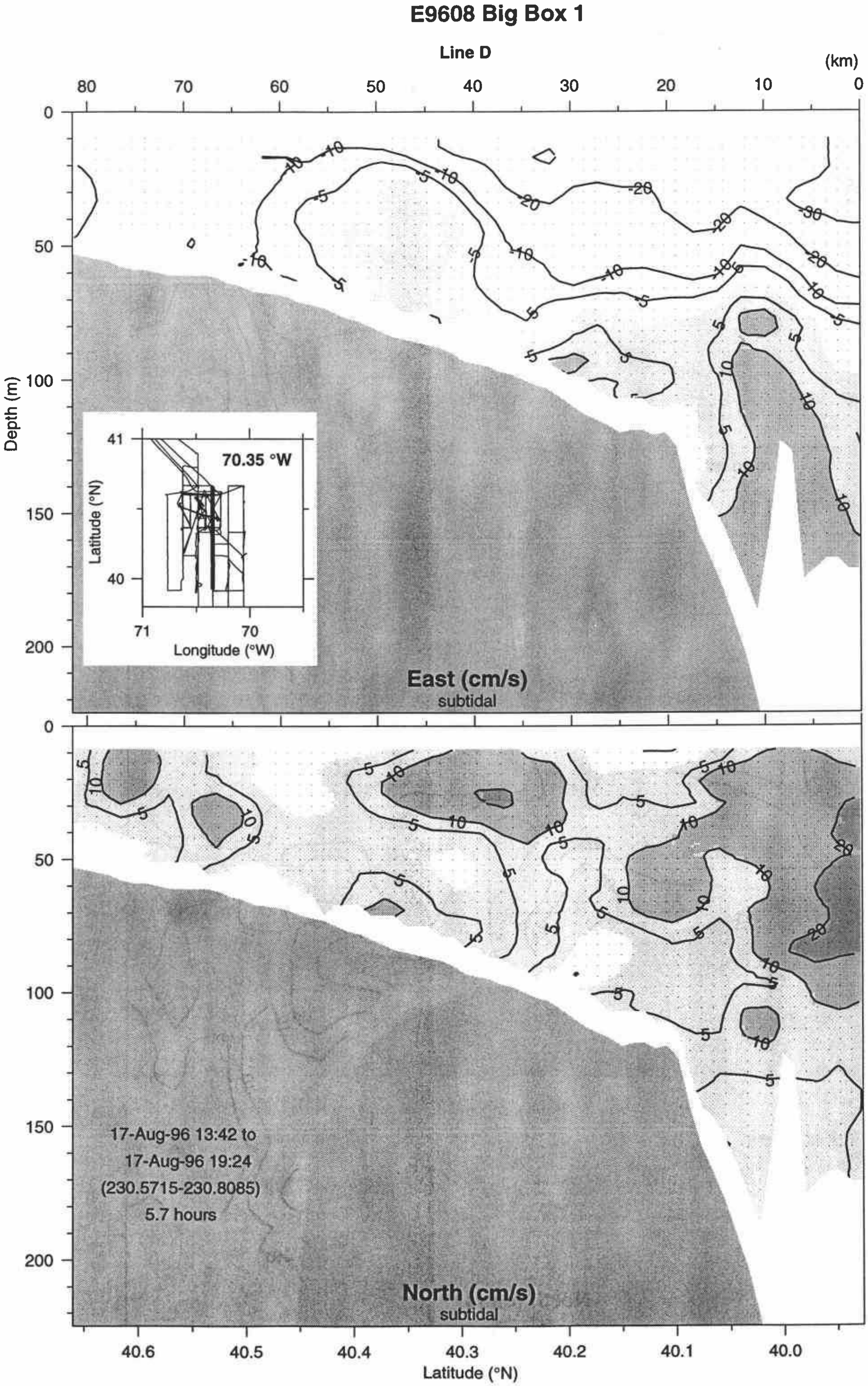
E9608 Big Box 1
Line D
(km)
80
70
60
50
40
30
20
10
0
Depth (m)
East (cm/s)
subtidal
70.35 °W
Latitude (°N)
Longitude (°W)
North (cm/s)
subtidal
17-Aug-96 13:42 to
17-Aug-96 19:24
(230.5715-230.8085)
5.7 hours
Latitude (°N)

E9608 Big Box 1

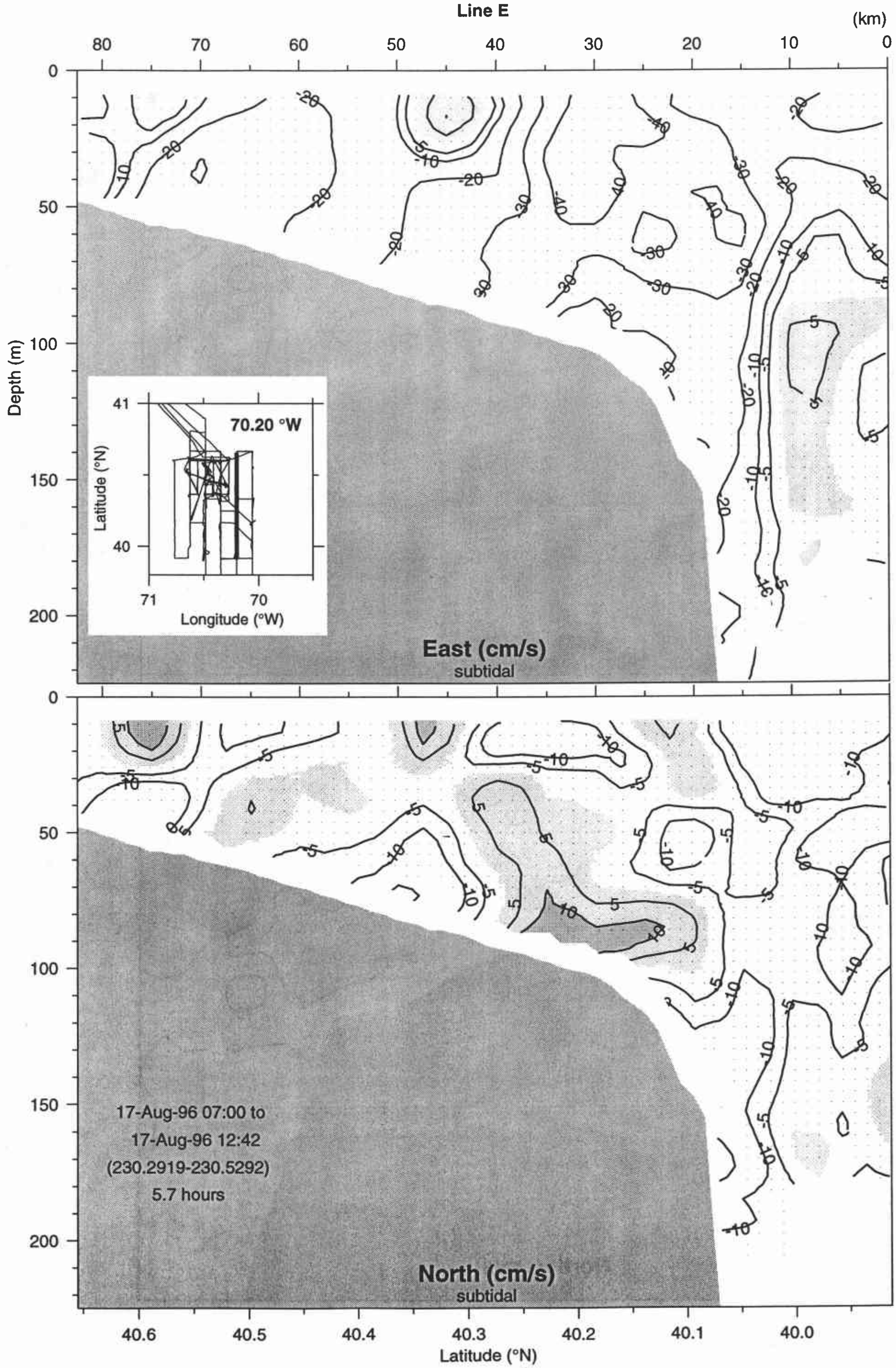

E9608 Big Box 1

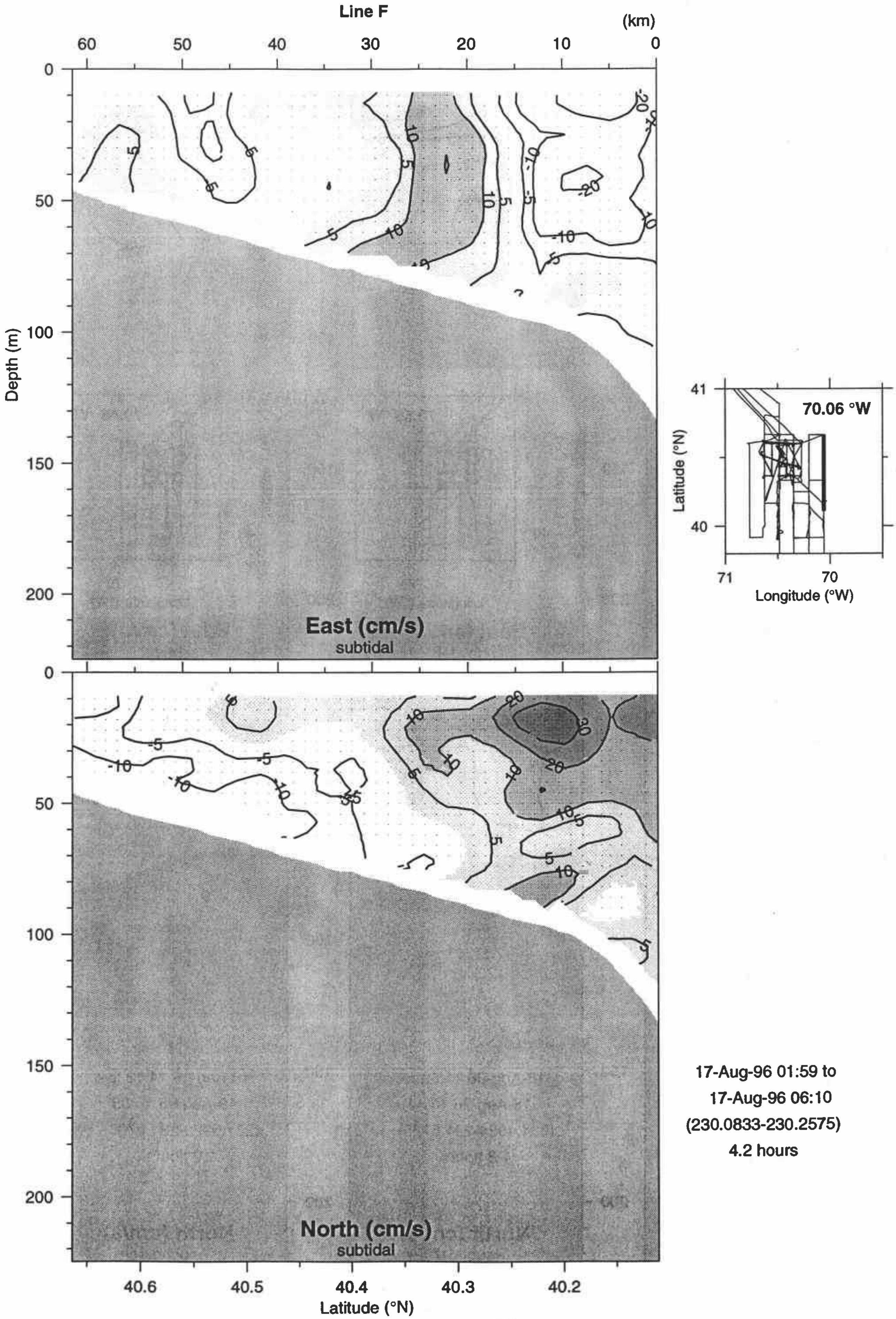

E9608 Small Box 2

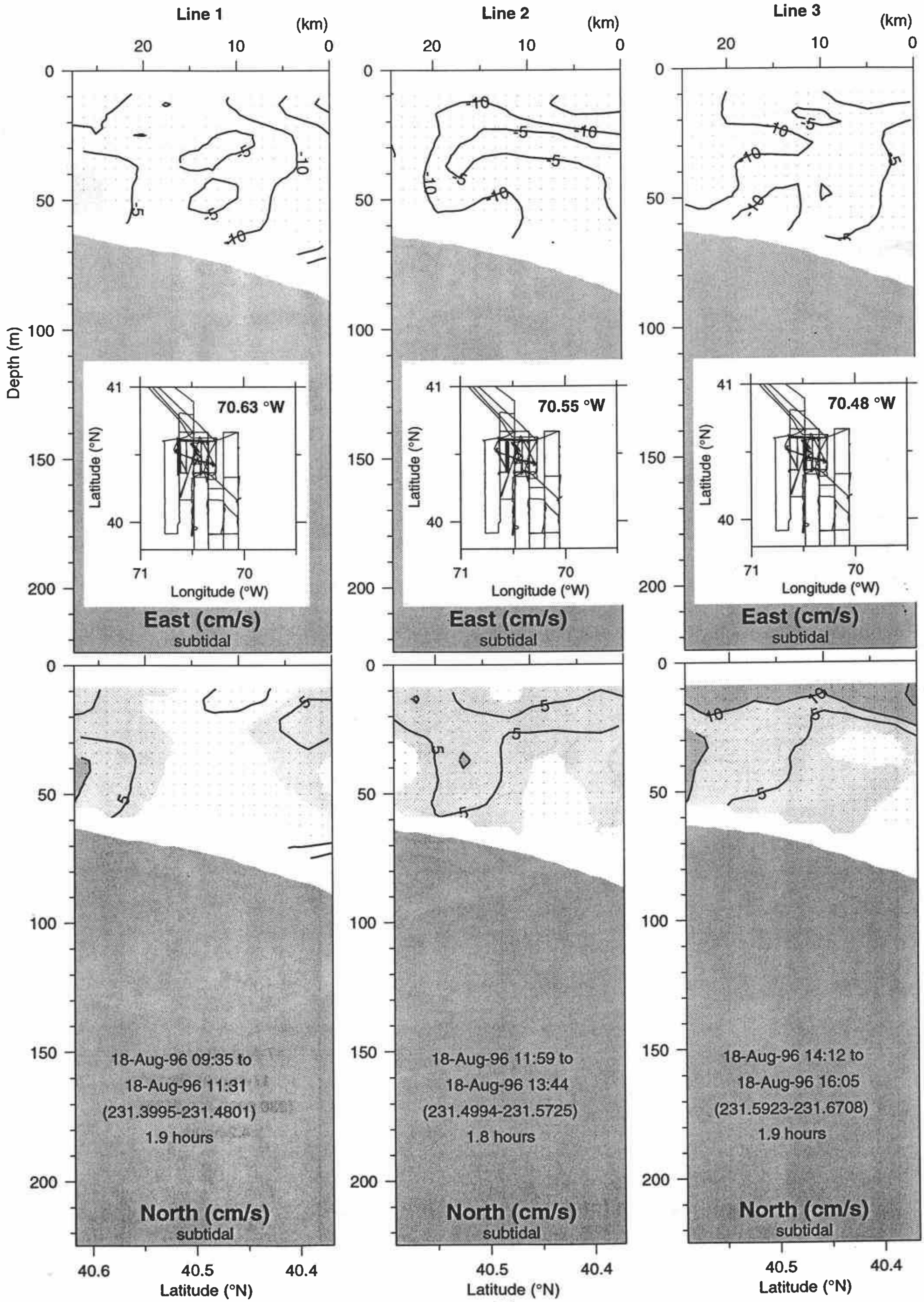

E9608 Small Box 2

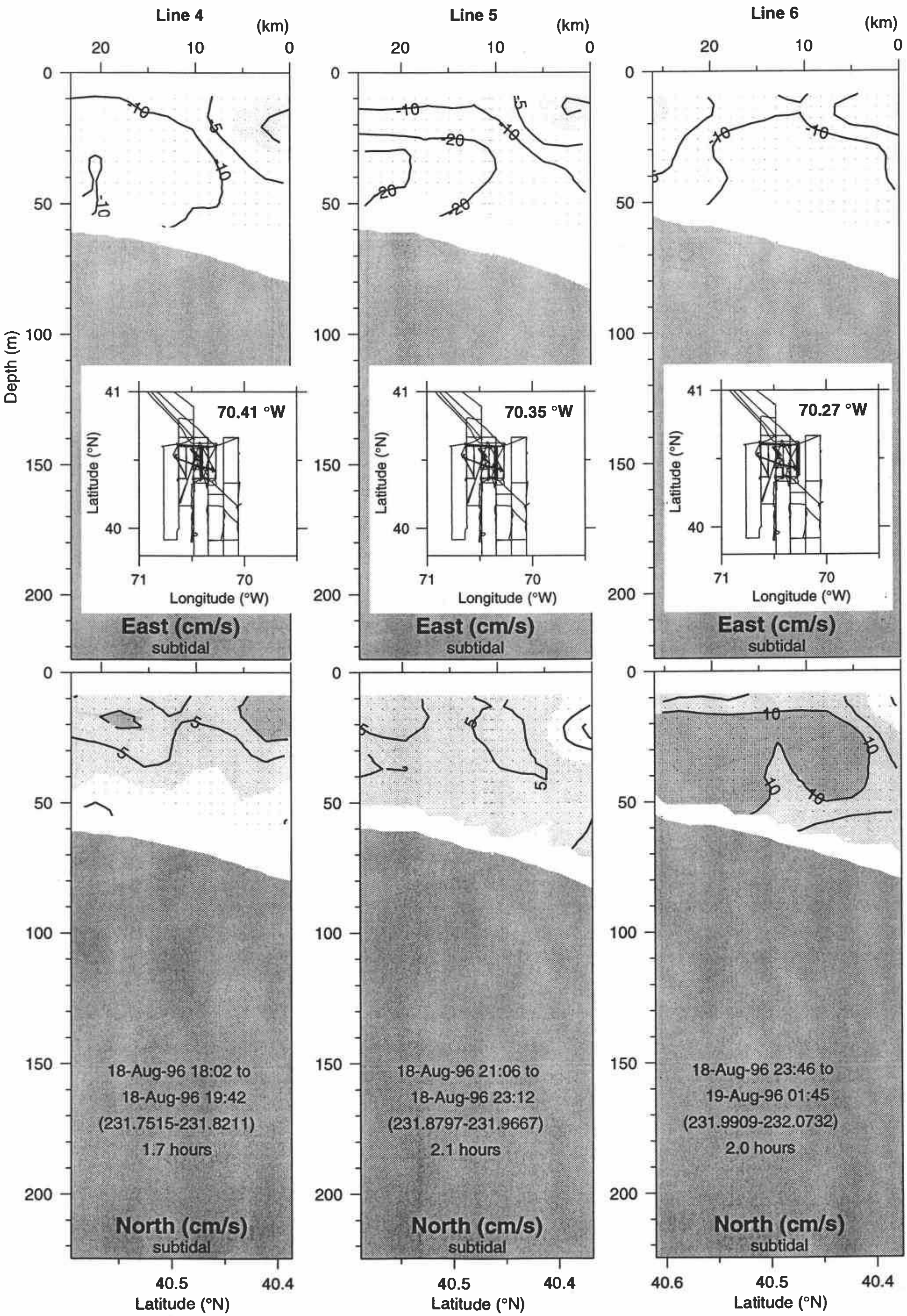

E9608 Small Box 3

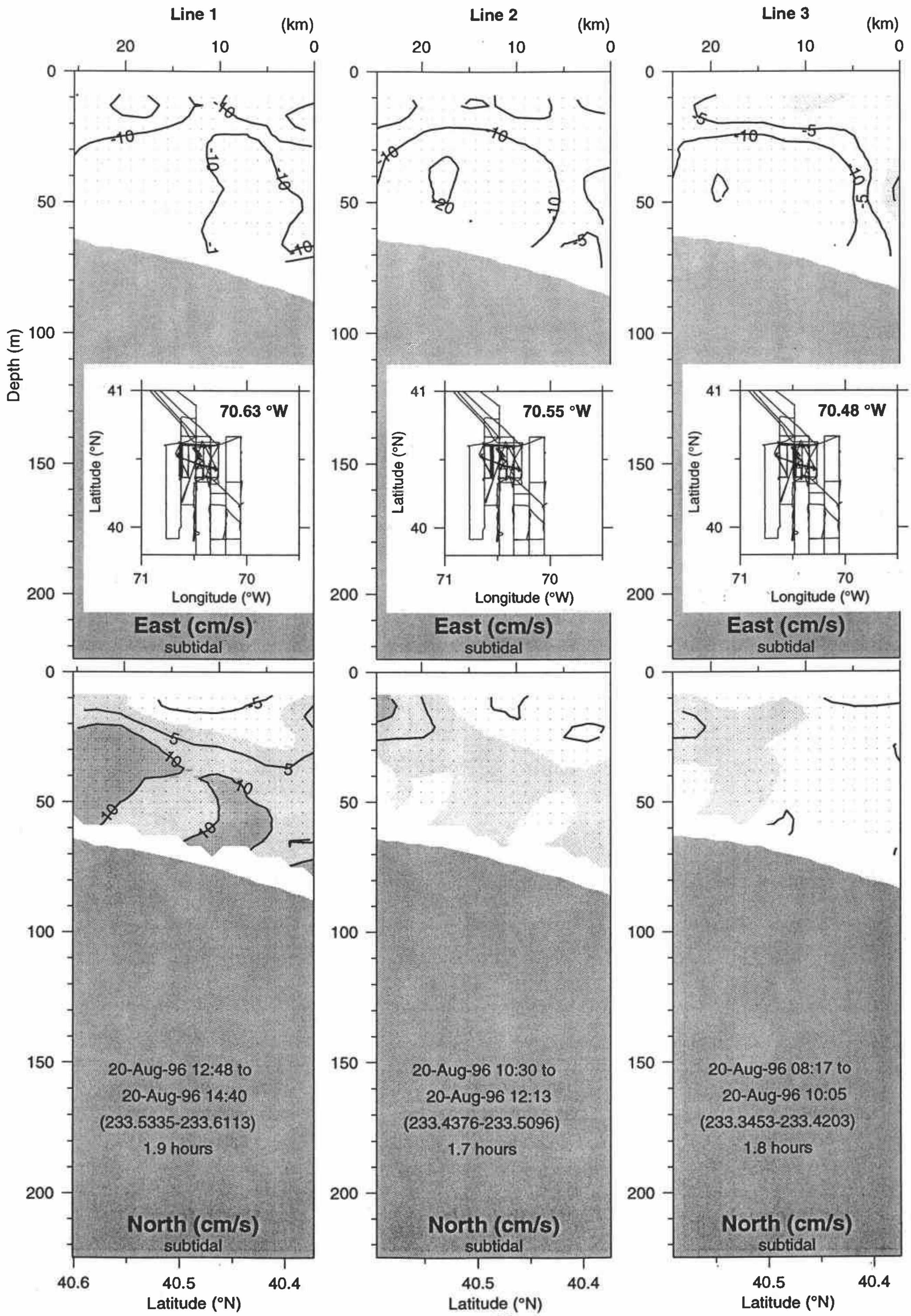

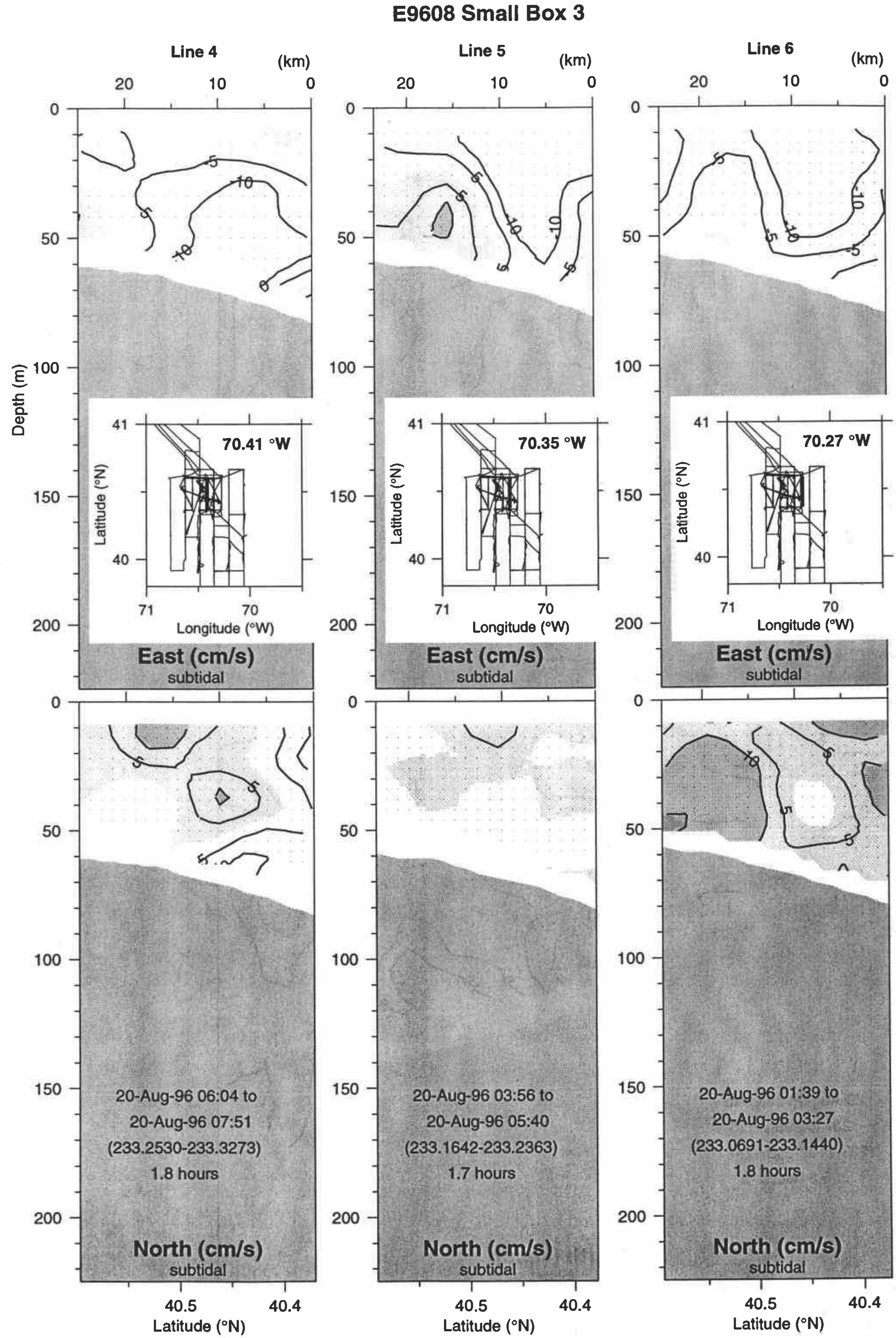
E9608 Small Box 3
Line 4
Line 5
Line 6
(km)
Depth (m)
70.41 °W
70.35 °W
70.27 °W
Latitude (°N)
Longitude (°W)
East (cm/s)
subtidal
North (cm/s)
subtidal
20-Aug-96 06:04 to
20-Aug-96 07:51
(233.2530-233.3273)
1.8 hours
20-Aug-96 03:56 to
20-Aug-96 05:40
(233.1642-233.2363)
1.7 hours
20-Aug-96 01:39 to
20-Aug-96 03:27
(233.0691-233.1440)
1.8 hours
Latitude (°N)

E9608 Big Box 2

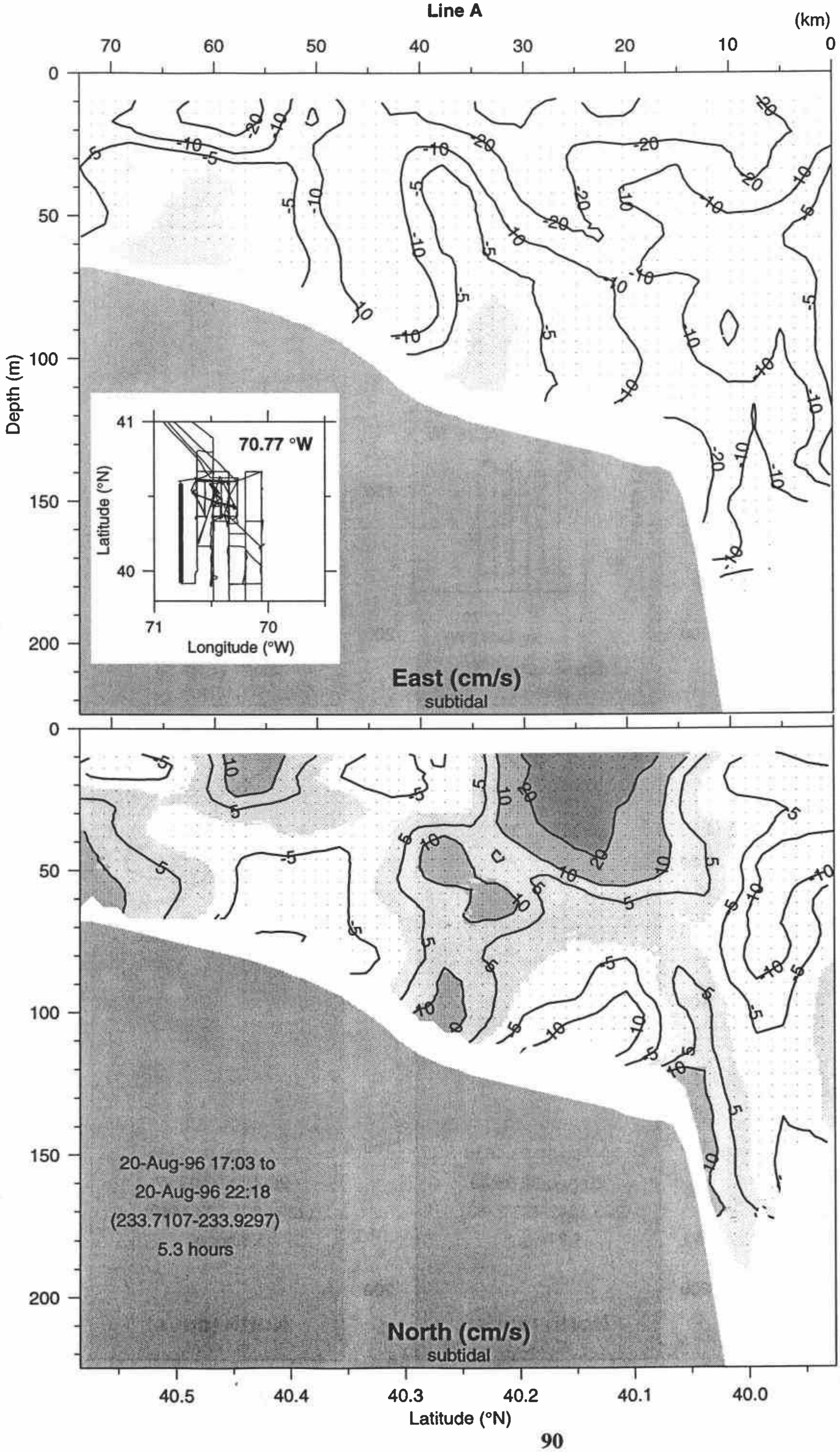

E9608 Big Box 2

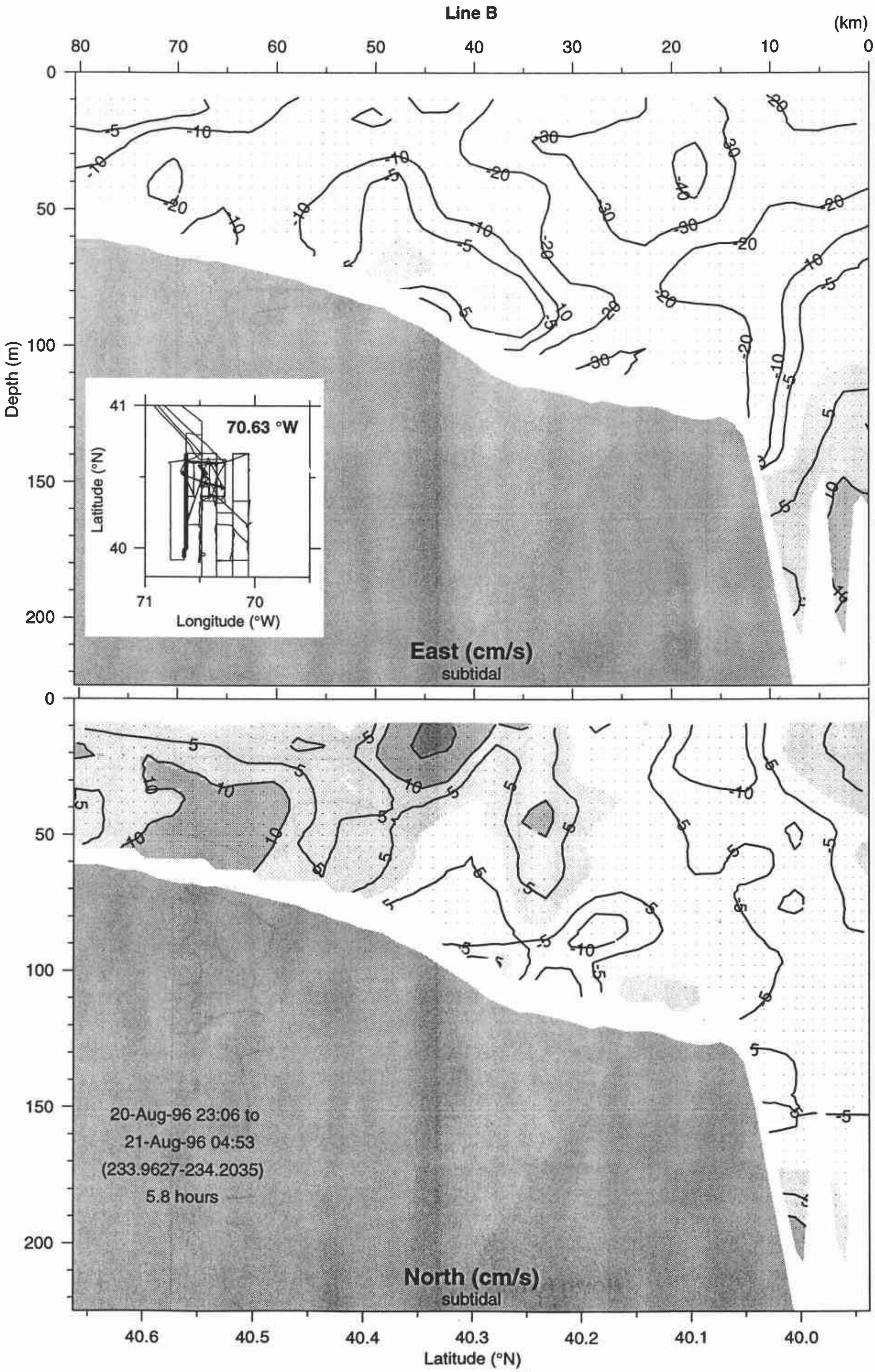

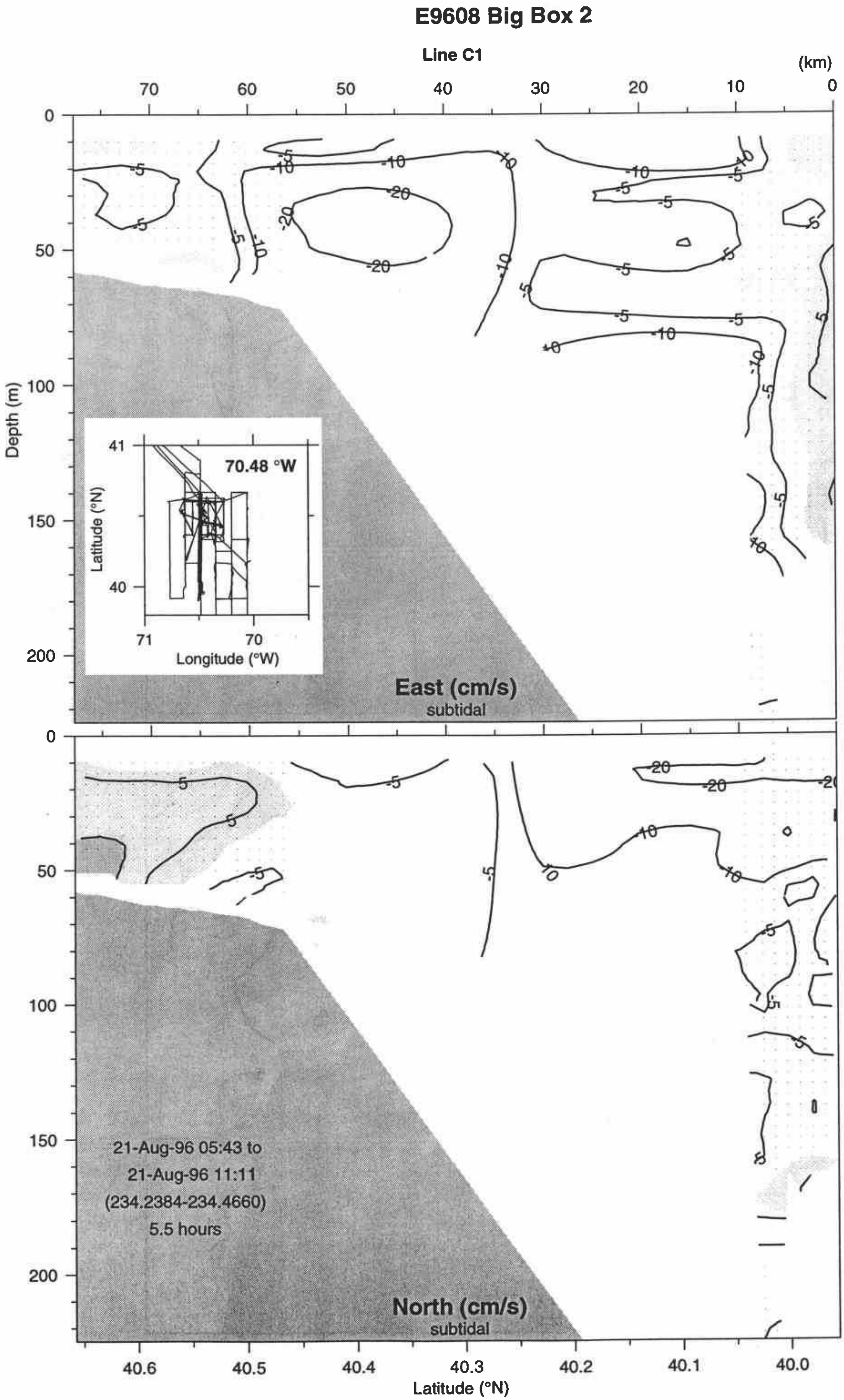
E9608 Big Box 2
Line C1
(km)
70
60
50
40
30
20
10
0
Depth (m)
East (cm/s)
subtidal
North (cm/s)
subtidal
Latitude (°N)
Longitude (°W)
70.48 °W
21-Aug-96 05:43 to
21-Aug-96 11:11
(234.2384-234.4660)
5.5 hours
Latitude (°N)

E9608 Big Box 2

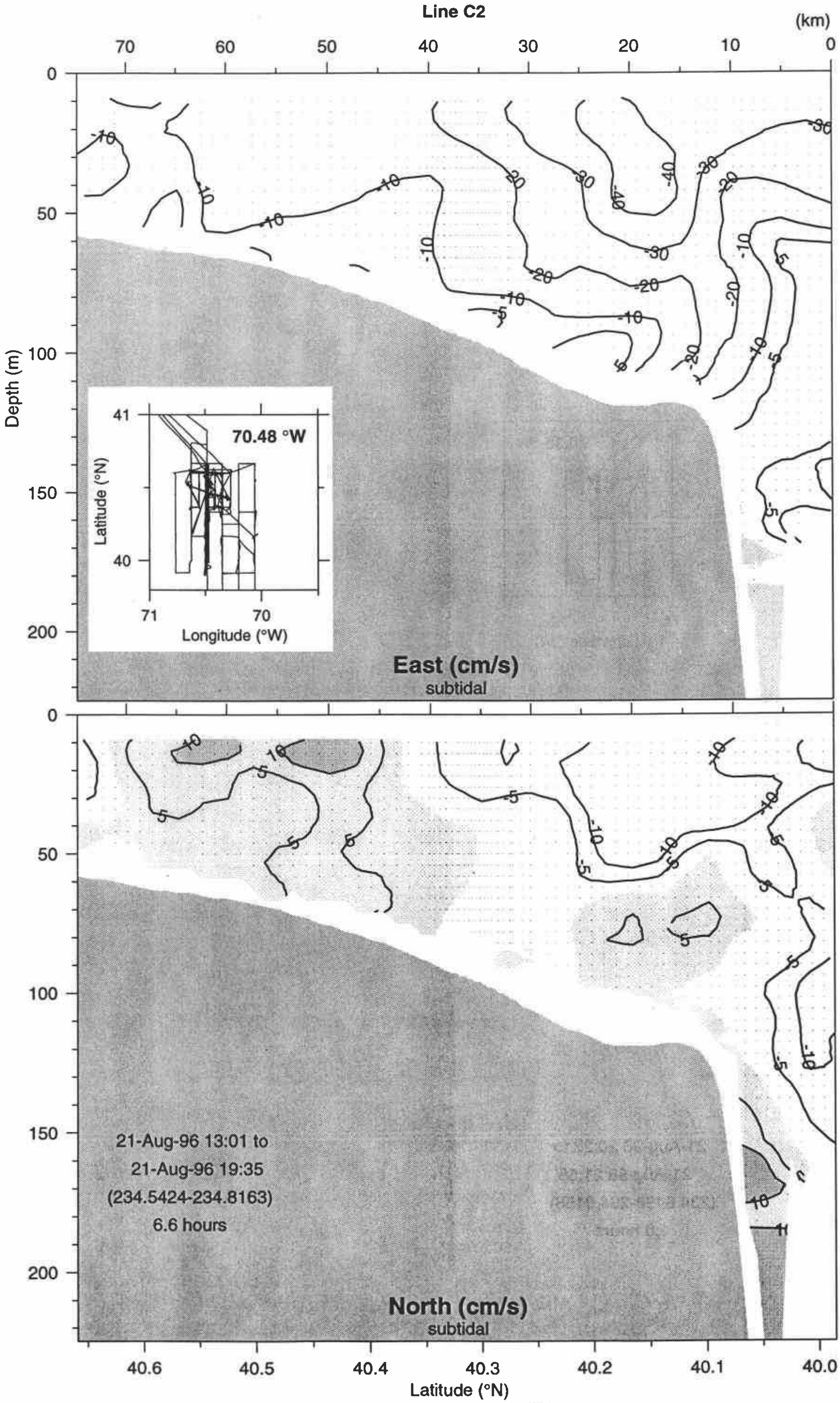

E9608 Big Box 2

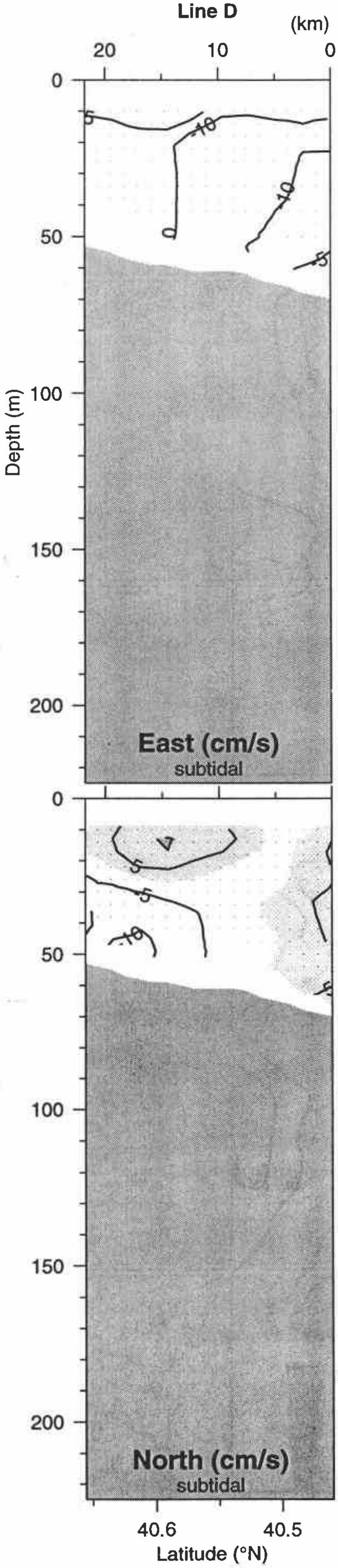

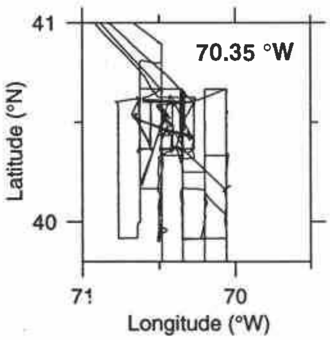

21-Aug-96 20:23 to
21-Aug-96 21:58
(234.8498-234.9158)
1.6 hours

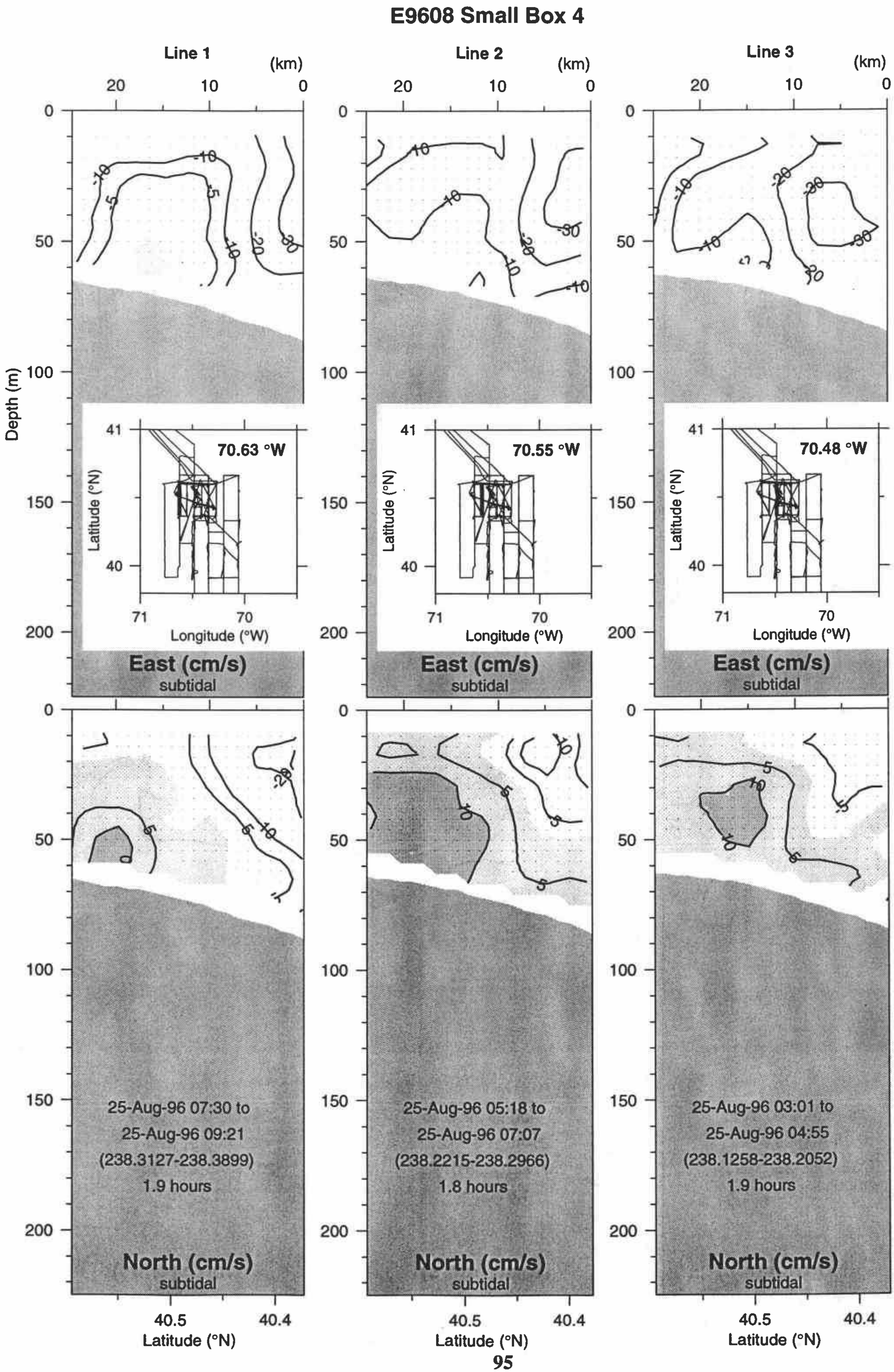
E9608 Small Box 4
Line 1
Line 2
Line 3
(km)
Depth (m)
70.63 °W
70.55 °W
70.48 °W
Latitude (°N)
Longitude (°W)
East (cm/s)
subtidal
North (cm/s)
subtidal
25-Aug-96 07:30 to
25-Aug-96 09:21
(238.3127-238.3899)
1.9 hours
25-Aug-96 05:18 to
25-Aug-96 07:07
(238.2215-238.2966)
1.8 hours
25-Aug-96 03:01 to
25-Aug-96 04:55
(238.1258-238.2052)
1.9 hours
Latitude (°N)

E9608 Small Box 4

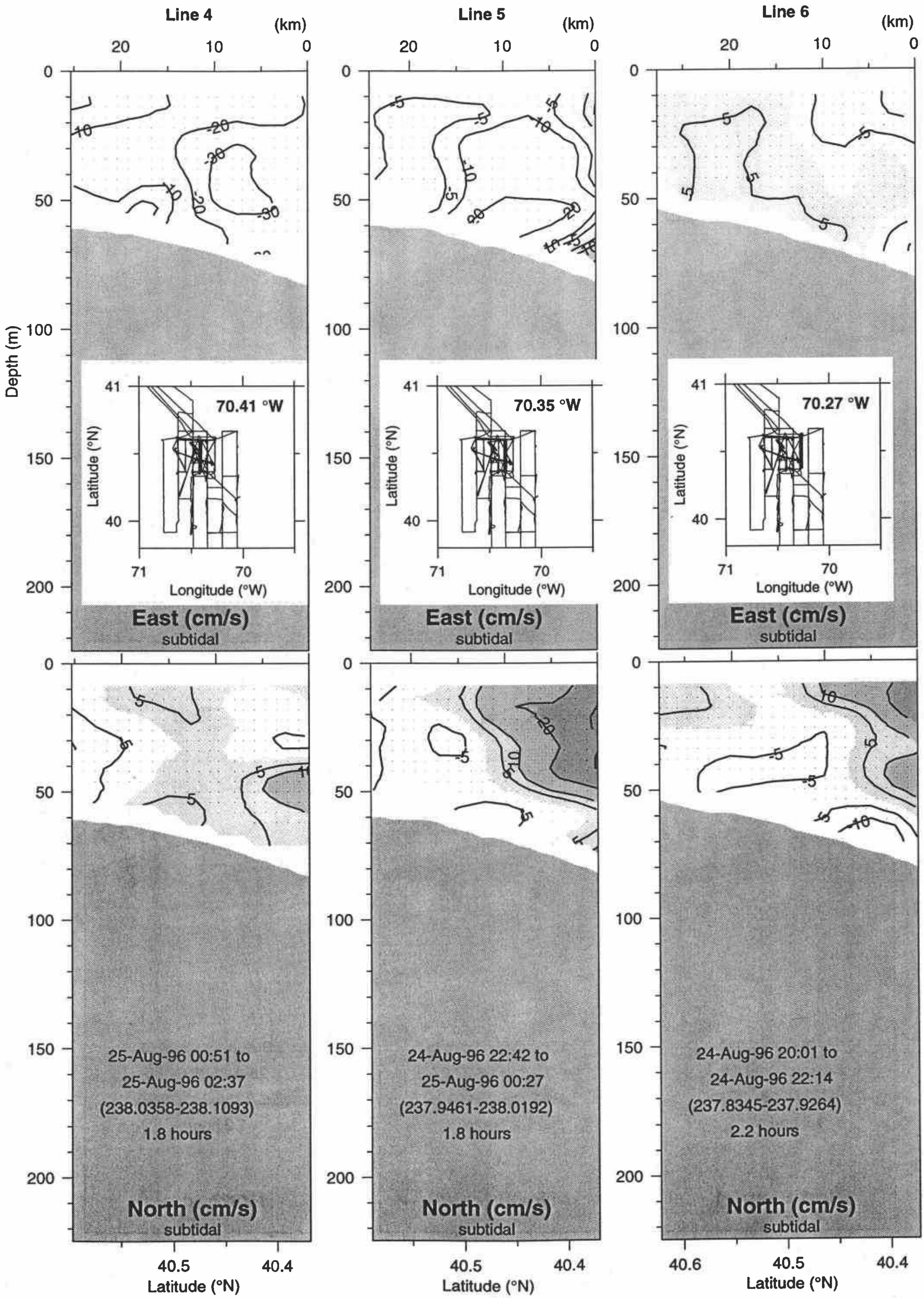

E9608 Small Box 5

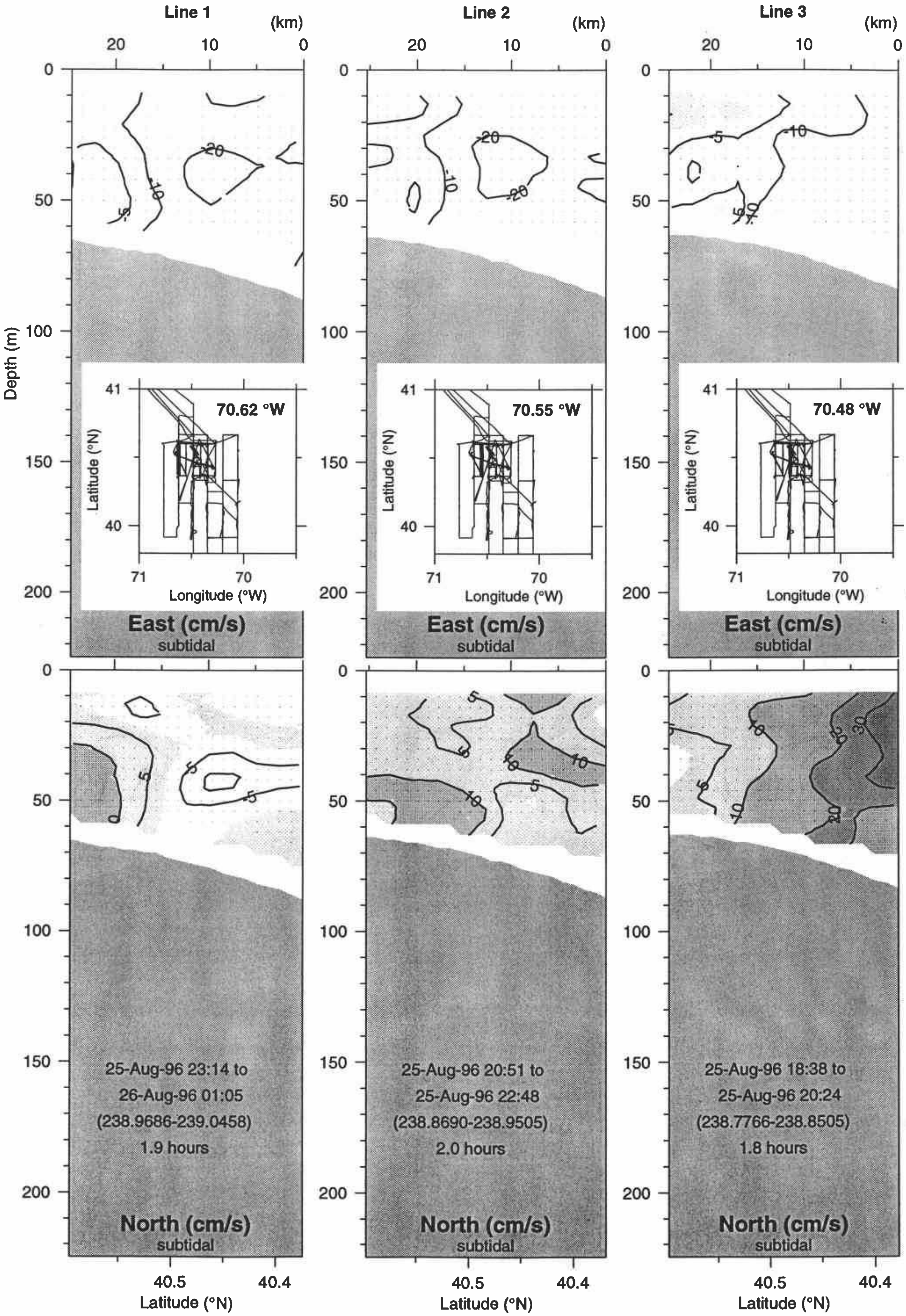

E9608 Small Box 5

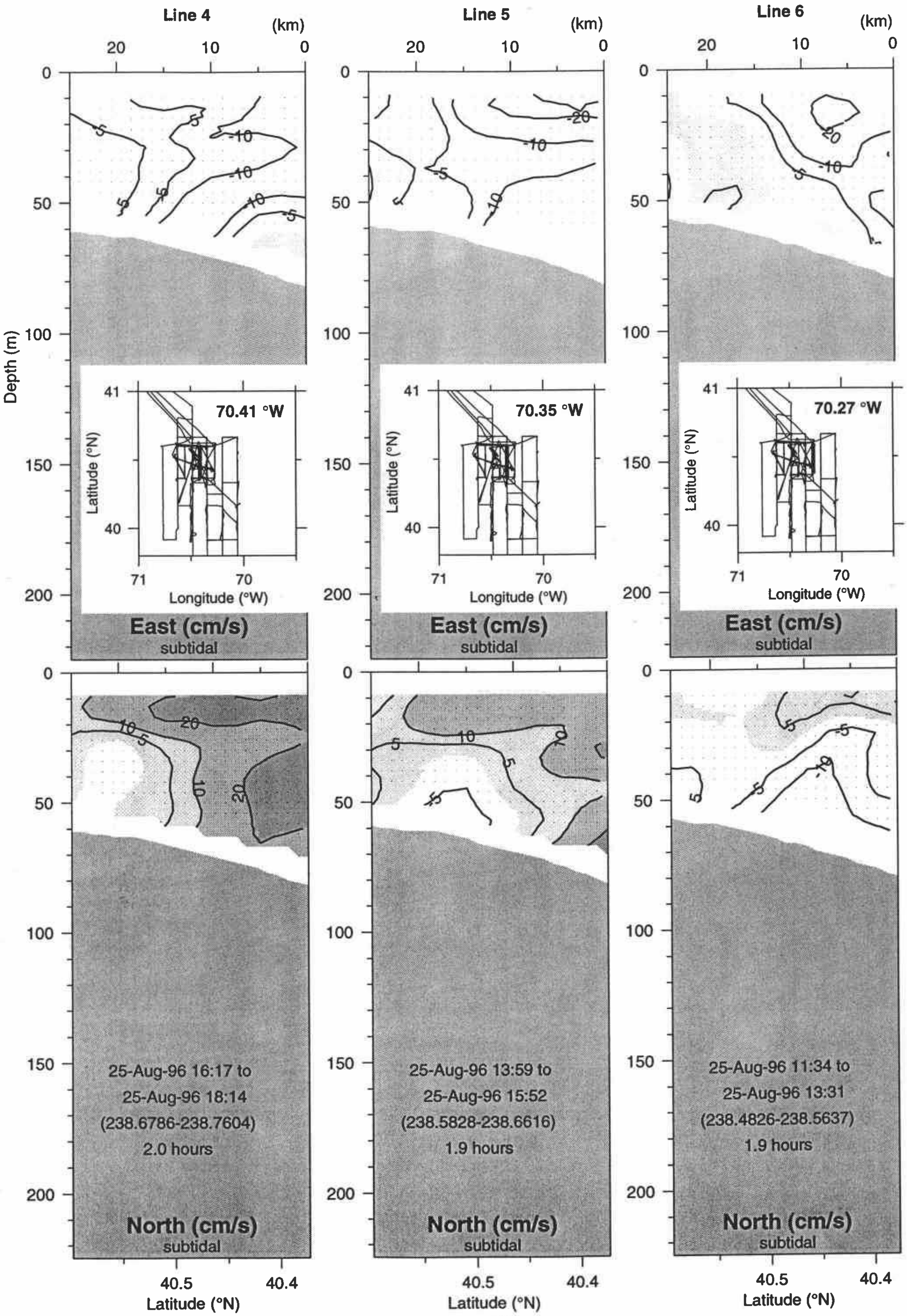

E9608 Small Box 6

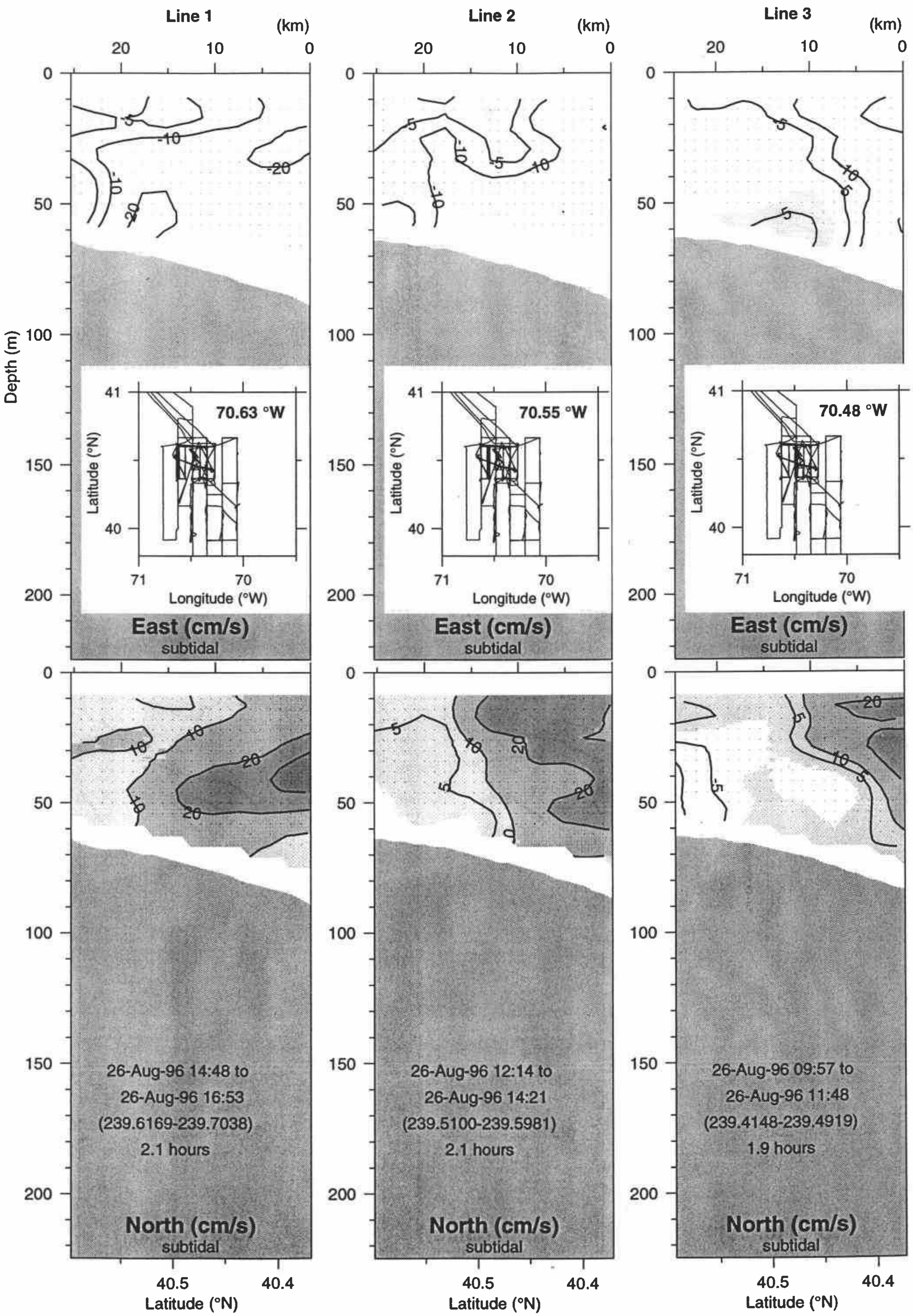

E9608 Small Box 6

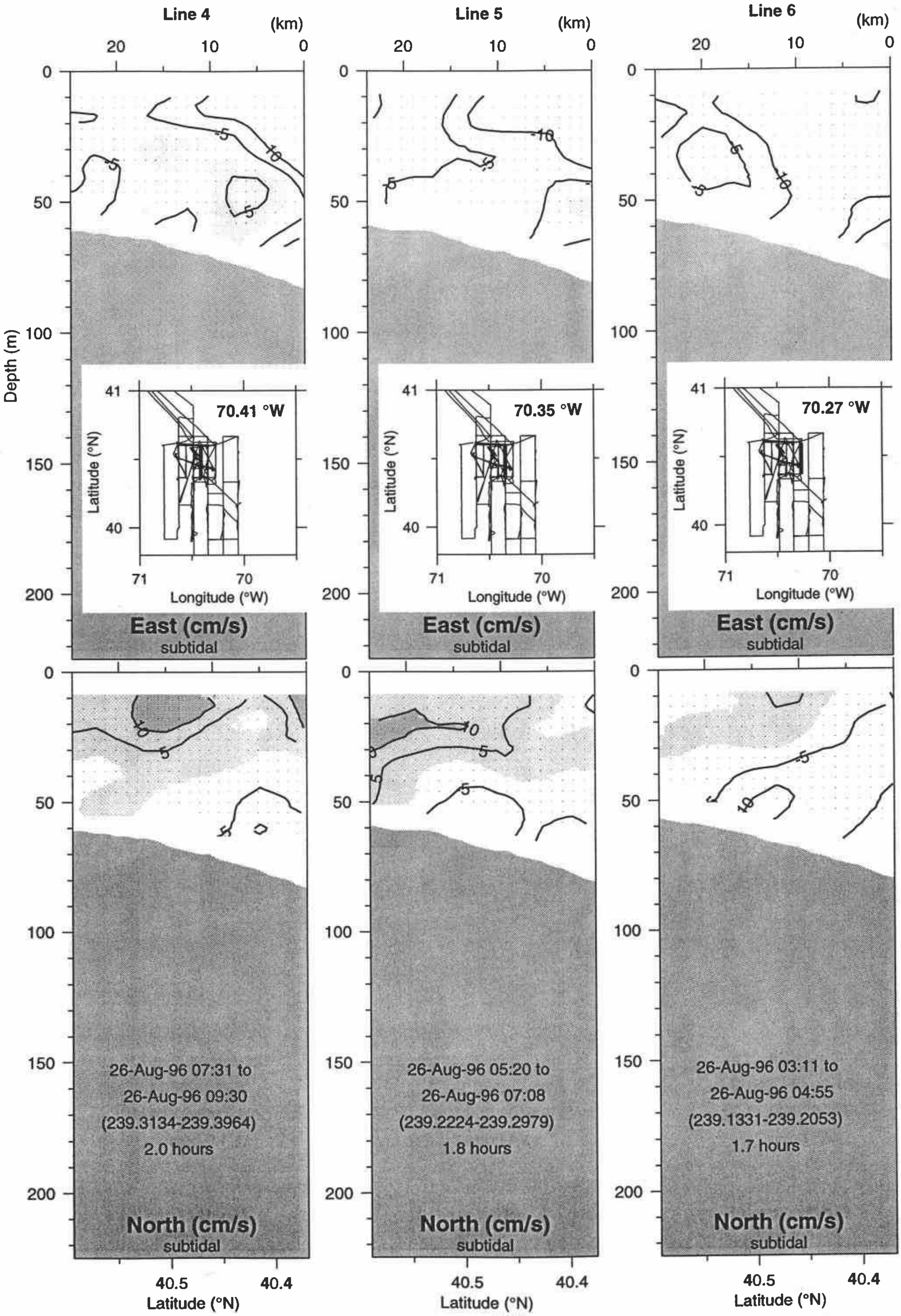

E9608 Butterfly 1

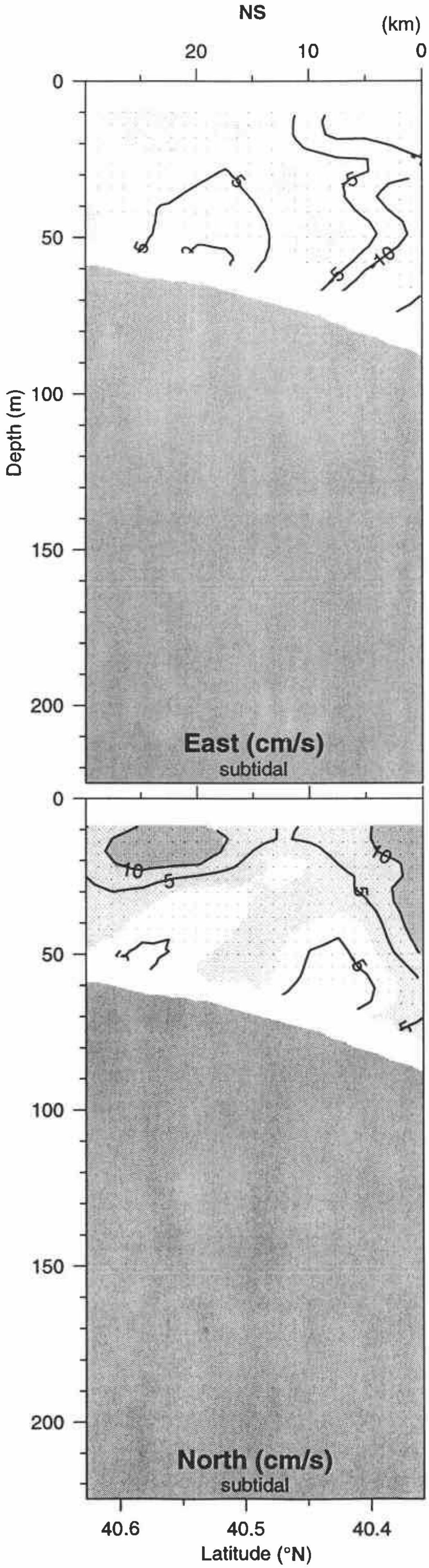

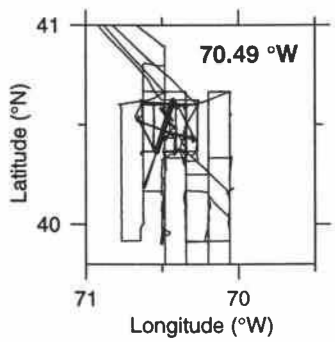

27-Aug-96 07:16 to
27-Aug-96 09:46
(240.3029-240.4072)
2.5 hours

E9608 Butterfly 2

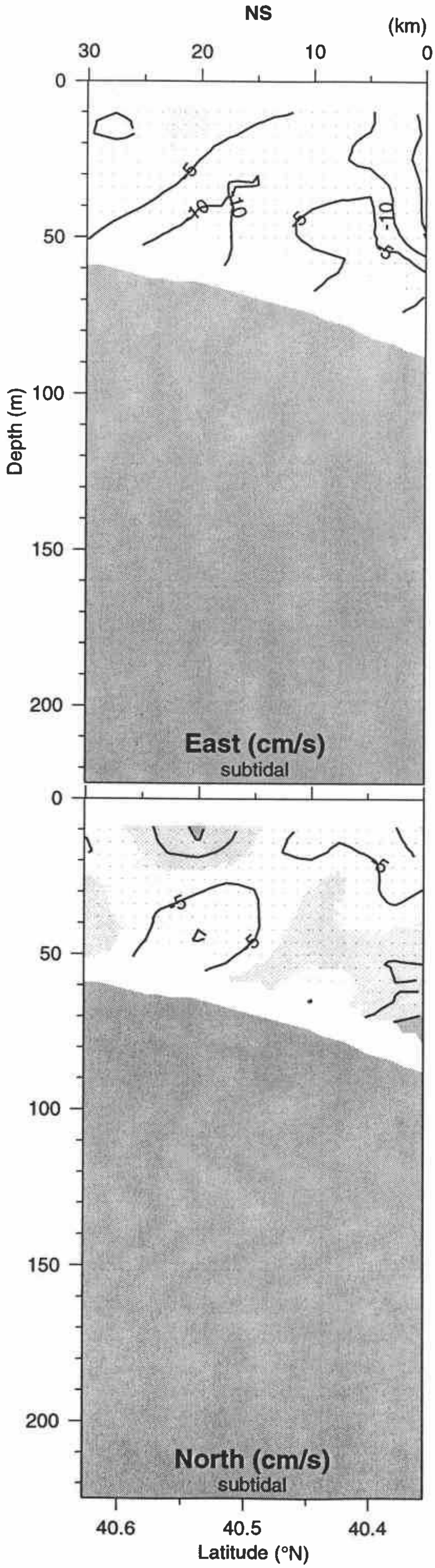

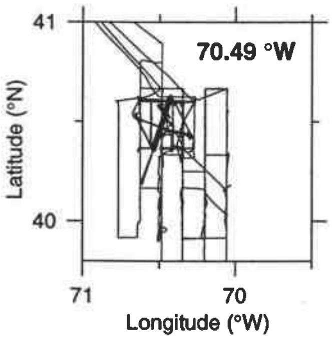

27-Aug-96 17:31 to
27-Aug-96 20:00
(240.7299-240.8335)
2.5 hours

E9608 Butterfly 3

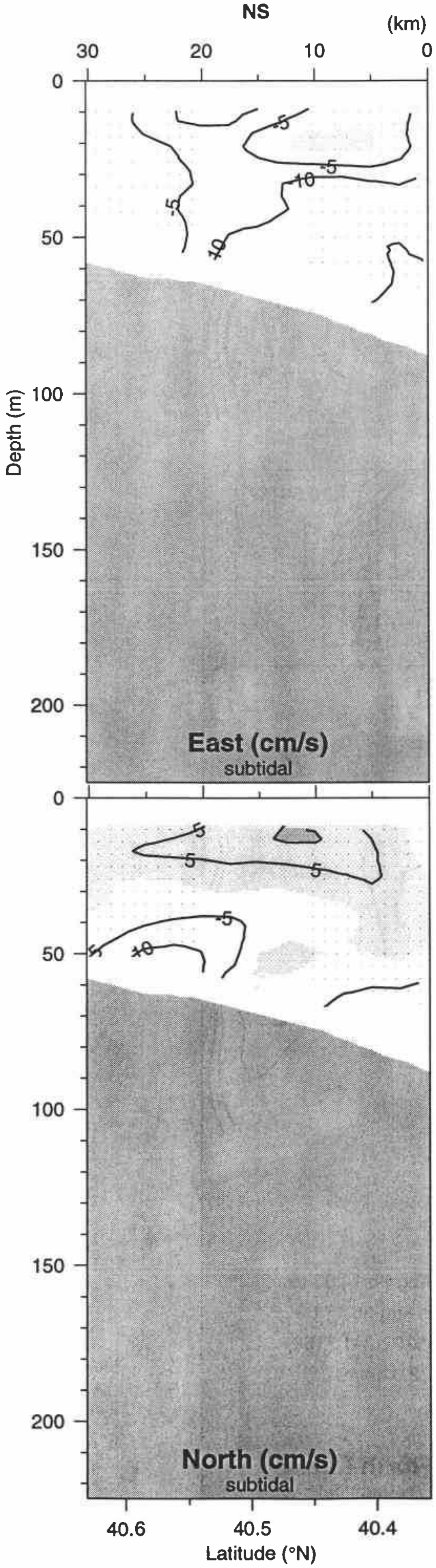

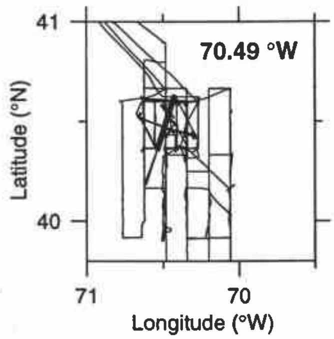

28-Aug-96 04:49 to
28-Aug-96 07:19
(241.2007-241.3052)
2.5 hours

E9608 Butterfly 4

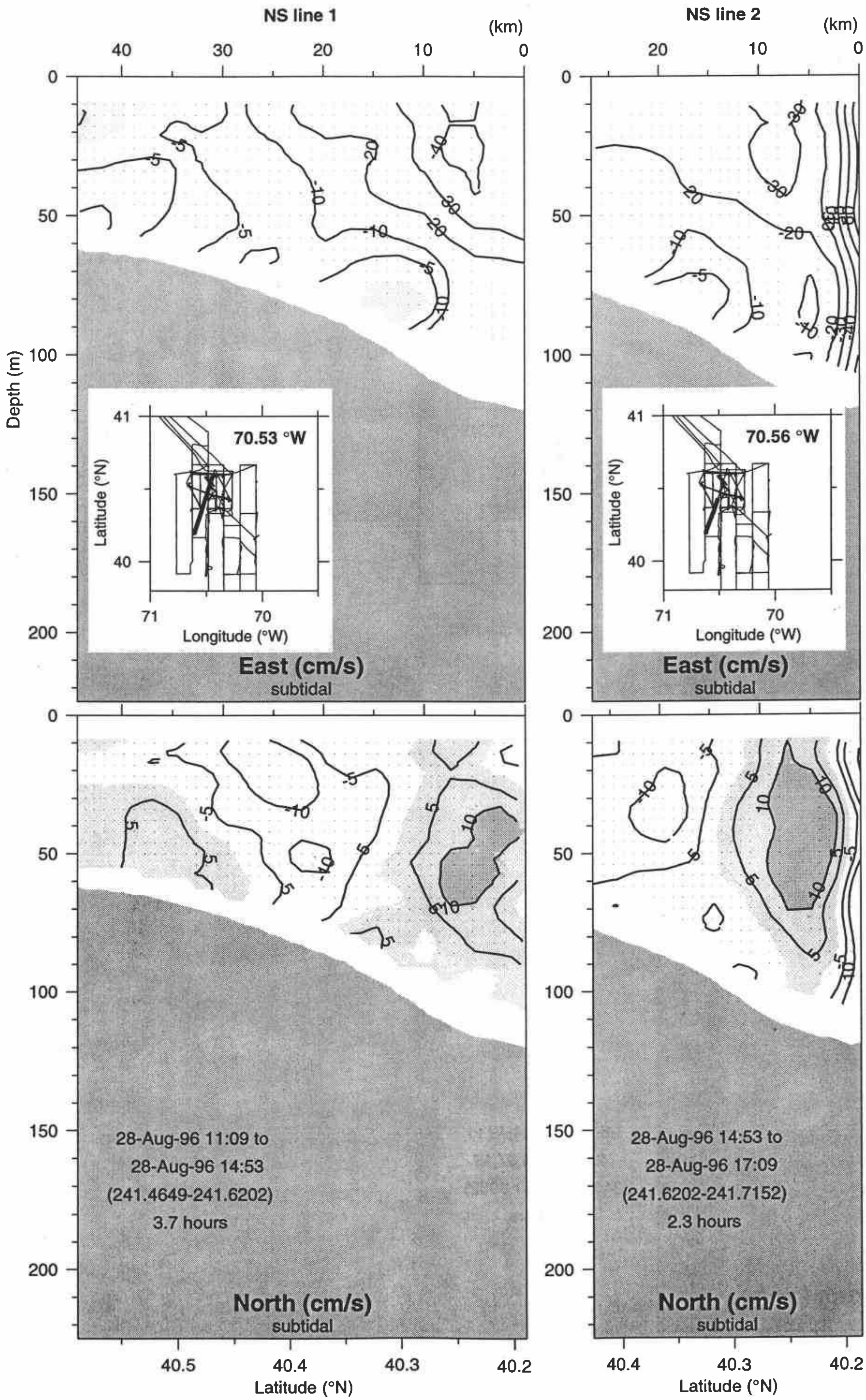

E9608 Small Box 7

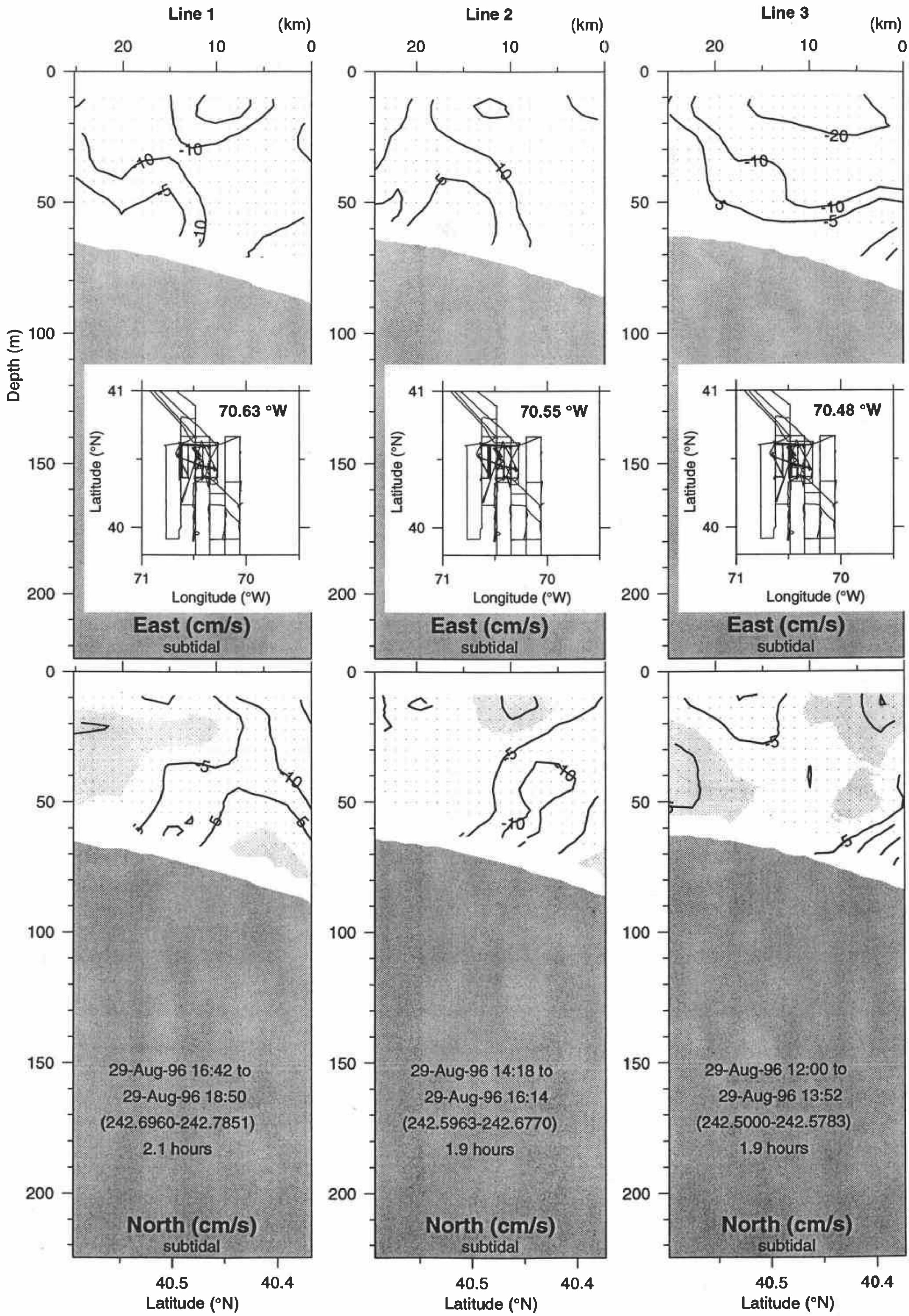

E9608 Small Box 7

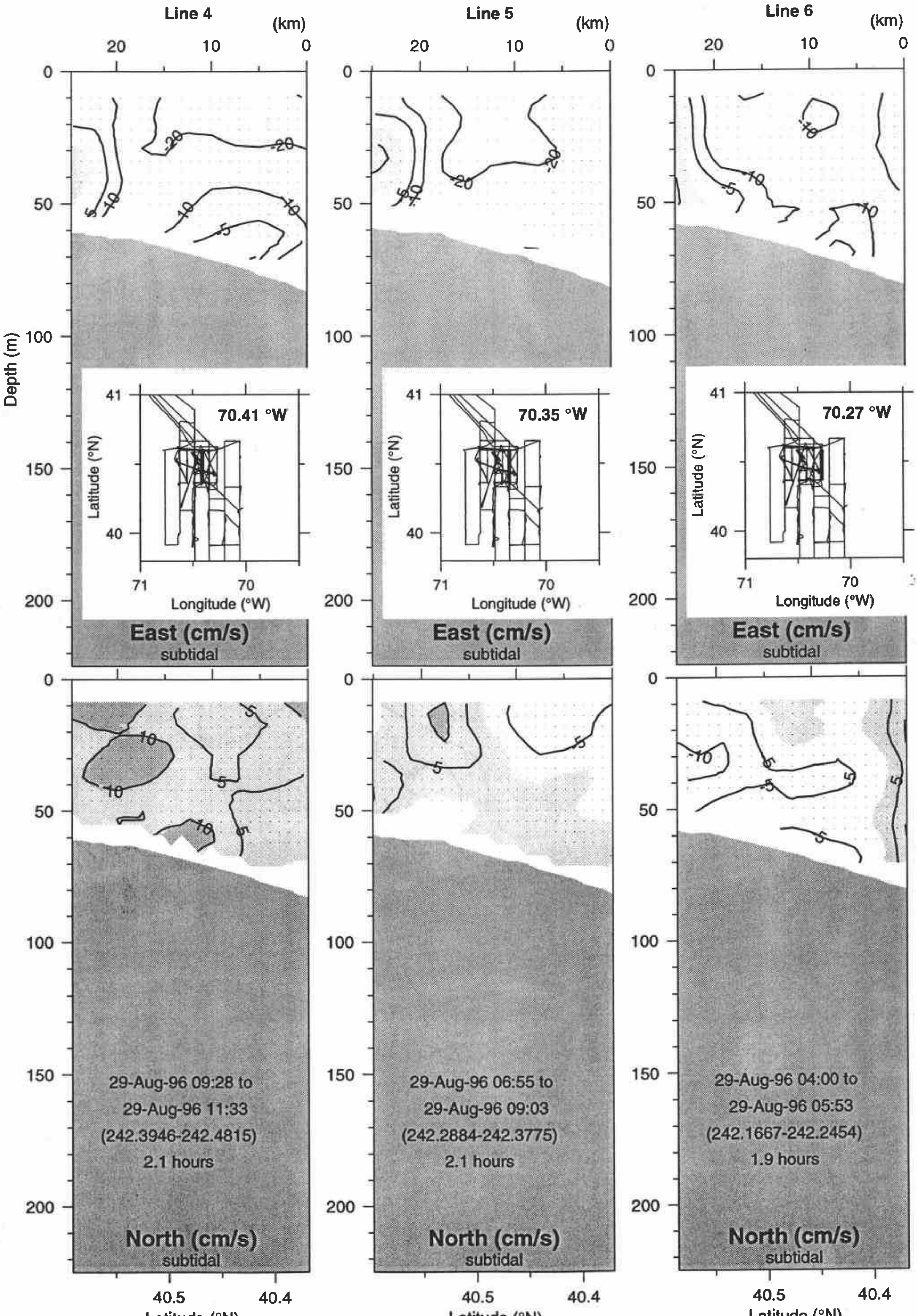

E9608 Small Box 8

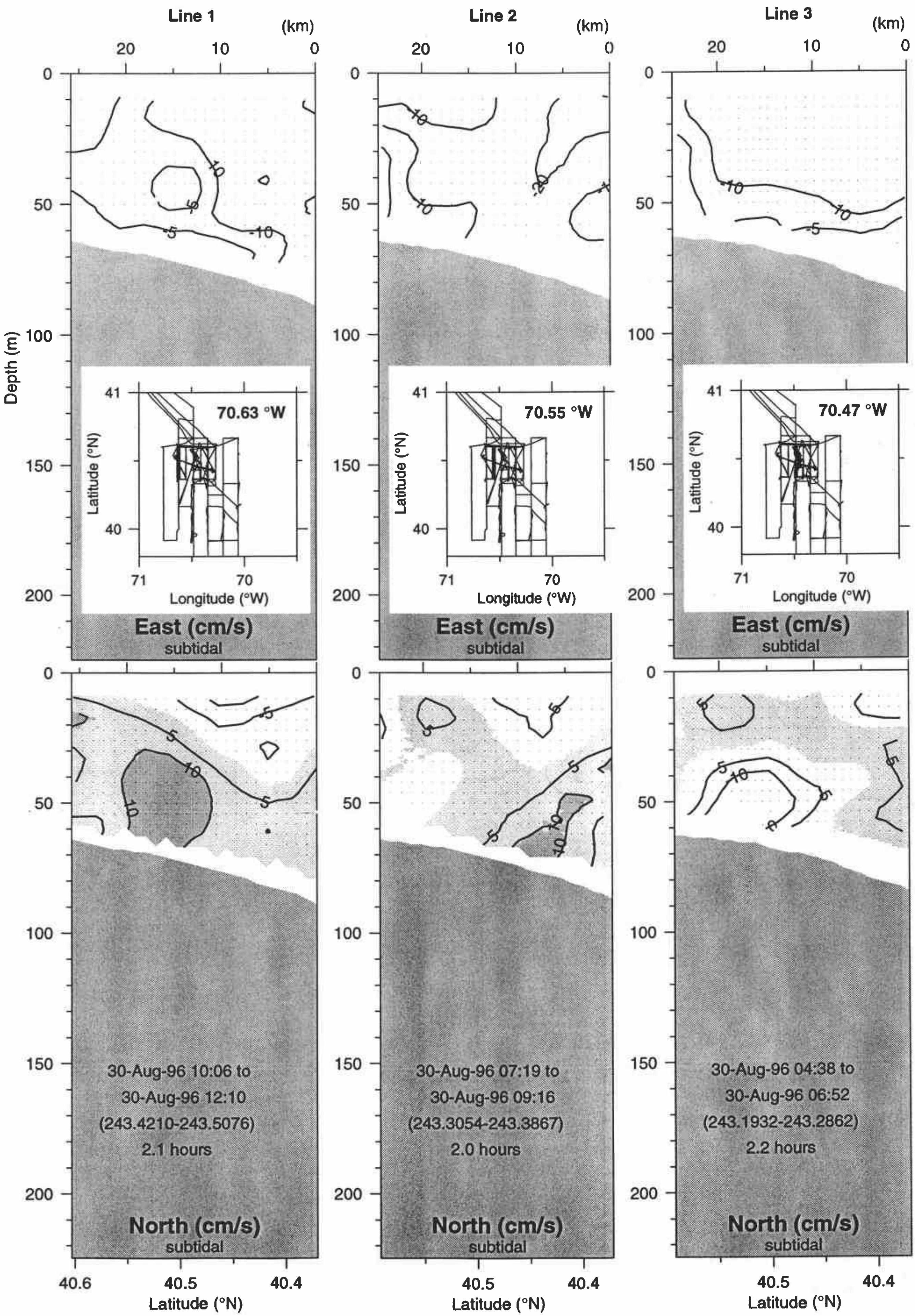

E9608 Small Box 8

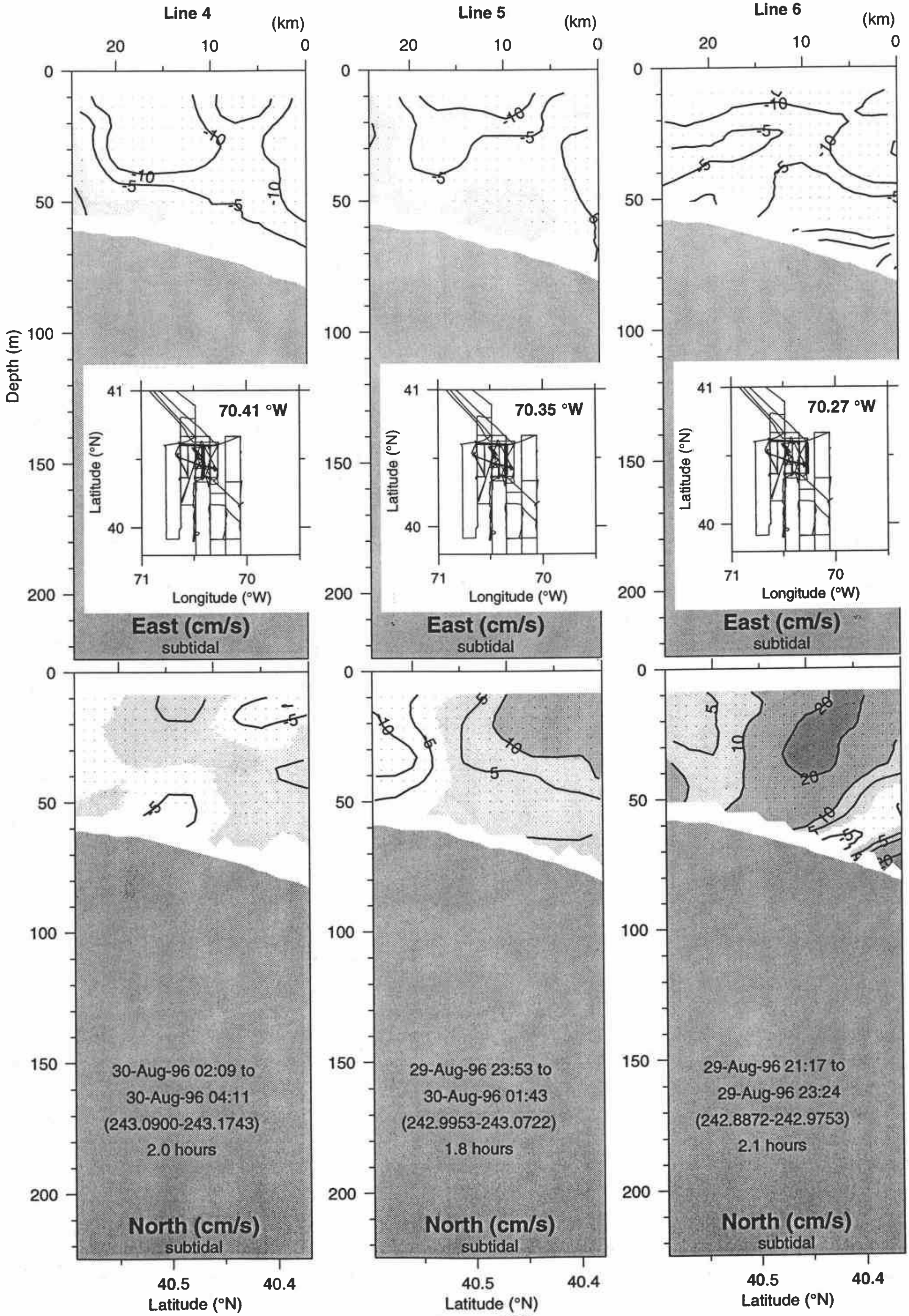

E9608 Small Box 9

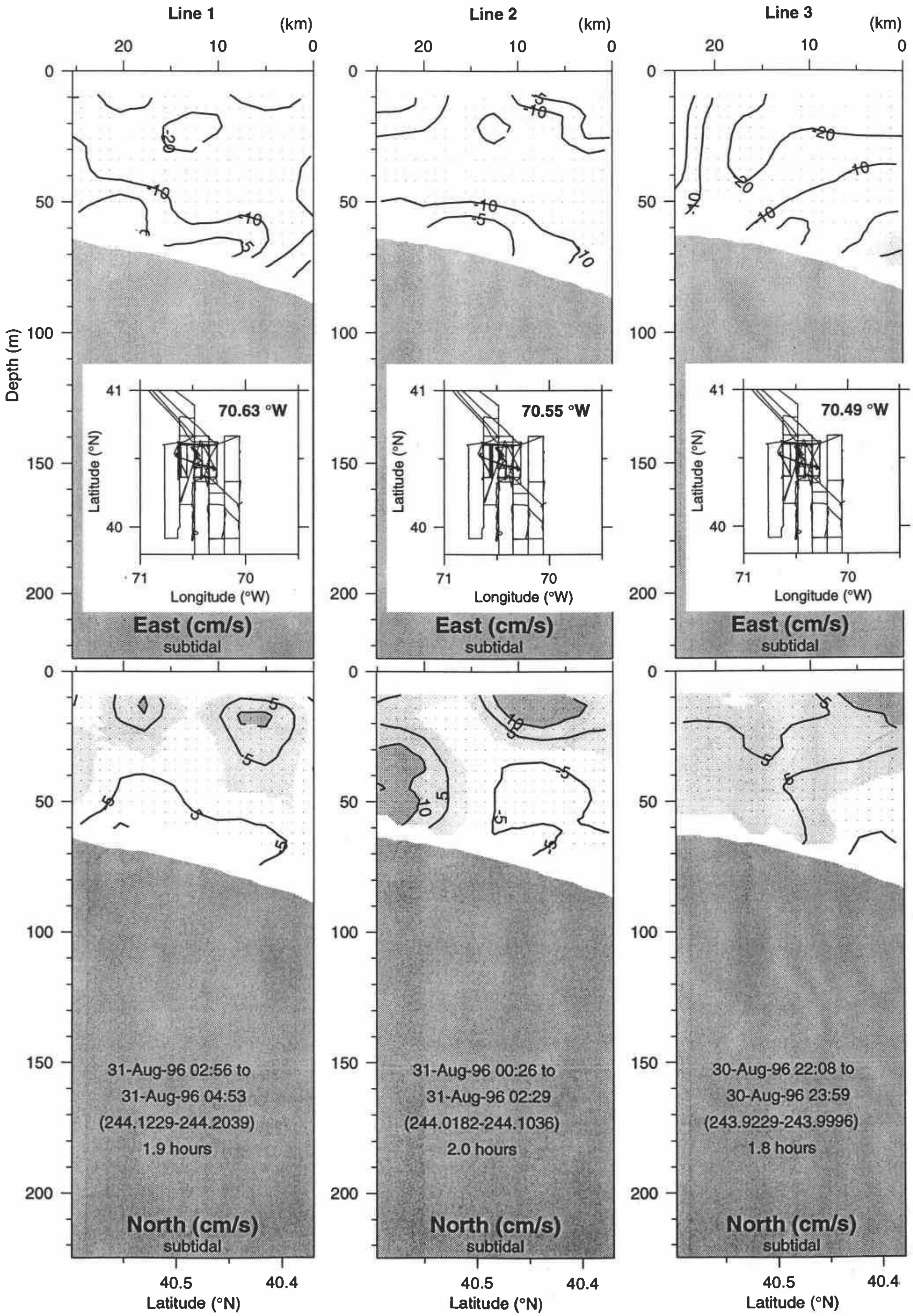

E9608 Small Box 9

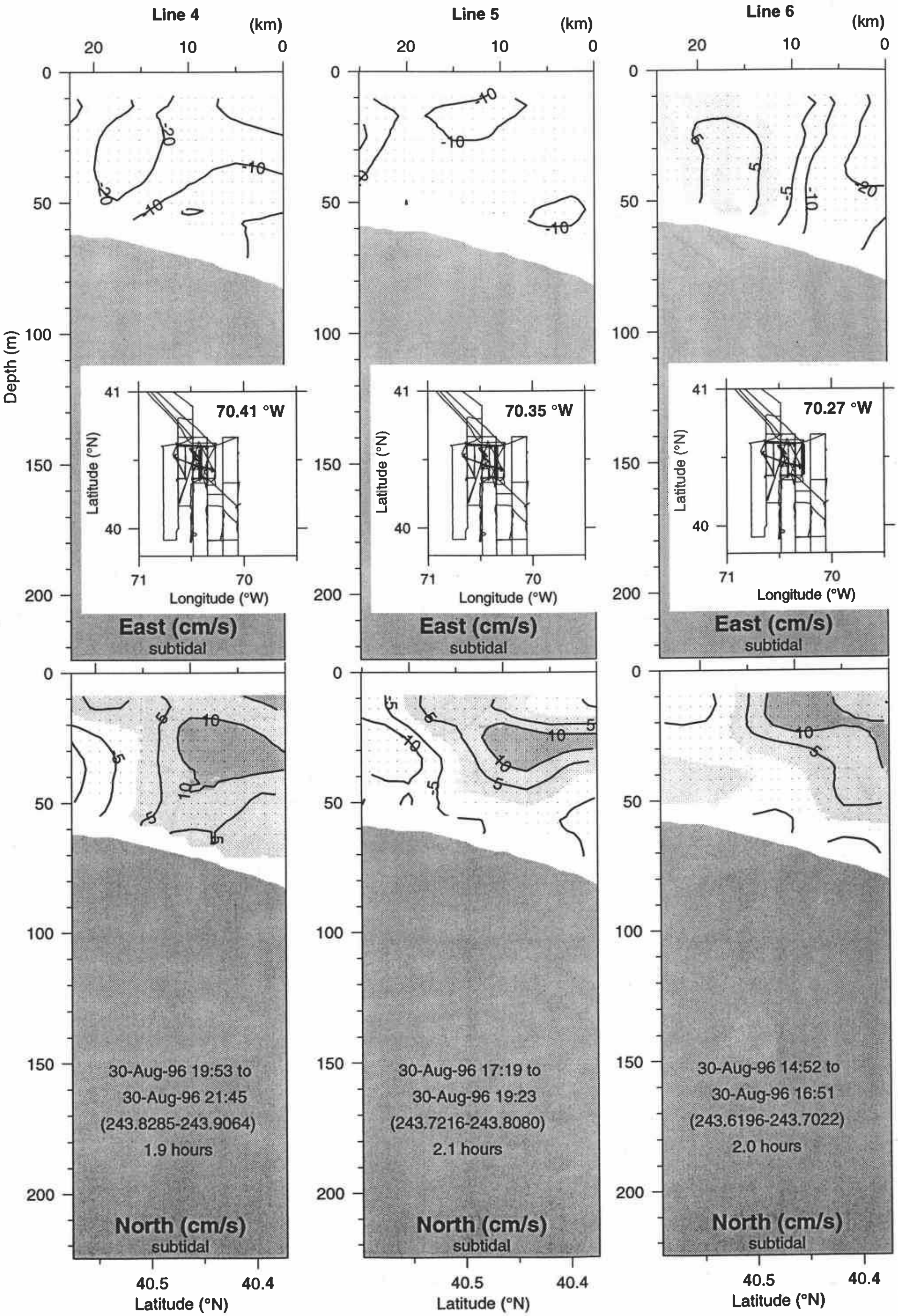

E9608 Big Box 3

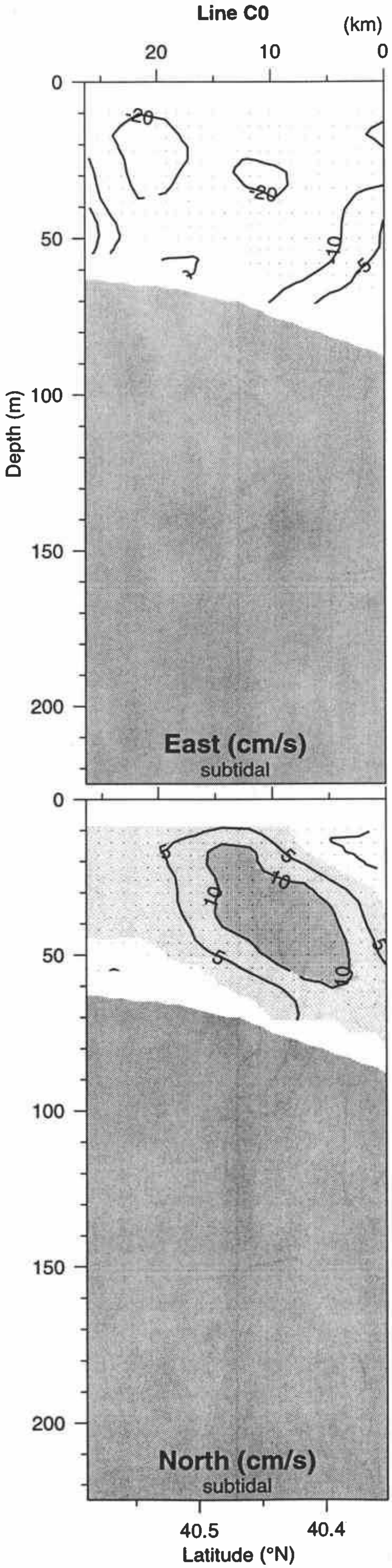

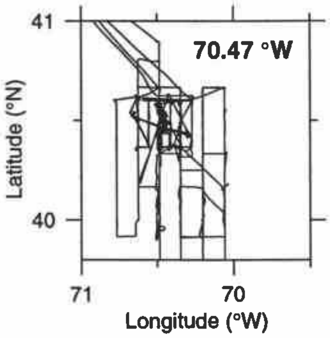

31-Aug-96 05:49 to
31-Aug-96 08:02
(244.2424-244.3352)
2.2 hours

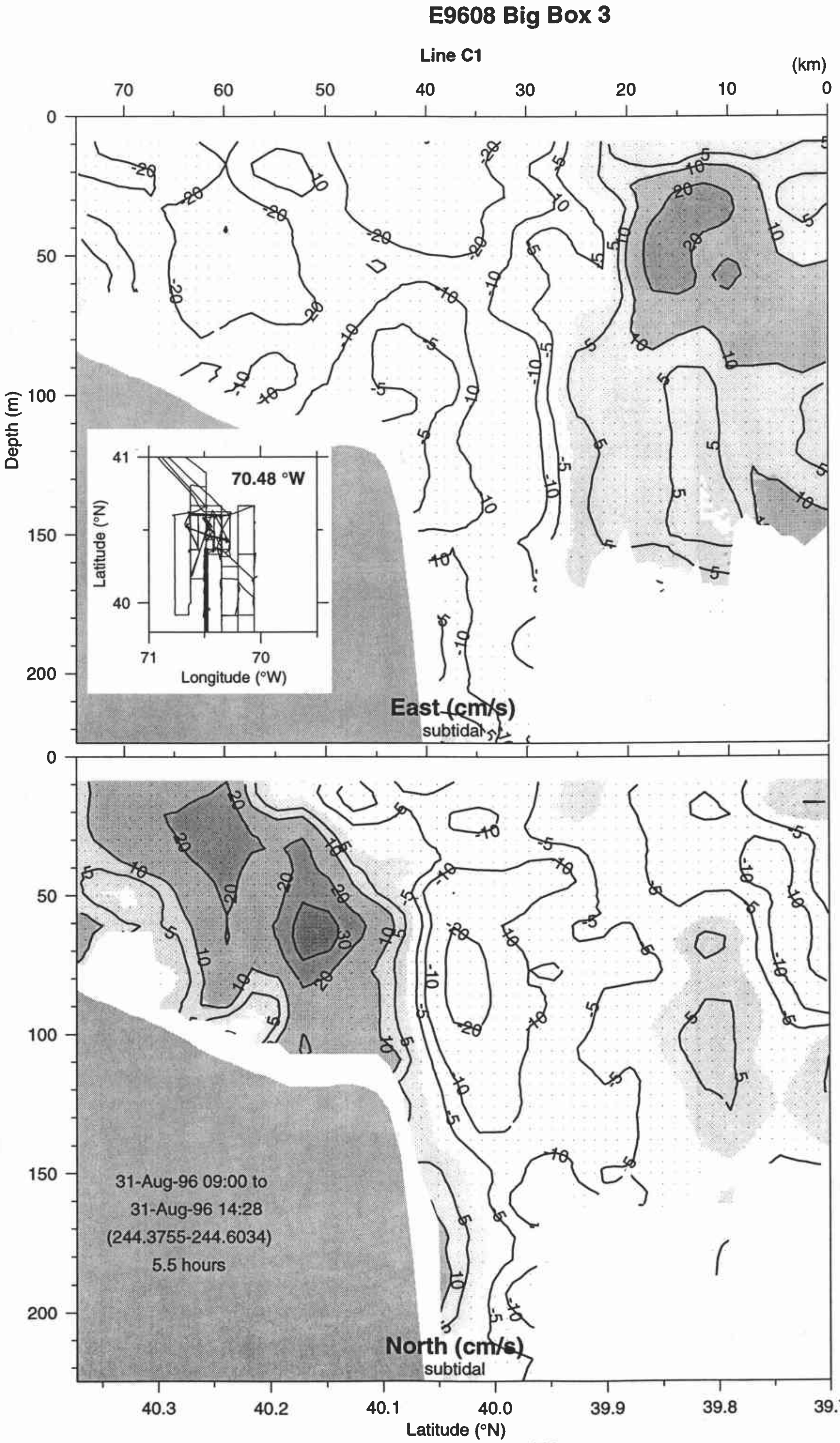
E9608 Big Box 3
Line C1
(km)
Depth (m)
East (cm/s)
subtidal
70.48 °W
Latitude (°N)
Longitude (°W)
North (cm/s)
subtidal
31-Aug-96 09:00 to
31-Aug-96 14:28
(244.3755-244.6034)
5.5 hours
Latitude (°N)

E9608 Big Box 3

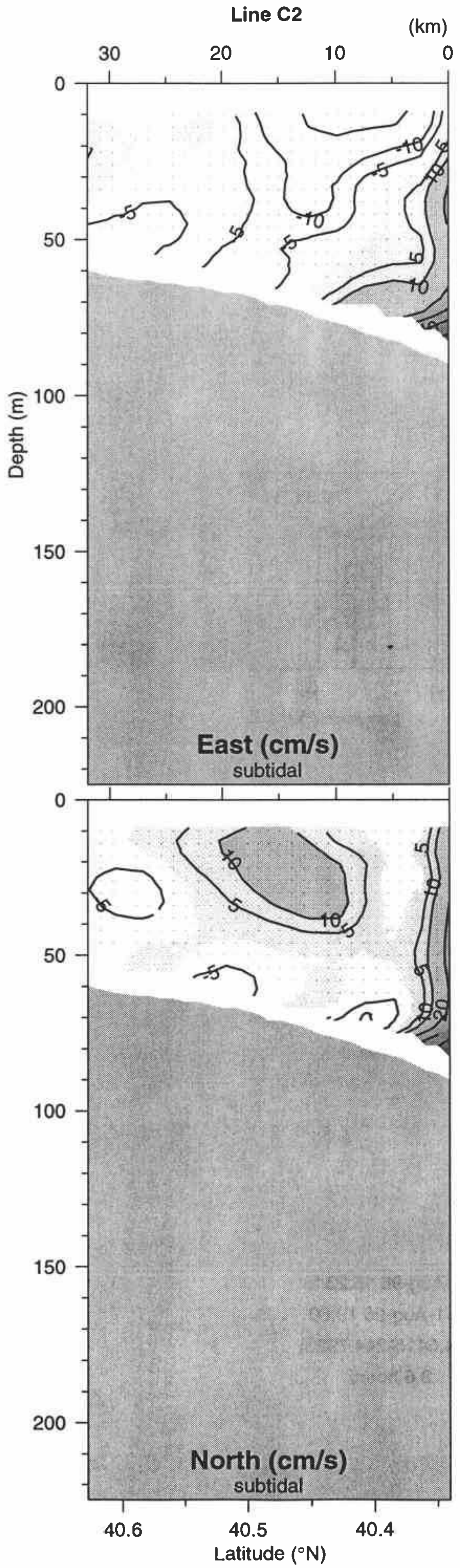

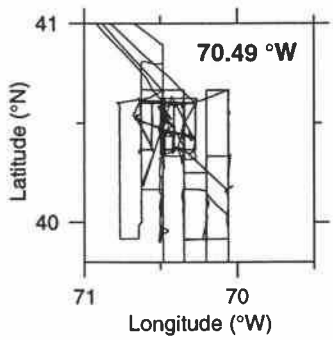

01-Sep-96 08:32 to
01-Sep-96 11:08
(245.3560-245.4640)
2.6 hours

E9608 Big Box 3

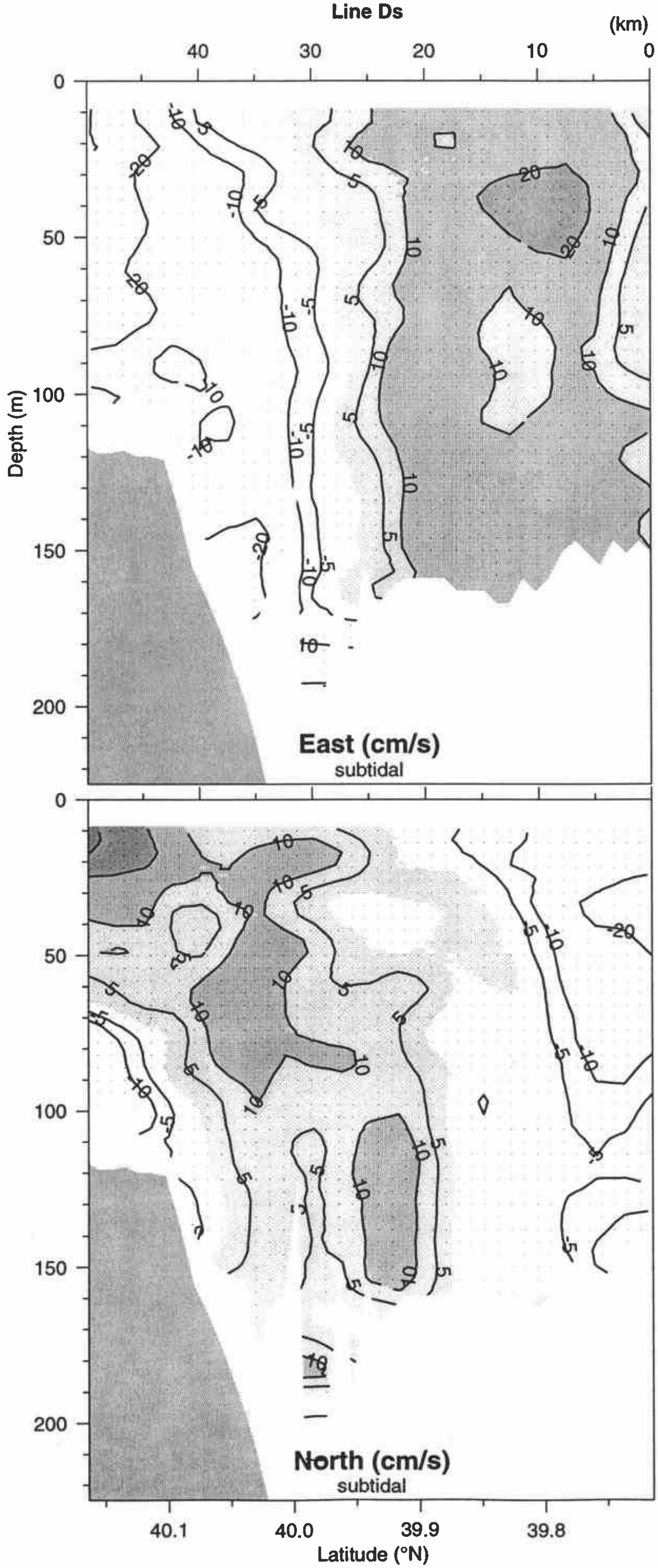

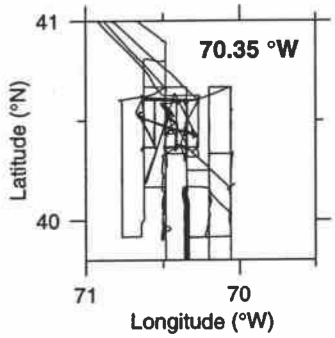

31-Aug-96 15:23 to
31-Aug-96 19:00
(244.6415-244.7923)
3.6 hours

E9608 Big Box 3

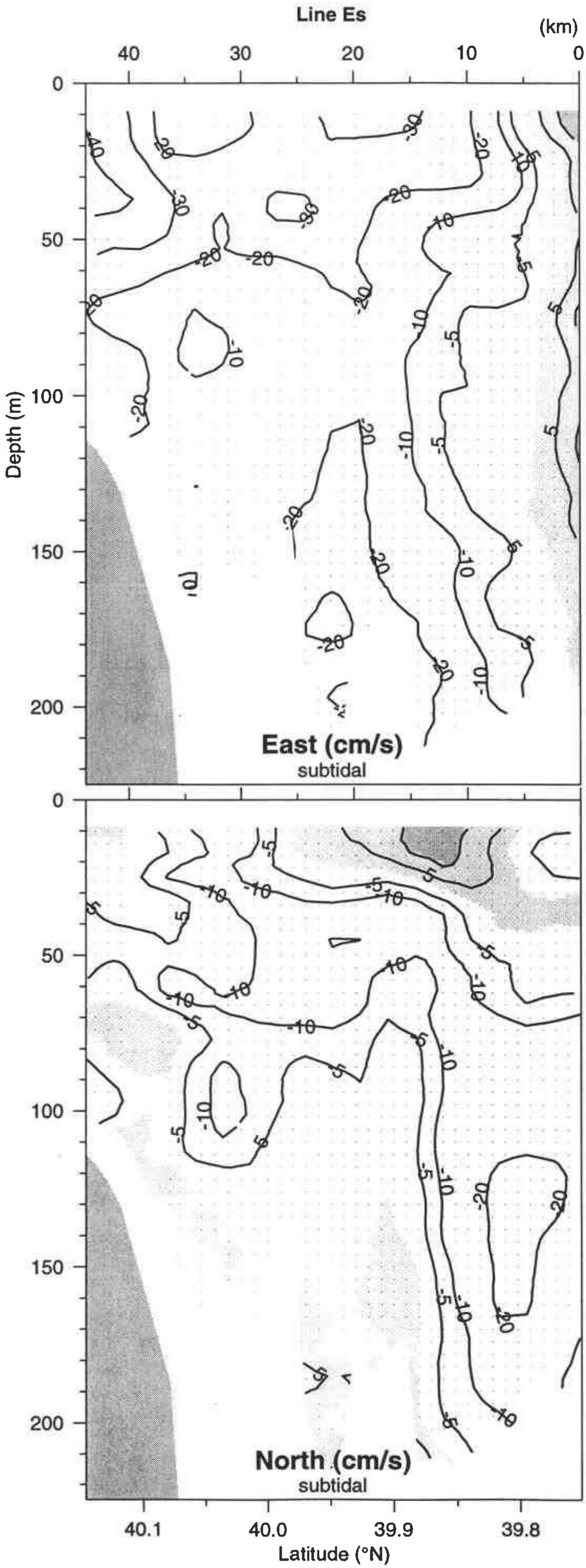

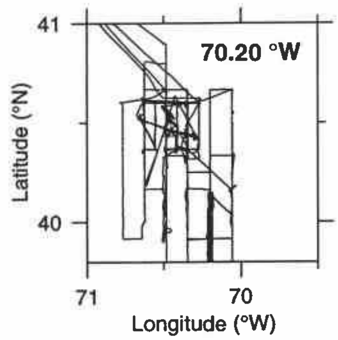

31-Aug-96 20:06 to
31-Aug-96 23:29
(244.8379-244.9790)
3.4 hours

E9608 Big Box 3

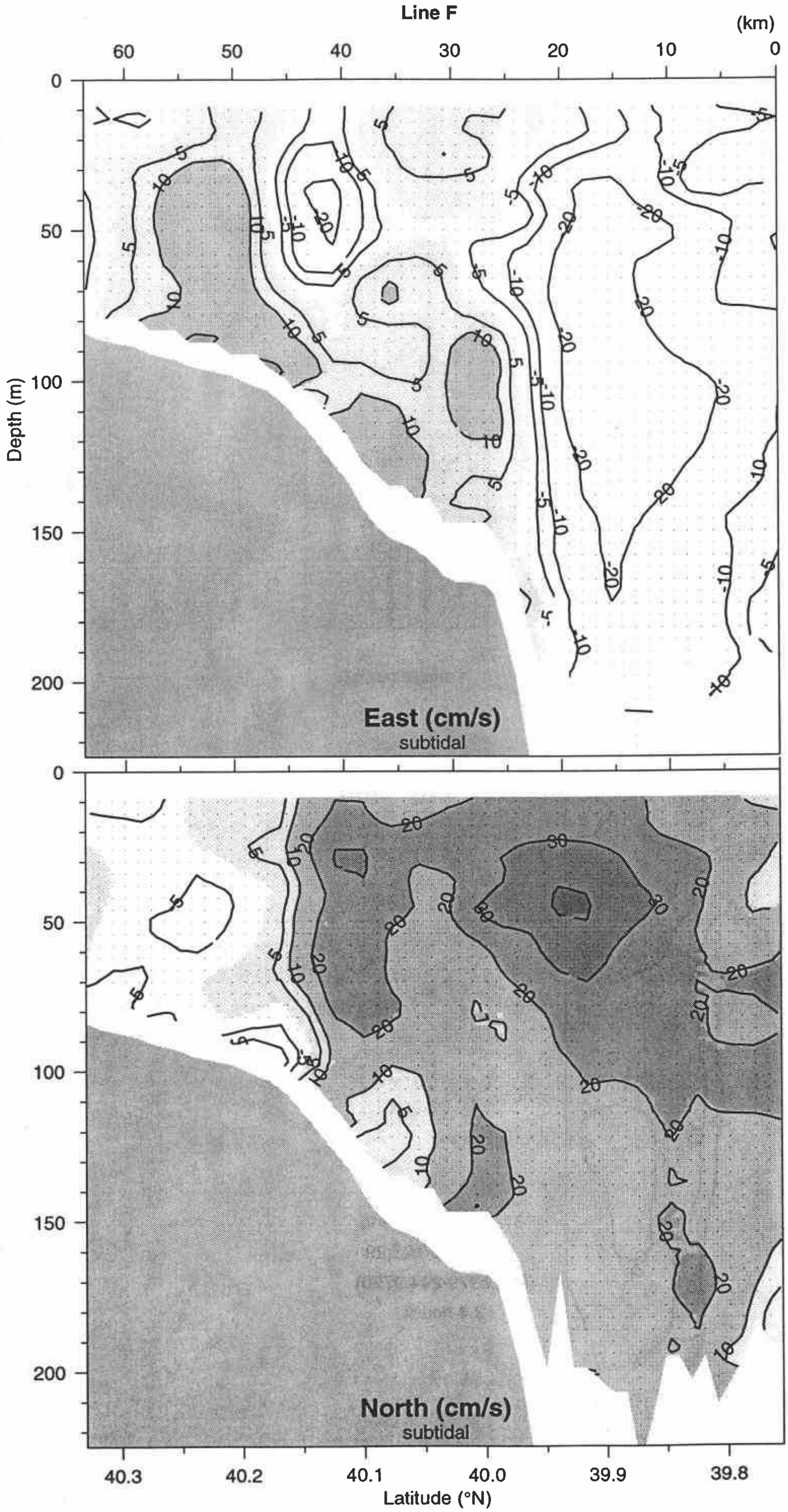

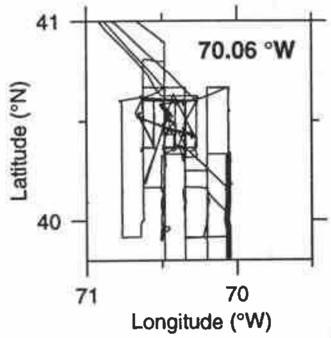

01-Sep-96 00:21 to
01-Sep-96 04:46
(245.0152-245.1987)
4.4 hours